ATOMISTIC SIMULATION OF SURFACE STRUCTURES AND ENERGIES OF ALKALINE EARTH HEXA-ALUMINATES

BY

DARREN M. STOHR

A THESIS

SUBMITTED TO THE FACULTY OF

ALFRED UNIVERSITY

IN PARTIAL FULFILLMENT OF THE REQUIREMENTS
FOR THE DEGREE OF

DOCTOR OF PHILOSOPHY

IN

CERAMICS

ALFRED, NEW YORK

APRIL, 2004

ATOMISTIC SIMULATION OF SURFACE STRUCTURES AND ENERGIES OF ALKALINE EARTH HEXA-ALUMINATES

BY

DARREN STOHR

B.S. CERAMIC SCIENCE ALFRED UNIVERSITY (1991)

M.S. CERAMIC SCIENCE ALFRED UNIVERSITY (1998)

SIGNATURE OF AUTHOR

APPROVED BY

(Signature on File)

ALASTAIR N. CORMACK, ADVISOR

(Signature on File)

ROBERT A. CONDRATE, ADVISORY COMMITTEE

(Signature on File)

PAUL F. JOHNSON III, ADVISORY COMMITTEE

(Signature on File)

DOREEN D. EDWARDS, ADVISORY COMMITTEE

(Signature on File)

WILLIAM B. CARLSON, CHAIR, ORAL THESIS DEFENSE

ACCEPTED BY

(Signature on File)

ALASTAIR N. CORMACK, DEAN, SCHOOL OF ENGINEERING

ACCEPTED BY

(Signature on File)

ALASTAIR N. CORMACK

DIRECTOR OF THE GRADUATE SCHOOL, ALFRED UNIVERSITY

ACKNOWLEDGMENTS

I am dedicating this work to my sons, Anthony Malachi Stohr and Cedric Cain Stohr. I would like to take this opportunity to especially thank my mother and father for their love and support. Many people also deserve to be mentioned for their support while working toward this accomplishment: my brother Brian, my sisters Marina and Peggy, brother-in-laws Henry and Dave, my sister-in-law Jen, my nieces Laura and Emma, my nephew Max, my former band members and still good friends; Gary, Phil, and Eric, their wives Tracy and Cindy, and many other friends who would fill far too much space to list here.

I would also like to say that my years at Alfred University were very good to me. I completed all three of my degrees here for a very good reason: the excellent faculty and staff of the NYSCC at Alfred University, without whom none of this would have been possible. Several members deserve special acknowledgement. I would first like to thank Dr. Varner and Dr. Burdick for their mentoring of my MS degree. It was a pleasure working with both of you. I would also like to thank my PhD committee members, Dr. Condrate, Dr. Edwards, and Dr. Johnson, for reading and critiquing this dissertation. The most thanks goes to my advisor Dr. Cormack. I greatly enjoyed working with him and truly appreciated the opportunity to work on such a interesting and challenging project.

Stay as far away from the Holiday Inn, Cambodia as you can.

TABLE OF CONTENTS

LIST OF TABLES

LIST OF FIGURES

ABSTRACT

Atomistic computer simulation techniques were used to model the surfaces of five crystal structures in the hexa-aluminate family. Calcium, strontium, and the theoretical barium hexa-alumunates with the magnetoplumbite structure and two barium β-alumina crystals were investigated. It was found in all the crystal structures that the [001] surface had the lowest surface energy. Each system modeled resulted in plate-like crystals.

Coordination of the exposed surface ions and the density of ions on the surface was found to be the dominant factor in the energy of the surfaces. The relaxation of ions to positions above the original surface (thus a low coordination with the other ions) was found to increase the energy of the surfaces for all the crystal systems.

The surface energy increased with increasing divalent cation size in the calcium and strontium magnetoplumbite surfaces. The theoretical barium magnetoplumbite had the lowest calculated overall surface energy value of the magnetoplumbite crystals. The lower values for barium magnetoplumbite were due to the rumpling of the oxygen layers above and below the mirror plane in the bulk crystal structure. The relaxed positions and the number of exposed divalent cations also had a large influence on the surface energy for a given orientation in these structures.

The location of the Ba^{2+} ion plays only a minor role in the lowering of surface energies in the β-aluminas. The coordination of the surface ions, mostly the number of dangling O^{2-} ions, and the reduction of polarization in the surface structure have the greatest impact on the surface energy of a given orientation.

It was concluded that surface energy stabilization of barium magnetoplumbite was not possible. The overall energy reduction caused by the formation of the two barium β-alumina crystals cannot be overcome by the lower surface energy of adopting the theoretical magnetoplumbite structure. The effect of isovalent cation substitution defects on the stability of the theorectical barium magnetoplumbite was also investigated. Calculation of isovalent substitution defects of the divalent cations and the aluminum ion on the surface was also examined. It was found that the addition of such surface defects did not stabilize the magnetoplumbite structure.

I. INTRODUCTION

The world of solid state chemistry and physics has enjoyed the explosion of computational power available in today's laboratories. The increasing complexity of the materials used in today's society has caused experimental researchers to improve and invent new characterization techniques. The sensitivity of these experiments has greatly increased in recent years, but cannot answer all the questions put forth. In most cases, accurate models are needed as a starting point for interpreting the experiment's results. The number of variables and the cost of the processing materials has also increased. The use of computer modeling in recent years has greatly helped the experimentalist improve designs and interpret their results. This is not to say, however, that computational material science will someday replace all experimentation, but that the partnership of these two disciplines can reduce costs and propose new solutions to contemporary materials science problems.

The development of nanotechnology, biomaterials, catalysis, and smaller components in electronic products relies on the knowledge of surface properties of existing and potentially new materials. Experimental characterization of these surfaces can be difficult. Low concentrations of surface defects are especially difficult to characterize. Additionally, existing models are sometimes necessary to interpret these experimental results. Atomistic surface modeling can be used with experimental characterization techniques to determine surface structure and properties. The investigation of surface defects via atomistic surface modeling has the potential to give a better understanding of surface properties, especially in the area of catalysis and biomaterials.

Hexa-aluminates are a class of poly-aluminate compounds that adopt a hexagonal structure that includes the magnetoplumbite, β-alumina, β”-alumina, and many other similarly related layered structures. This class of materials has applications in nuclear waste disposal,[1,2,3] laser processes,[4] fluorescence,[5,6,7,8] high-temperature combustion catalysis,[9,10] high temperature thermal coatings,[11] and crack deflection coatings.[12,13,14] The work presented here is the calculation of the surface structures and defects of the alkaline earth hexa-aluminates using a semi-classical atomistic computer simulation technique.

A. Hexa-Aluminates

Although they are related, the differences in the structures of the hexa-aluminates can lead to profound changes in their properties. The major difference between the magnetoplumbite and β-alumina type structures is the configuration of the mirror plane. For example, sodium β-alumina is known for its very high ionic conductivities. This is due to the open nature of the mirror/conduction plane and its defect structure. On the other hand, the magnetoplumbite type materials do not work well as ionic conductors because of the close-packed nature of the mirror plane. This lack of ionic conduction can be used to trap radioactive ions within its structure.[1,2]

Hexa-aluminates involved in this study fall into three crystal structures. The first is the magnetoplumbite structure. The second and third are β-alumina type structures. Calcium and strontium hexa-aluminates adopt the magnetoplumbite crystal structure. The barium hexa-aluminate magnetoplumbite phase was found previously not to be a thermodynamically stable phase, but separates into a mixture of two phases with two different β-alumina structures, a barium poor (β(I)) and a barium rich (β(II)) phase.[15,16,17,18] The work carried out in this study on the barium magnetoplumbite phase is based on its theoretical structure.

1. Magnetoplumbite Crystal Structure

The magnetoplumbite structure was originally determined by Adelskold.[19] Additional neutron diffraction work by Amin *et al*[20] further refined the structure. The original magnetoplumbite structure was named for the compound $PbFe_{12}O_{19}$. A generalized formula for magnetoplumbite compounds is given by $AB_{12}O_{19}$, with A=Sr, Ca, Pb, or Ba and B=Fe, Al, and Gd. The unit cell, with the space group $P6_3/mmc$, is composed of two-dimensional slabs perpendicular to the c-axis. These slabs are made up of four oxygen layers that closely resemble the spinel structure. The oxygens are in a cubic close packed array with the "B" cations occupying one tetrahedral (B(3)) site and three octahedral sites (B(1), B(4), and B(5)). The B(1) sites lie in the middle of the spinel block. The B(4) site is coordinated with six oxygens that make up a significantly distorted octahedron and is the

most abundant position for the "B" ions. The B(5) sites are coordinated to three oxygens in the mirror plane and three oxygens in the spinel block. The spinel-like blocks are separated by an oxygen close-packed plane having mirror symmetry that is composed of three oxygen ions O(3) and the divalent cation in a triangular dodecahedral site, A(1). There is also a "B" ion that occupies a five-fold coordination site, B(3), in the mirror plane. The mirror planes are situated about 11A apart, which results in the c-axis of the unit cell being approximately 22 A. Structural data for the strontium magnetoplumbite from Lindop *et. al.*[21] are given in Table I.

The instability of barium magnetoplumbite is due to the large size of the Ba^{2+} atoms. In order to accommodate its larger size, a rumpling of the O layers around the mirror plane occurs. This results in a lowering of the symmetry in the crystal structure[17] to the $P6_3mc$ space group. Although this rumpling relaxation lowers the lattice energy of the crystal, the phase separation into β(I)- and β(II)-alumina has an overall lower lattice energy thus making the barium magnetoplumbite phase thermodynamically unstable.[17]

2. Barium β(I)-Alumina Crystal Structure

The structure of barium β(I)-alumina calculated by Park and Cormack[17] uses a 2a x 2a x c quadruple supercell. The formula for this supercell is $Ba_6Al_{88}O_{138}$. There are eight half cells, two of which are defective, relative to the sodium hexa-aluminate structure, to maintain charge neutrality. There are several ways in which the defective half cells can be distributed. It was found that there was little difference in the lattice energy for the different distributions of the defect half cells. This agrees well with the lack of superstructure reflections. The defect half cell contains a Ba^{2+} vacancy and a Reidinger defect. The Reidinger defect is a string of point defects running parallel to the c-axis: V_{Al} - Al_i - O_i - Al_i - V_{al}.

The oxygen interstitial is a charge-compensating defect situated in the mirror plane. The two interstitial Al^{3+} defects help stabilize the mirror plane structure. Atomic positions calculated by Park[22] are given in Table II.

Table I. Crystallographic Data for Strontium Aluminate Magnetoplumbite, $SrAl_{12}O_{19}$

Space Group: $P6_3/mmc$				
Hexagonal Crystal System				
Lattice Parameters: a= 5.562 A, c= 21.972 A				
Atomic Positional Parameters				
Atom	Wyckoff Position	x	y	z
Sr	2d	2/3	1/3	1/4
Al(1)	2a	0	0	0
Al(2)	2b	0	0	1/4
Al(3)	4f	1/3	2/3	0.0276
Al(4)	12k	0.1685	0.3370	0.9918
Al(5)	4f	1/3	2/3	0.1903
O(1)	4e	0	0	0.1481
O(2)	4f	1/3	2/3	0.9462
O(3)	6h	0.1822	0.3644	1/4
O(4)	12k	0.1552	0.3104	0.0523
O(5)	12k	0.5025	1.0050	0.1476

Table II. Equilibrated Pseudo-Hexagonal Perfect Cell for the Barium β(I) Alumina Structure

Space Group: $P6_3/mmc$
Hexagonal (for equilibrated supercell)
Lattice Parameters: **a'** = 11.2510 A, **c'** = 22.7539 A for equilibrated supercell
Atomic Positional Parameters

Atom	Wyckoff Position	Site Type	x	y	z
O(1)	12k	tetrahedral	0.157	-0.157	0.050
O(2)	12k	tetrahedral	0.503	-0.503	0.000
O(3)	4f	tetrahedral	1/3	2/3	0.056
O(4)	4e	tetrahedral	0	0	0.143
O(5)	2c	Linear	1/3	2/3	0.025
Al(1)	12k	octahedral	0.832	-0.832	0.106
Al(2)	4f	tetrahedral	1/3	2/3	0.025
Al(3)	4f	tetrahedral	1/3	2/3	0.176
Al(4)	2a	octahedral	0	0	0
Ba(1)	2c	Beever-Ross	2/3	1/3	1/4
Ba(2)	6h	mid-O site	0.873	-0.873	1/4

3. Barium β(II)-Alumina Crystal Structure

The structure of barium β(II)-alumina calculated by Park and Cormack[17] uses a √3a x √3a x c supercell. Diffraction evidence supports a triple superstructure of the basic β-alumina structure. The thermodynamically stable structure was proposed by Iyi *et. al.*[23,24] In this structure, there are two kinds of cell; a perfect cell that has the ideal β-alumina structure and a defective cell that contains the excess Ba^{2+} of this phase. The defect cell has three Reidinger defects located around a Ba^{2+} vacancy in the mirror/conduction plane and the presence of a Ba^{2+} interstitial in the spinel block. The spinel block interstitial forces the removal of an Al^{3+} and O^{2-}. Thus, the interstitial Ba^{2+} ion becomes coordinated by 12 oxygens. The charge neutrality for the supercell requires that there be one defective cell for every two perfect cells. The formula for Ba-β(II) is $Ba_7Al_{64}O_{103}$. The calculated atomic positions of barium β(II)-alumina are given in Table III.[23]

B. Surface Science

Surfaces have become an increasing important research topic in the last few years.[25] The effect of surface properties on the material as a whole becomes more relevant as the size of components decreases. The properties of catalysis materials rely completely on both the non-defective and defective surface structures.[26] The longevity and viability of biomaterials depends on how the body chemistry reacts to these materials.[27] These chemical reactions are associated with the surface chemistry and structure of the biomaterials. Product development can be improved by a better understanding of the materials' surfaces.

There are several different methods for experimentally probing surface structure, its energetics, and surface adsorbates. A large part of surface physics and chemistry is concerned with the adsorption, both chemical and physical, of other species. Microcalorimetry, temperature programmed desorption, ultra-violet photoelectron spectroscopy, x-ray photoelectron spectrography, and infra-red absorption spectroscopy have all been used to examine adsorbed species on the surfaces of materials. Microcalorimetry[28] is a destructive technique that measures the equilibrium pressure, adsorbed amount, and the amount of heat released after a gaseous adsorbate is reacted with

the surface of the material

Table III. Calculated Atomic Positions of the Equilibrated of Barium β (II) Alumina

Space Group: P6m2
Hexagonal Crystal System
Lattice Parameters: a'= 9.88348 A, c'= 22.97005 A
Atomic Positional Parameters

Atom	Site	x	y	z
Ba(1)	2c	0.3333	0.6667	0.0000
Ba(2)	3g	0.3297	0.0000	0.5000
Ba(3)	2e	0.0000	0.0000	0.2336
Al(1)	12l	0.3208	0.4928	0.1530
Al(2)	12l	0.1674	0.3328	0.3563
Al(2)'	6i	0.4971	0.0000	0.3565
Al(3)	6i	0.3471	0.0000	0.2310
Al(4)	4h	0.3333	0.6667	0.2781
Al(5)	6i	0.3626	0.0000	0.0748
Al(6)	4h	0.3333	0.6667	0.4242
Al(6)'	2e	0.0000	0.0000	0.4231
Al(7)	6i	0.6660	0.0000	0.2528
Al(8)	6i	0.8098	0.0000	0.0710
O(1)	12l	0.3555	0.1762	0.2106
O(1)'	6i	0.5168	0.0000	0.2024
O(2)	12l	0.6535	0.1560	0.3028
O(2)'	6i	0.7953	0.0000	0.3073
O(3)	12l	0.1694	0.5071	0.1108
O(4)	12l	0.1654	0.4959	0.3958
O(4)'	6i	0.1719	0.0000	0.3972
O(5)	4h	0.3333	0.6667	0.1985
O(6)	6i	0.3346	0.0000	0.3096
O(7)	6i	0.6661	0.0000	0.1160
O(8)	6i	0.6613	0.0000	0.3914
O(9)	3f	0.3947	0.0000	0.0000
O(10)	2d	0.3333	0.6667	0.5000
O(10)'	1b	0.0000	0.0000	0.5000
O(11)	3f	0.7658	0.0000	0.0000
O(12)	6i	0.1743	0.0000	0.0832

being investigated. Initial preparation of the sample involves using vacuum conditions to remove any species that were previously adsorbed. The evolution of heat with time and change in pressure with time are used to calculate the adsorption behavior of the sample.

Another method of determining adsorption of species on the surface of a sample is temperature programmed desorption.[29] As with microcalorimetry, this is a destructive technique. The sample is heated until the adsorbed species dissociates from the surface. The desorbed species is detected using a mass spectrometer. The mean stay time, τ, of the adsorbed species is plotted versus the reciprocal of the temperature of the sample on a logarithmic scale. The energy needed to desorb the species, E_d, is determined by the slope of the plot.[29,30] In the case where there is more than one species present on the surface, additional peaks can be observed in the mean stay time vs the reciprocal of the temperature (non-logarithmic) plot.[31] One must be careful to realize that more than one peak does not automatically indicate additional adsorbed species. It is possible that the same species could be adsorbed in a different chemical environment (i.e., another site on the same surface, adsorption on different faces of the sample or a different orientation of the adsorbed species). The presence of other peaks can make it very difficult to determine E_d for a given species, and it is sometimes necessary to carry out the investigation under vacuum conditions.

Another method for determining adsorbed species on the surface of a sample is to bombard the surface with radiation. The radiation does not appreciably damage the sample, and thus this type of technique is considered nondestructive. Using this type of method also requires that the sample be placed in an ultra-high vacuum. There are two different results of bombarding the surface with radiation. The electrons are ejected from either the valence orbitals or the core orbitals. The former is called ultra-violet photoelectron spectrography[32] (UPS) and the latter is called x-ray photoelectron spectroscopy[33] (XPS).

The valence electrons are those involved in the bonding of the species. The binding energies of the valence electrons are on the order of 10 eV. The kinetic energies examined, using UPS, of the electrons ejected are therefore about 10-30 eV. Since these binding energies are much higher for the core electrons than for valence electrons, XPS looks at

kinetic energies on the order of hundreds of eV.

In both techniques, differences in binding energies for the different observed peaks leads to determination of which species have been absorbed, whether the species are physically or chemically adsorbed, and if the adsorption is occurring at more than one site. The ability of these methods to distinguish between different possibilities, including the ejection of electrons from different shells of the same species subjected to the same environment, depends on the instrument's resolution.

Infra-red absorption spectroscopy [34] is another nondestructive method of examining adsorbed species. IR radiation penetrates about 1000 nm into a sample. The material must not adsorb IR radiation for this technique to work for surface studies. In this technique, a thin sample of the material under investigation is exposed to potentially adsorbed species. Since the IR penetrates to large distances, the wafer of material is thus transparent to the IR. This leaves only the adsorbed species interacting with the IR radiation. Shifts or new features in the absorption band for the adsorbate can distinguish the site at which the species is adsorbed as well as the type of adsorption.

Determining the composition of surfaces can be done using a variety of techniques. Secondary Ion Mass Spectrometry[35] (SIMS) is one such technique. Particles, usually Ar ions, are accelerated toward the sample's surface. The high-energy collision of the Ar ions remove ions from the surface. A mass spectrometer is used to detect the ejected surface species. The detected ion's is determined by its mass and charge. Based on the time and number of species detected, a concentration gradient for each detected species can be determined by plotting the number of each species detected vs time. This data shows the surface composition and depth profile of the species in the sample. This can then determine if there is any segregation of species (i.e., if there are surface defects or other phases present on the sample's surface). To avoid detecting adsorbed species, this technique is performed under vacuum conditions. The surface structure cannot be determined using this destructive technique, only the surface composition.

X-ray diffraction[36] (XRD) has been used for many years to determine the atomic structure of the bulk. Under its normal use, the x-rays usually penetrate too deep into the

material to obtain any useful knowledge of the surface structure. A surface sensitive technique, x-ray photoelectron diffraction[37] (XPD), utilizes x-rays to obtain surface structural information. The x-rays knock out electrons from the atoms in the surface layer. The observed electron diffraction pattern can be used to determine the surface structure.

Another technique for determining the structure of surfaces is low energy electron diffraction[38] (LEED). Under an ultra high vacuum, electrons are accelerated toward the surface at low monochromatic energies, equal to the de Broglie wavelength corresponding to interatomic distances. The diffraction patterns produced by the scattered electrons determine interatomic distances, adsorbed species, symmetry of the surface structure, and the regularity of the surface. One problem with using LEED is that it is necessary to have a model to compare the diffraction results against.

Scanning tunneling microscopy[39] (STM) uses a tip from which accelerated electrons tunnel through the sample. A micrograph of the atomic surface can be used to determine structure due to different conduction rates of the electrons. A major drawback of this technique is that the surface must be conductive. Oxide surfaces, which encompass a large class of ceramics, are generally insulators. In order to get around this problem, thin oxide films are placed on a conducting substrate. This can lead to questions of the validity of the surface structure for larger sized samples.[39]

Atomic force microscopy[40] (AFM) is a technique similar to STM. A tip is placed close to the sample's surface. The tip is deflected, either toward, or away from, the sample surface as repulsive and attractive forces interact between the surface species and the tip. The amount of deflection is measured using a laser beam. The image produced is of atomic resolution. One advantage over STM is that the sample need not be conductive.

The use of both experimental and modeling techniques can lead to a greater understanding of a material's surface structure and thus its properties. Atomistic modeling can predict surface structures that then can be proven or disproved by experimental techniques. Surface modeling can also compare different theories arising from experimental results. Surface modeling can be used in conjunction with microcalorimetry, TPD, UPS, XPS, and IR spectroscopy to determine where species are adsorbed on a material's surface.

Surface modeling can also be used with SIMS, XPD, STM, and AFM to determine the surface structure, especially in cases where competing theories are involved. The use of the LEED technique requires pre-existing models, which can be created via atomistic modeling, to compare against the experimental results.

C. Computational Materials Science

The world of computational materials science is made up of two major branches.[41] Classical based atomistic simulations are based on the Born model of solids[42] in which ions are treated as point charges. The interatomic forces are obtained from pair-wise interatomic potentials that include both long-range and short-range interactions. The long-range forces are due to coulombic interactions. The short-range forces include the attractive Van der Waals potentials and the repulsive forces due to the overlapping electron orbitals. Materials with a higher degree of covalency sometimes include three-body terms that account for the bond geometry more accurately.[42] The interatomic potentials may be modified for the specific crystal being modeled, based on experimental data, such as crystal structure, elastic constants, and dielectric constants.

The second major type of model involves electronic structure calculations. These models are based on quantum mechanical principles and thus involve the solving of the Schrodinger equation.[43] Classically-based atomistic simulations work on a larger length scale than electronic structure calculations. The number of variables for each atom is less in the classical-based calculations than those used in electronic structure calculations. This means that the classically based simulations can have larger numbers of atoms modeled in a system using the same amount of computer resources. The long-range coulombic interactions are also not used in electronic structure calculations. This larger length scale allows for a better examination of the presence or lack of long range order in the materials being modeled.

Electronic structure calculations can themselves be divided into two major methods, Hartree-Fock and density functional theory. The Hartree-Fock method is a variational method which has its origins in chemistry.[44] The wave function of the many electron system

is assumed to be an antisymmetrical product of one-electron wave functions. The result is varied using the Schrodinger equation for individual one-electron wave functions with a potential determined by the wave functions of other electrons. The coupling between the wave functions results in nonlinear equations. These equations are then solved using an iterative process until the system becomes self-consistent. Approximations are needed to include the coulombic interactions between the electrons of the system, namely the exchange and correlation potentials. This method relies on solving wave equations for each individual electron in the system. As the number of electrons in the system increases, the number of equations and thus the computation time increases dramatically. This drawback can severely limit the size of the system being modeled.

The density functional theory[45] (DFT) is plane wave based with its origins in physics. DFT calculates solutions to the electronic orbitals not by solving the Schrodinger equation for individual electron orbitals but as a function of the electron density. This density is, in principle, non-local, as in the Hartree-Fock method. In the local density approximation[45] (LDA), the Hamiltonian is taken to depend on the local value of the density only. The exchange and correlation potentials are included in the Hamiltonian. This method is used extensively in the modeling of solids. Although this method reduces the number of equations needed to model a system compared to the Hartree-Fock method, a large number of equations are still needed because of the plane wave expansion of the electron wavefunction. Modeling large systems is still computationally expensive. In both types of electronic structure calculations, a matrix of eigenvalues is generated. Using the solutions to the matrix, calculations of the total energy and excitation spectra can be compared with experimental data.

Atomistic simulation has been used in a variety of applications and was the method of investigation of this study. The basis of atomistic simulations is the pair potential. They sometimes include three and four-body terms when materials have a higher degree of covalency to more accurately account for directionality of the bonds. Interatomic potentials between ions are used to calculate the potential energy of an ion relative to the other ions. The potentials of individual ions are summed over all ions to calculate the total potential

energy of the system.

There are several applications that employ atomistic simulation. The most widely used application is the refinement and prediction of the crystal structure of ionic solids.[46] These static lattice calculations do not include thermal vibrations and thus are considered to be done at 0 K. Other problems of solid state chemistry can also be modeled, including point defects,[47] dislocations, and grain boundaries.[48] It is also possible to model dynamic properties of crystals including the vibrational and entropic effects of higher temperature conditions.[49] Monte carlo and molecular dynamics techniques have been used to model atomic diffusion, conductivity,[50] and the structure of glasses.[51]

The main use of atomistic simulation in this study is the calculation of surface structure and energy. This type of model is also a static lattice problem. Surface modeling has major potential applications in the catalysis industry,[52] biomaterials development,[53] and phase stability prediction via surface energy stabilization. Early work on surface defects was done by Stewart and Mackrodt[54] and by Tasker[55,56] on surfaces. Tasker defined three different types of surfaces that occur in ionic crystals.[56] Type I surfaces are electrically neutral, i.e., equal numbers of cations and anions. Type II and Type III surfaces do not have equal numbers of cations and anions and are therefore charged surfaces. The difference between these surfaces is the dipole moment perpendicular to the surface. Type II surfaces have no dipole moment while Type III surfaces do have a net dipole moment perpendicular to the surface. Type III surfaces result in a divergence of the surface energy and are not physically possible. Type III surfaces require surface roughening, i.e. major reconstruction, or the adsorption of foreign atoms, to be stabilized.

The early work of atomistic surface simulations was performed on the (100) surface of simple binary oxides and alkali halides.[57] Later, the quantum mechanical techniques of Hartree-Fock and LDA both gave results that had very good agreement with the classical atomistic simulations. Table IV shows the agreement between experiment, atomistic simulations, Hartree-Fock, and LDA models for the {100} surface of MgO.[58] The success of atomistic simulations has also been demonstrated in modeling of the basal plane of alumina. The LDA calculations supported the earlier results showing large displacement of the surface cations found by atomistic simulations.[59]

Table IV: Surface Energies and Surface Structure for MgO

Parameter	Experiment	Shell Model	Hartree-Fock	LDA
Surface Energy (J/m^2)	1.04 ± 1.2	1.07	1.16	1.03
Rumple (%)	2.0 ± 2.0	3.0	2.5	1.7
Relaxation (%)	0.0 ± 0.75	1.0	-0.7	0.7

Two terms that are relevant to both bulk and surface modeling are relaxation and rumpling. Relaxation is the adjustment of the atomic coordinates relative to the initial configuration due to the minimization of the system's energy. Rumpling is the result of the relaxation of the system. Rumpling refers to movement of atoms alternatively below and above a plane that initially contained the relaxing atoms. Rumpling in the bulk phase is due to differences in the size of cations (or anions) in similar compounds such as calcium and the theoretical model of barium magnetoplumbite.[22] This occurs because the structure is too small to accommodate the larger cation. Rumpling of surfaces is due to the need of atoms to increase the coordination of neighboring surface atoms and thus satisfy bonds lost due to the creation of a surface.

The surfaces of several materials have been investigated using the classically based technique presented in this thesis. Early investigations were performed on simple surfaces such as the cubic rock-salt oxides of NiO, CaO, and MgO[60,61,62] and the alkali halides.[55] Allan *et al.*[63] investigated the surface of La_2CuO_4. The surfaces of different perovskites have been modeled, including $CaCO_3$ by Parker *et al.*[62] Zeolites[64] and calcite[65] surfaces have also been investigated using this technique. Lawrence performed surface structure and energy calculations on Cr_2O_3.[66] α-Alumina (0001) surfaces were modeled by Gautier *et al*.[67]

Surface defects have also been investigated using the classically-based atomistic simulations. Mackrodt and Stewart investigated both intrinsic surface defects of NaCl and MgO and substitutional defects in NaF.[54] The surface structure and defect chemistry of the $LaCoO_3$ perovskite was investigated by Read *et al.*[26]

II SIMULATION PROCEDURE

The basis of classical atomistic simulations is the Born theory of solids[42] that treats all ions in a crystal lattice as point charges. The interactions of the ions include both short-range forces, which include attractive van der Waal and repulsive forces due to valence orbital overlap between neighboring ions, and the long-range electrostatic forces.

A. Perfect Lattice Simulations

1. Description of a Perfect Lattice

There are two terms generally associated with the perfect lattice property; these are the lattice energy and cohesive energy. The cohesive energy is the energy of a crystal with reference to its component atoms at infinity, thus it is used for non-ionic systems. The lattice energy is its counter-part for ionic systems. It is the energy of a crystal with reference to its component ions at infinity. The ions have no potential interactions between them at infinite distances. A potential develops as they are brought together. This potential energy of the ions on their equilibrium lattice sites is the lattice energy. A general expression for the lattice energy is given by:

$$U = \Sigma\, q_i q_j / \mathbf{r_{ij}} + \Sigma\, \Phi_{ij}(\mathbf{r_{ij}}) + \Sigma\, \Phi_{ijk}(\mathbf{r_{ijk}}) + \ldots$$

(1)where the summations are for all pairs of ions i and j, and in the case of the third term for the trio of ions i, j, and k.

The first term in the lattice energy equation is the long-range contribution, which is the sum is the coulombic interaction between all pairs of ions i and j separated by a distance r_{ij} where q_i and q_j are the charges of ion i and j respectively. One problem with the evaluation of this first term is that it converges rather slowly as the distances between the ions is increased. The summation used here relies on a technique developed by Ewald.[68] In the Ewald method, the point charges of the ions are replaced with a Gaussian charge distribution representing the long-range potentials that is then transformed into reciprocal space. The Fourier series converges very rapidly. The near-neighbor coulombic interactions are represented in the real space. This summation also rapidly converges. The overlap between the Gaussian distributions that occurs in real space is subtracted out of the

summation. The total electrostatic forces converge rapidly since both terms converge very rapidly.

The remainder of the terms on the right hand side of equation (1) are the short-range interactions between the ions. Short-range interactions include the repulsive terms associated with ions' electron orbital overlap and the attractive terms associated with dispersion interactions and van der Waals attractions. Two-body terms represented by $\Phi_{ij}(\mathbf{r_{ij}})$ are based only on the distance between the ions. This covers the repulsive, dispersive, and van der Waals interactions. These are the dominant component of the short-range interactions and therefore are included in all ionic and semi-ionic systems. Three-body terms can also be included because of directionality in the bonding orbitals of semi-ionic and covalent materials. Four-body terms might also be necessary to model torsion of bonds in these materials.

There are many different models used for the two-body interactions. The Bond Harmonic Function is the simplest potential used in two-body interactions. It is a simple harmonic model given by:

$$\Phi(\mathbf{r_{ij}}) = \tfrac{1}{2}\, k_{ij}(\mathbf{r_{ij}} - \mathbf{r_o})$$

(2)where k_{ij} is the bond force constant, $\mathbf{r_{ij}}$ is the distance between ions i and j, and $\mathbf{r_o}$ is the equilibrium bond distance. This model's simplicity does not lend itself well to anything but very small deviations from the equilibrium bond lengths. This is because k_{ij} is valid for a particular value of $\mathbf{r_{ij}}$; thus, as $\mathbf{r_{ij}}$ changes so does the value of k_{ij}. Re-evaluation of k_{ij} makes this model problematic for all but very small deviations of r_{ij}. Any systems with large deviations from equilibrium, which are present in any real system, cannot use this type of potential model. Anharmonicity in the bond lengths quickly makes this model ineffectual.

A second type of short-range interaction is the Morse Potential. The Morse potential includes the anharmonicity present in real systems and is given by:

$$\Phi_{ij}(r_{ij}) = D(1-\exp[-\alpha(\mathbf{r_{ij}} - \mathbf{r_0})])^2 - D$$

(3)where $\mathbf{r_{ij}}$ and $\mathbf{r_0}$ are the same as in the Bond Harmonic Function, D is the dissociation energy of the bond, and α is a variable which is determined from spectroscopic data. The variable α is determined by the slope of the energy well. The Morse potential is designed so

that the two ions have a minimum potential energy at the equilibrium distance and is zero at infinite separation. This type of potential is often used in the modeling of organic molecules.

Another short-range model used is the Lennard-Jones potential:

$$\Phi(\mathbf{r_{ij}}) = A\mathbf{r_{ij}}^{-12} - B\mathbf{r_{ij}}^{-6}$$

(4)where $\mathbf{r_{ij}}$ is the separation between ions and A and B are variable parameters. The first term is the repulsive term, and this acts only over a very short range. The second term is an attractive term. It acts over a larger distance than the repulsive term and thus is the dominant term for the Lennard-Jones potential.

The Buckingham Potential, used in this study, is one of the most widely used in atomistic simulations, and is given by:

$$\Phi_{ij}(\mathbf{r_{ij}}) = A_{ij} \exp[-\mathbf{r_{ij}} / \rho_{ij}] - C_{ij}\mathbf{r_{ij}}^{-6}$$

(5)where the attractive second term is identical in form to the attractive term used in the Lennard-Jones potential. The shorter-ranged repulsive term used in the Lennard-Jones potential has been replaced by an exponential term in which the parameters A_{ij} and ρ_{ij} are related to the size and the hardness of the ion respectively.

The terms represented by $\Phi_{ijk}(\mathbf{r_{ijk}})$ are the three-body terms. These terms are used to incorporate bond geometry into the model. One general form is given by the expression:

$$\Phi_{ijk}(\mathbf{r_{ijk}}) = \tfrac{1}{2}\, k_{ijk}(\Theta_{ijk} - \Theta_o)^2$$

(6)where k_{ijk} is a force constant and $(\Theta_{ijk} - \Theta_o)$ is the deviation from the equilibrium bond angle (i.e., it is a simple harmonic term). The subscript ijk represents the labels of the central atom i and the two bonded atoms j and k. The forces associated with the three body terms are usually much smaller in magnitude than the coulombic and short range forces. Three body terms, in these cases, contribute only very small amounts of energy to the lattice energy. A three body term is often included to properly model the directional properties of the covalent bond. Most semi-ionic systems show some degree of covalency in the directionality of bonding. As the degree of covalent nature of the bonding increases, the relevance of three body terms also increases. Three body terms do have a significant effect on the vibrational properties of the system.[22]

Although additional terms may be added to the potential model, it is very rare to use terms of higher order than three ions due to their very small contributions to the lattice energy. It is used only when the bond geometry is highly important to the overall structure of the material as in inorganic molecular crystals such as sulfates and carbonates.

The following is an example of a four-body term, as used in modeling of the torsional properties of carbonate groups by Pavese.[65]

$$\Phi_{ijkl} = K_{ijkl} [1 - s \cos[N\Theta]]$$

(7)where K_{ijkl} is a force constant, s is either +1 or -1, and N is an integer that gives the periodicity of the torsion.

There are also contributions to the lattice energy from vibrational energy. One approximation used in this work is that the lattice is static, effectively carrying out the work at 0K. This allows the neglect of any vibrational terms to the lattice energy. This also means that entropic effects are also effectively ignored. The contributions of the lattice vibrations and the entropy to the lattice energy are relatively small. Valid results are still obtained with their omission.[69]

The work described in this thesis was carried out without the use of three-body terms. The potential models and crystal structures used in this work were determined previously.[22] Park previously showed, because of the high degree of ionic nature of the materials, that the three-body terms do not have a significant effect on the lattice energy of these crystal structures, thus the three-body terms were not included.

The properties of the crystal being modeled, such as the elastic constants, can be derived from the first and second derivatives of the lattice energy. Based on the derivatives of the lattice energy, the forces acting on individual ions within the unit cell can be calculated. The bulk and basis strains can also be calculated.

The potential models thus far introduced are called rigid ion models. The ions are treated as if they are only point charges, i.e., no polarization of the ions is taken into account. This implies that the high-frequency dielectric constant is one. This type of potential model is adequate for many systems as shown by Harding.[70] Several problems can be encountered when using this type of potential model, though. Dynamic properties of

crystal lattices will be poorly modeled due to the fact that lattice vibrations are coupled to the polarizability of the crystal.[71] The rigid ion model is also inaccurate when atom positions within the crystal structure result in a high degree of polarization. The distortion of the "electron cloud," in the presence of an electric field (polarization), is also known to have a significant effect on the relaxation of ions around defects.[71] This distortion can greatly reduce the defect energy and thus stabilize the defect. Gillan[72] showed that it is possible in a static lattice simulation to modify the short-range interactions to obtain experimentally accurate static dielectric constants. This has the drawback that lattice relaxations associated with the polarization are overestimated in the absence of electronic polarizability.

As previously stated, dielectric properties of the system depend on the ionic polarization. Polarization that arises from the distortion of the "electron cloud" surrounding each ion can be modeled with the simple point polarizable ion model. In this model, ion type i is assigned a polarizability, α_i. The dipole moment, μ is given by:

$$\mu=\alpha_i E \quad (8)$$

when subjected to an electric field, E. The use of this model does not greatly increase the amount of time needed to minimize the lattice energy. Thus it is computationally inexpensive and has been used in defect calculations.[73] This model performed poorly in calculating lattice dynamical and dielectric properties of solids.[72] As in the use of rigid ion model, it does not take into account the coupling between the polarizability of the ion and its short-range interactions due to the ion's environment. The polarization is overestimated and results in smaller defect energies than expected. The ions have a critical distance, for which, when exceeded, the energy becomes divergent.[74] The polarization due to the ion's environment can be included in a model by coupling the short-range interaction and the polarization as in the shell model.

Dick and Overhauser[75] developed the shell model to include this coupling of the short-range interactions and the polarization of the ions. This study incorporates the shell model. This model uses a mass-less shell representing the valence electrons and the ion's core connected by a harmonic spring. The short-range interactions are between the shells of the neighboring ions. The cores and shells are allowed to relax, thus allowing for

polarization of the ion. The polarization is thus affected by ion's environment. The functional form of the shell model is given by:

$$\varphi_i (r_i) = \tfrac{1}{2} k_i d_i \quad (9)$$

where the spring constant is k_i and d_i is the separation of the shell and its core. The polarizability of the free ion is thus:

$$\alpha_i = Y^2 / (4\pi\varepsilon_0 k_i) \quad (10)$$

where Y is the shell charge. The core is assigned a charge X. Although it is not necessarily the case, in this study all ions use their formal charge state, i.e., X + Y equals the integer valence state charge. Both k_i and Y are fitted to match the experimentally measured dielectric constants, elastic properties or dispersion curves of the material. It should be noted that not all ions in the system need explicitly to use a core-shell model. Ions that are small and highly charged, i.e., Al^{3+} as in this study, might not be easily polarized and thus including the shell for that ion increases the computation time but does not increase greatly the accuracy of the model.

In the shell model, the short-range interactions are assumed to act between shells or the core and its neighboring ion's shell, when no shell is present for a particular ion. This is based on the assumption that only the shell overlap will be involved over such short distances. However, the long-range coulombic interactions include the interaction between all cores and shells not of the same ion. A diagram of the shell model can be seen in Figure 2.1.

2. Lattice Energy Minimization

Nature is always seeking its lowest energy state. The minimization of the lattice energy in computational physics is the goal in determining crystal structures. The atomic coordinates and cell dimensions are adjusted until the lowest energy configuration is achieved.

There are two conditions under which the lattice energy can be minimized in order to achieve the lowest energy configuration. The first is under constant volume and the second

is

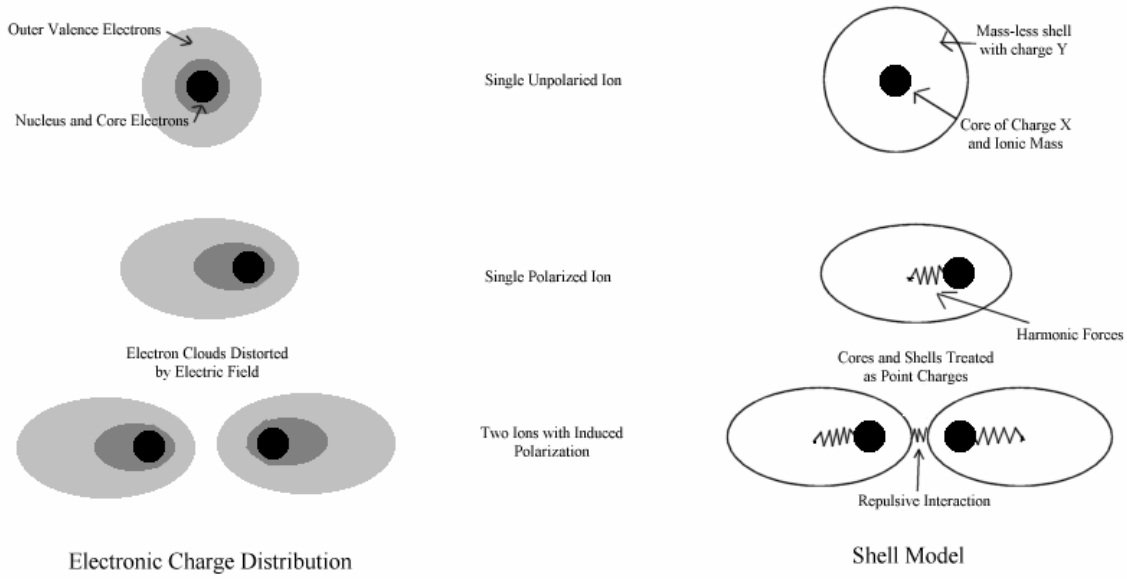

Figure 2.1. Electronic Charge Distribution and Shell Model Schematic[22]

under constant pressure. Constant volume minimization relies only on equilibrating the ions' coordinates, removing any basis strain. This is the simpler method. Constant volume minimizations are performed when the cell dimensions of the crystal must be maintained. Constant pressure minimization equilibrates the lattice by adjusting the unit cell parameters as well as the ionic coordinates. Since most investigations of crystals are under the conditions of constant pressure (namely one atmosphere), most calculations are done under the conditionof constant pressure.

There are many different minimization techniques. One method of lattice energy minimization, known as the conjugate gradient technique, involves only the first derivative of the energy with respect to a parameter r_i ($g_i = \partial E_i / \partial r_i$). The value of the (k+1)th configuration is related to the kth by:

$$\mathbf{r}^{(k+1)} = \mathbf{r}^{(k)} + h^k \mathbf{s}^{(k)} \qquad (11)$$

where $h^{(k)}$ is a scalar parameter and $\mathbf{s}^{(k)} = -\mathbf{g}^{(k)}$. The speed of convergence is greatly influenced by the choice of parameters.

The Newton-Raphson procedure is another minimization technique that is widely used in crystal lattice modeling. The lattice energy, U, for a lattice containing N atoms per unit cell can be expanded around a point **r** to second order in the total strain with the expression:

$$U(\mathbf{r'}) = U(\mathbf{r}) + \mathbf{g}^T \cdot \delta + (1/2)\delta^T \cdot \mathbf{W} \cdot \delta$$

(12)where **g** is defined as above and the new configuration **r'** is generated by the strain vector δ. The strain vector has 3N+6 dimensions. The 3N components given by δ are defined as:

$$\delta = \mathbf{r'} - \mathbf{r} = \delta\mathbf{r}$$

(13)which is the displacements in the x, y, and z positions of the ions. The final 6 components, δ=δε which are the bulk strain components of the symmetric strain matrix Δε:

$$\Delta\varepsilon = \begin{matrix} \delta\varepsilon_1 & (1/2)\delta\varepsilon_6 & (1/2)\delta\varepsilon_1 \\ (1/2)\delta\varepsilon_6 & \delta\varepsilon_2 & (1/2)\delta\varepsilon_4 \\ (1/2)\delta\varepsilon_5 & (1/2)\delta\varepsilon_4 & \delta\varepsilon_3 \end{matrix} \qquad (14)$$

with the vector of the first derivatives, $\mathbf{g}=(\partial U/\partial\delta\boldsymbol{\varepsilon})$.

The second derivative matrix, **W** is given by:

$$\mathbf{W} = \begin{matrix} \partial^2 U/\partial\delta\mathbf{r}^2 & \partial^2 U/\partial\delta\mathbf{r}\partial\varepsilon \\ \partial^2 U/\partial\varepsilon\partial\delta\mathbf{r} & \partial^2 U/\partial\delta\varepsilon^2 \end{matrix} = \begin{matrix} \mathbf{W_{rr}} & \mathbf{W_{r\varepsilon}} \\ \mathbf{W_{\varepsilon r}} & \mathbf{W}_{\varepsilon\varepsilon} \end{matrix} \quad (15)$$

r' is also related to **r** by:

$$\mathbf{r'} = \Delta\varepsilon\cdot(\mathbf{r} + \delta\mathbf{r}).$$

(16)Equation (12) is then differentiated and equilibrium conditions applied:

$$\partial U/\partial\delta\mathbf{r} = 0$$

(17)giving:

$$\mathbf{g} + \mathbf{W_{rr}}\boldsymbol{\delta}\mathbf{r} = 0.$$

(18)The lattice energy is at a minimum when:

$$\mathbf{g} = -\mathbf{W_{rr}}\boldsymbol{\delta}\mathbf{r}.$$

(19)The displacement of the ions can thus be found by inverting the **W** matrix:

$$\boldsymbol{\delta}\mathbf{r} = -\mathbf{W_{rr}}^{-1}\mathbf{g}.$$

(20)The iterative minimization uses the expression:

$$\mathbf{r}^{(k+1)} = \mathbf{r}^{(k)} - \mathbf{g}^{(k)}\cdot\mathbf{H}^k$$

(21)where the matrix $\mathbf{H} = \mathbf{W}^{-1}$. This method converges much more rapidly than just using the gradient technique. The improved speed at which the convergence occurs can be lost in the extra computation time used in calculating the second derivative matrix **W** and its inverse matrix **H**. One way of decreasing the time needed for each iteration is to avoid calculating the second derivative and inverting it at each step.

The Davidon-Fletcher-Powell algorithm[76] can be used to calculate the matrix **H**. The matrix **H** is updated at each iteration by the following equation:

$$\mathbf{H}^{(k+1)} = \mathbf{H}^{(k)} + (\delta^{(k)}\cdot\delta^{T(k)} / \delta^{T(k)}\cdot\delta\mathbf{g}^{(k)}) - (\mathbf{H}^{(k)}\cdot\delta\mathbf{g}^{(k)}\cdot\delta\mathbf{g}^{T(k)}\cdot\mathbf{H}^{(k)} / \delta\mathbf{g}^{T(k)}\cdot\mathbf{H}^{T(k)}\cdot\delta\mathbf{g}^{(k)}) \quad (22)$$

where

$$\delta \mathbf{g}^{(k)} = \mathbf{g}^{(k+1)} - \mathbf{g}^{(k)}$$

(23)and

$$\delta = \mathbf{r}'^{(k+1)} - \mathbf{r}^{(k)}$$

(24)and the superscript T indicates the transpose of the vector. The use of such matrix updating without recalculating the second derivative and its inversion of the Newton-Raphson minimization is the basis of most studies in solid state physics and chemistry.

3. Calculation of Crystal Properties

Once the crystal lattice has been equilibrated, crystal properties can be then calculated. The net force acting on all ions is zero at equilibrium, $\mathbf{g} = 0$. The presence of an external field, E_{ext} is given by:

$$U(\mathbf{r}) = U(\mathbf{r}^{e}) + (½)\delta^{T}\cdot\mathbf{W}\cdot\delta - q^{T}\cdot\delta r^{\alpha}\cdot E^{\alpha}_{ext}$$

(25)where $\mathbf{r}^{e}$ is the equilibrium configuration in the absence of an external field, q is an N dimensional vector of the charges and the coordinate index α, which represents the summation over all components. This can be expanded to obtain:

$$U(\mathbf{r}) = U(\mathbf{r}^{e}) + (½)\delta\mathbf{r}^{T}\cdot\mathbf{W}_{rr}\cdot\delta\mathbf{r} + \delta\varepsilon\cdot\mathbf{W}_{\varepsilon\mathbf{r}}\cdot\delta\mathbf{r}$$

$$(26) \quad + (½)\delta\varepsilon\cdot\mathbf{W}_{\varepsilon\varepsilon}\cdot\delta\varepsilon - \mathbf{q}^{T}\cdot\delta\mathbf{r}^{\alpha}\cdot\mathbf{E}^{\alpha}_{ext}.$$

The equilibrium condition from equation (17) gives:

$$\delta\mathbf{r}^{\alpha} = -[\mathbf{W}_{\mathbf{rr}}^{-1}\cdot\mathbf{W}_{\mathbf{r}\varepsilon}\cdot\delta\varepsilon]^{\alpha} + [\mathbf{W}_{rr}^{-1}]^{\alpha\beta}\cdot\mathbf{q}\cdot\mathbf{E}^{\boldsymbol{\alpha}}_{\mathbf{ext}.}$$

(27)The definition of the electric displacement field **D** results in:

$$\mathbf{D}^{\alpha} = \mathbf{E}^{\boldsymbol{\alpha}}_{\mathbf{ext}} + (4\pi/v)\mathbf{q}^{T}\delta\mathbf{r}^{\boldsymbol{\alpha}}$$

(28)where v is the unit cell volume.

The dielectric and piezoelectric constants can be defined using:

$$\mathbf{D}^{\boldsymbol{\alpha}} = \Sigma\,\boldsymbol{\lambda}^{\alpha}\varepsilon_{i} + \Sigma\,\mathbf{k}^{\alpha\beta}\,\mathbf{E}^{\boldsymbol{\alpha}}_{\mathbf{ext}}$$

(29)where **λ** is the piezoelectric tensor and **k** is the dielectric tensor. This gives expressions for

the piezoelectric tensor:

$$\lambda^{\alpha}_{i} = -(4\pi/v)\mathbf{q}^{T} \cdot [\mathbf{W}_{rr}^{-1}\mathbf{W}_{r\varepsilon}^{-1}]^{\alpha}_{i}$$

(30)and the dielectric tensor:

$$k^{\alpha\beta} = \delta^{\alpha\beta} + (4\pi/v)\mathbf{q}^{T\cdot}\cdot[\mathbf{W}_{\mathbf{rr}}^{-1}]^{\alpha\beta}\cdot\mathbf{q}$$

(31)where $\delta^{\alpha\beta}$ is the Kronecker delta.

The elastic constants are defined as the second derivatives of lattice energy with respect to strain when the lattice energy is normalized to unit volume. The elastic constant tensor C is given by:

$$C = (1/v)[\mathbf{W}_{\varepsilon\varepsilon} \cdot \mathbf{W}_{\varepsilon r} \cdot \mathbf{W}_{rr}^{-1} \cdot \mathbf{W}_{r\varepsilon}].$$

(32)

B. Defect Energy Calculations

1. Description of a Defective Lattice

Lidiard and Norgett[77] and Norgett[78] developed a convenient general formulation for modeling the defective lattice. The internal energy of the perfect lattice is defined as zero. The change in the internal energy at constant volume is then considered the defect energy. Using this approach, the energy needed to remove a bulk lattice ion to infinity is always positive.

The basis of the method is that the lattice will always relax around a defect in order to minimize the total energy of the system. The surrounding ions move to a minimum energy configuration. The biggest problem in calculating static lattice defects is the treatment of the relaxation around the defect and the loss of periodicity. The effect of the relaxation is rather large since there is an extensive perturbation of the atomic positions in the surrounding lattice. In the case of ionic crystals, the defect is mainly coulombic in nature and thus causes the relaxation field to be a long-range perturbation.

The method used to overcome the problem of long-range perturbations and calculate realistic results for defect relaxation energies is to use a two-region approach. The crystal is divided into two regions, I and II. The inner region (Region I) immediately surrounds the defect and contains a few hundred atoms. These atoms are allowed to relax atomistically, i.e., explicitly using the interatomic potentials. The outer region (Region II) appears to the

defect as a dielectric continuum. Within Region II, the ion displacements are dependent on the electric field created by the defect. These displacements are treated by methods based on continuum theories of Mott and Littleton.[79]

The total energy, E, of the formation of the defect in the two-region approach can be expressed as:

$$E = E_1(\mathbf{r}) + E_2(\mathbf{r},\zeta) + E_3(\zeta)$$

(33)where $E_1(\mathbf{r})$ is the energy of Region I, $E_3(\zeta)$ is the energy of Region II, and $E_2(\mathbf{r},\zeta)$ is the interaction energy between Regions I and II. The positions of the ions in Region I are given as **r** and the displacements of the ions in Region II are ζ. The difficulty of this method is that $E_3(\zeta)$ cannot be calculated exactly since there are in principle an infinite number of displacements. Two assumptions are made to overcome this difficulty. The first is that the energy of Region II be expressed as a quadratic function of the displacements ζ:

$$E_3(\zeta) = \tfrac{1}{2}\,\zeta^{T}\cdot \mathbf{A}\cdot\zeta$$

(34)where **A** is the force constant matrix. The second assumption is that equilibrium conditions hold, thus the following equation obtains:

$$\delta E/\delta\zeta = 0.$$

(35) $E_3(\zeta)$ can be evaluated by differentiating equation (24) with respect to ζ and using equations (25) and (26), gives:

$$0 = |\,(\delta E_2(\mathbf{r},\zeta)/\delta\zeta)\,|_{\zeta=\zeta'} + \mathbf{A}\cdot\zeta'$$

(36)where ζ' is the equilibrium value of ζ corresponding to an arbitrary values of r determined from this equation. This leads to:

$$-1/2\ |\,(\delta E_2(\mathbf{r},\zeta)/\delta\zeta)\,|_{\zeta=\zeta'}\cdot\zeta = \tfrac{1}{2}\,\zeta^{T}\cdot\mathbf{A}\cdot\zeta.$$

(37)The total energy of the system can then be expressed by:

$$E = E_1(\mathbf{r}) + E_2(\mathbf{r},\zeta) - \tfrac{1}{2}\ |\,(\delta E_2(\mathbf{r},\zeta)/\delta\zeta)\,|_{\zeta=\zeta'}\cdot\zeta$$

(38)which depends only on terms that involve interactions within Region I and those between Regions I and II.

When using pair potentials, the calculation of each of these terms is rather straightforward. The energy of the perfect lattice is given by:

$$E_L = \Sigma\, \Phi_{ij}(|\, \mathbf{R}_i - \mathbf{R}_j\,|)$$

(39)where $\{\mathbf{R_i}\}$ is the equilibrium configuration and the summation is over i and j. The defective lattice is expressed as:

$$E_D = \Sigma'\, \Phi_{ij}(|\mathbf{r}_i - \mathbf{r}_j\,|)$$

(40)where $\{\mathbf{r_i}\}$ are the displaced lattice coordinates and the summation of the defective lattice, Σ', is over again i and j. The defect energy is the difference between the two summations:

$$E = \Sigma'\, \Phi_{ij}(|\mathbf{r}_i - \mathbf{r}_j\,|) - \Sigma\, \Phi_{ij}(|\, \mathbf{R}_i - \mathbf{R}_j\,|).$$

(41)The summations extend over all ions in a spherical region of the crystal radius equal to the Region I radius plus a short-range interaction cut-off distance. Conditions must be met to make the partitioned energy a single summation for each component for defects involving vacancies and interstitials. The convention that needs to be adopted contains three conditions. The first is that the initial position of the interstitial ion is at infinity. The second is that a vacancy is formed when the ion in question is removed to infinity. The third is that ionic substitution is the combination of both an interstitial and vacancy. The complete expression of the energy of the lattice defect, E is given by:

$$E = \Sigma_{i(I),j(I)}\, \langle \Phi_{ij}(|\mathbf{r}_i - \mathbf{r}_j|) - \Phi_{ij}(|\mathbf{R}_i - \mathbf{R}_j\,|)\rangle$$

$$(42)\quad + \Sigma_{i(I),j(II)}\, \langle \Phi_{ij}(|\mathbf{r}_i - \mathbf{r}_j|) - \Phi_{ij}(|\mathbf{R}_i - \mathbf{R}_j\,|)\rangle$$

$$-1/2\Sigma_{i(I),j(II)}\, \langle(\partial\Phi_{ij}(|\mathbf{r}_i - \mathbf{r}_j|)/\partial\mathbf{r}_j) - (\partial\Phi_{ij}(|\mathbf{R}_i - \mathbf{R}_j\,|)/\partial\mathbf{r_j})\rangle \cdot (\mathbf{r_j} - \mathbf{R}_j)$$

where $\mathbf{r}_i$ is the atom coordinates of the defective lattice and $\mathbf{R_i}$ of the perfect lattice. The coulombic interaction is evaluated by subtracting the Gaussian charge distribution at each site and adding the contributions from ions in Region I. When a neutral defect is being examined, the displacement of ions in Region II is zero (i.e., $\zeta = 0$).

The Mott-Littleton approach is used when there is a charged defect. This approach relates the polarization, **P(r)**, at a distance of r from a defect that has an effective charge of Q in Region I. For dielectrically isotropic crystals by:

$$\mathbf{P} = (1/4\pi)(1-1/\varepsilon_o)(Q\mathbf{r}/|\mathbf{r}|^3).$$

(43)In using this approach, Region II is further subdivided into Region IIa and Region IIb.

Region IIa is the inner region which must be defined to be larger than the size of Region I plus the specified short-range potential energy cut off distance. Thus only the ions in Region IIa interact explicitly with the ions in Region I. The coulombic contribution to E_2 from Region IIb is a charge induced dipole interaction due to the effective charge of the defect which is expressed by:

$$E_2^{IIb}\,(\text{coulombic}) = -Q\Sigma_{j(IIb)}\,\mathbf{q}_j(\zeta_j\cdot\mathbf{R}_j)\,/|\mathbf{R}_j|^3$$

(44)where Q is the charge of the defect, q_j is the charge of ion j, ζ_j is the displacement position, and $\mathbf{R}_j$ is the equilibrium position of the jth ion in Region IIb.

Another consideration is the size of Region I. The larger the Region I size, the better the convergence of the defect formation energy. The validity of this approach comes from the convergence of this energy. The number of ions in Region I is dependent on the size of the defective lattice under investigation. Region I containing 100 to 400 ions is usually sufficient to ensure that the defect energy is not dependent on the region size.[22]

2. Defect Energy Minimization

The theoretical basis of the defective lattice is the same as for the perfect lattice, that is to say, the defective lattice will relax to its minimum energy configuration. The use of a modified Newton-Raphson minimization method was originally used to calculate defect energies. As stated earlier, the inverted second derivative matrix is updated by an approximation method in order to lower the amount of computation time.

Two strategies have been used to calculate the minimized defect energies. The first is to minimize the total energy E(r) with ζ used as an explicit function of r:

$$dE/d\mathbf{r} = 0.$$

(45)The second method has **r** and ζ as independent variables. The equilibrium condition is that all ions in Region I have a net force of zero:

$$|\partial E(\mathbf{r},\zeta)\,/\partial\mathbf{r}\,|_{\zeta=\text{constant}} = 0. \qquad (46)$$

The complete net force-balance equations are then given by:

$$\partial E_1/\partial\mathbf{r} + |\partial E_2(\mathbf{r},\zeta)\,/\partial\mathbf{r}\,|_{\zeta=\zeta'} - \tfrac{1}{2}\,|\partial^2 E_2(\mathbf{r},\zeta)\,/\partial\mathbf{r}\partial\zeta|_{\zeta=\zeta'}\cdot\zeta' = 0. \quad (47)$$

The equilibrium configuration calculated by both methods is equivalent as long as the

condition:

$$|\partial E/\partial \zeta|_r = 0 \qquad (48)$$

is true. The defect formation energies used in this investigation use the force-balance method.

C. Surface Energy Calculations

1. Description of a Surface

The surface of a crystal can be treated as a two dimensional infinite lattice (i.e., periodic) with the third direction normal to the surface treated as a finite lattice. As in the bulk static lattice calculations, the simulation is effectively carried out at 0K. The modeling of the surface does not include the vibrational properties of the crystal since they do not significantly contribute to the energy of the system. The second is that the calculation of the vibrational modes at the surface is extremely difficult. The zero point energy, due to quantum mechanical effects, is also omitted from surface energy calculations. The basis of using these two simplifications is that the energy contributions from vibrational and zero point sources to the surfaces free energy is zero. This approximation has yielded good results.[55,80]

The calculation of the excess energy of the surface block was defined by Stoneham[81] as the following:

E_s = [surface lattice energy] - [bulk lattice energy of the same number of ions].

The surface energy can be then defined as:

$$\gamma = (E_s / \text{Area}) \times 16.021\ JA^2/eVm^2 \qquad (49)$$

where γ is in J/m^2, E_s is in eV and the area is in A^2.

As stated earlier, Tasker developed the idea that there are three types of surfaces for ionic crystals. Type I surfaces have an overall zero charge and consist of both anions and cations in their stoichiometric ratio. Type II surfaces are made up charged layers but the overall repeat unit of the surface lattice has a symmetry such that there is no dipole moment perpendicular to the surface. The lack of a dipole moment perpendicular to the surface allows the surface energy to converge. Type III surfaces are made up of charged layers that

are alternately charged. This causes a dipole moment perpendicular to the surface. When a surface has a dipole moment perpendicular to the surface, the energy diverges and is infinite.[82] Oliver *et al*[83] found that removing half the anions (or cations) and placing them on the bottom of the lattice results in a neutral surface and removes the dipole moment perpendicular to the surface. In other systems, the number of ions placed at the bottom of the lattice does not have to be exactly half as long as the surface configuration results in a zero net dipole moment.

2. Surface Energy Minimization

The code METADISE developed by Watson *et al.,*[84] and supplied by Dr. S.C. Parker, was used to model the surfaces in this study, and thus calculate surface energies. In this approach, the crystal is considered to be composed of a series of charged planes parallel to the surface and periodic in the other two dimensions. The crystal is then divided into two blocks, each of which is divided into two regions, Region I and Region II. This is similar to the two region approach used in defect calculations[77,78] but instead of spherical regions, the regions are slabs of atoms.[84] The ions in Region I are allowed to relax explicitly. Ions in Region II are held fixed at their bulk equilibrium positions. The Region II of both blocks are allowed to move relative to each other as the explicitly relaxing ions within each Region I conceivably can expand or contract. Block I is represented in Figure 2.2. It should be noted that only Block I is used for surface simulations. The top of Block I is the exposed surface of the crystal. Blocks I and II would be used for the modeling of interfaces. It is necessary to include Region II to ensure that ions that lie at the "bottom" of Region I experience the correct potential energy environment.[55]

The code METADISE orients the crystal so that a low Miller index plane is

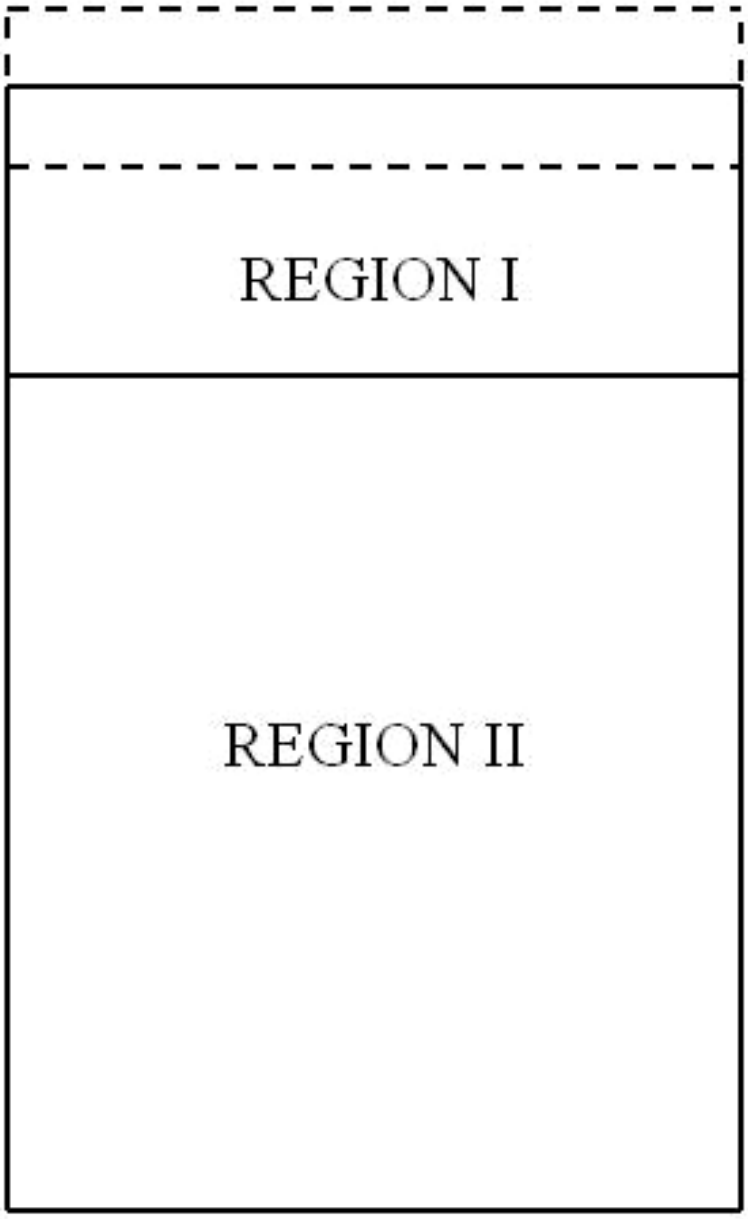

Figure 2.2. Two dimensional representation of Region I and II of Block I.
Dashed lines represent possible expansion or contraction of Region I terminations.

perpendicular to the normal of the surface. The reoriented lattice has its top ion removed, one at a time. At each step, the configuration is considered as a possible termination for the given surface. The dipole moment normal to the surface is calculated. The only termination planes that are accepted are those with a zero dipole moment: for practical purposes, that is those which are less than 1.6×10^{-31} C m. The process is continued until the "bottom" of the lattice is reached. The lattice is then reoriented to a new low Miller index and the process repeated.

Some surfaces of interest have high dipole moments unless surface reconstruction is allowed. The researcher must then remove atoms manually to find surfaces suitable for calculation. In this study, it was necessary to use surface reconstruction to calculate the {001} surface structure in the magnetoplumbite systems.

3. Surface Defect Energy Calculations

The code METADISE uses the code CHAOS to calculate surface defects. The lattice is divided into two regions, Region I and Region II. Region II is divided into two regions, a and b. This is very similar to the set up used for bulk defect calculations. The difference is that in bulk defect calculations the regions are spherical. This is not possible since half the bulk is removed in creating the surface. The regions used in surface defect calculations must then be hemispheres. The interactions between ions in Region I and Region IIa are explicitly calculated as in bulk defect calculations. The dipole created by the surface defect induces dipoles in the rest of the crystal. The ions in Region IIb are treated as a dielectric continuum, also as in bulk defect calculations. The total energy of the system is the same as in equation (33). There are modifications to the bulk defect calculations. The ionic displacements and the energy of the continuum need to be modified to use planar integrals for the surface planes. The energy of Region IIb is given by:

$$E_{IIb} = -(1/2)Q^2(E_{planar} + E_{volume}) \quad (50)$$

where E_{planar} is:

$$E_{planar} = \Sigma_{p \in I,IIa} \Sigma_j q_j M_j \int (r^2 - r^2_p)^{-1} 2\pi r dr \quad (51)$$

with the limits of integration being from ∞ to $(R^2_{IIb} - r^2_p)^{1/2}$. The E_{volume} is expressed as:

$$E_{volume} = \Sigma_j q_j M_j \int (1/r^4) 2\pi r^2 dr$$

(52)where the limit of integration being ∞ to R^2_{IIb}. Q is the total charge of Region I, q_j is the defect charge, M_j is the Mott-Littleton displacement factor, R_{IIb} is the cut-off radius, r_p is the perpendicular distance from the origin to plane p, and r is the distance from the defect.[54]

There is an additional problem when calculating charged defects at the surface. Surfaces cause a discontinuity in the dielectric constant. The charged defect induces an image charge situated half an interplanar distance above the plane containing the defect. The field of the image charge needs to be taken into account when calculating the displacements of ions in Region IIa and the polarization energy in Region IIb. The image charge is given by:

$$q_i = q_{defect} [(\varepsilon_1 - \varepsilon_2) / (\varepsilon_1 + \varepsilon_2)]$$

(53)where ε_1 and ε_2 are the different dielectric constants of the adjoining material. Since surfaces are being examined, ε_2 is equal to the value of free space, that is, unity.

D. Interatomic Potentials

The interatomic potentials used in the short-range interactions can be derived either empirically or non-empirically. The short-range cation-cation interactions are sometimes ignored and only their coulombic interactions are included. This assumption is valid, in most cases, since cations are generally small and thus their "electron clouds" do not overlap.

Empirically derived parameters are those fitted to experimental crystal data. The starting point for the derivation of these parameters is a least-squares fitting of crystallographic data. Those include atomic positions and the dimensions of the unit cell. Other data, such as elastic or dielectric constants and phonon dispersion curves, can also be used to fit the parameters.

One major problem with using empirically derived parameters is that the model will only be valid if the ions are at equilibrium distances when the fitting occurs. Transferring of potentials from one system to another does not ensure an accurate model. Parameters must be tested against experimental values such as elastic and dielectric data for each new system being modeled. The second major problem is the unavailability of experimental data or, in

some cases, inaccurate data.

Non-empirical derivation of short-range potential parameters involves fitting directly to a calculated potential energy surface. The interaction energy is found to be a function of the distance between ions. There are two methods used to calculate the potential parameters.

The electron-gas method was reported by Jensen.[85] In this method the electrons are treated as a degenerate Fermi gas. The Hartree-Fock procedure is used to determine the charge clouds of the separated ions. The electron density of the ions is the sum of these charge clouds.[86] A density functional method is then used to obtain electrostatic and kinetic energies. The exchange and correlation contributions of the total energy are also determined.

The second method of non-empirical fitted of potential parameters is one of the *ab initio* methods. These were generally only used when the electron-gas calculations were inadequate since these methods are very computationally expensive. The use of these techniques are now the norm do to the increase in computational power.

Non-empirical methods for determining the potential parameters are usually valid over a wide range of interatomic separations. The problem is that they generally overestimate the lattice parameters[87] and are more difficult to obtain than the empirically derived parameters. The lack of electron-gas and quantum mechanical non-empirical potentials for some systems makes empirically derived parameters still very useful.

The validity of transferring interatomic potentials from one crystal system to another is something that each researcher must consider. In many cases, the transfer of potentials from one crystal system to another still results in acceptable models. This was the case for using potentials derived by fitting to the rock salt and corundum structural data for use in spinels.[88] Differences in the environment of an ion can make the transfer of potential parameters unacceptable.[70] The crystalline environment can cause large variations in the electronic polarizability, especially in oxides. It is always prudent to check the calculated crystal structure and properties with experimental data to ensure that the transfer of potentials is valid.

The main focus of this study involves calculation of surfaces. The validity of transferring of potentials in this case is of great importance to ensure a valid model of the

surface structure. The potential parameters are fitted to ions in the bulk crystal lattice. However, the surface changes the environment that an ion occupies. The surface relaxation restores the ions as closely as possible to the bulk configuration. The use of bulk potentials on surfaces facilitates this type of relaxation.[26] Electronic structure calculations also show that there is little change in the parameters between a surface and bulk site.[59] This indicates that use of bulk potentials in surface structure calculations is a reasonable assumption.

The non-empirical fitting method cannot be used on the shell parameters since no theoretical methods have yet been developed for their derivation. This means that only empirical fitting to the structure, high and low dielectric constants, and elastic constants can be done at this time. In most cases, fitting to the high and low dielectric constants has been found to be sufficient. The derivation of reliable potential parameters for strongly ionic solids results in accurate models. The reliability decreases as the covalent nature of bonds increases, although for most oxides, the results are still acceptable.

III RESULTS AND DISCUSSION

A. Crystal Potentials and Structures

Interatomic potential parameters used for the calcium, strontium, and barium hexa-aluminates are given in Tables V and VI. These potential parameters were developed by Park and Cormack.[17] The Mn^{2+} and Mn^{3+} potentials were those derived by Lewis and Catlow.[89] One feature of these models is the use of two different potential parameters for Al^{3+}. The different coordination of the Al^{3+} ions has been accounted for included by modifying the potential parameters, using the Huggins-Mayer relationship:

$$A = b \exp[r_o / \rho]$$

(54)where r_o is the equilibrium separation, b is the Goldschnidt correction factor, and ρ represents the hardness of the ion. The difference between the equilibrium radii for the two coordinations is given by Δr. The relationship then becomes:

$$A_{tetra} = A_{octa} \exp[\Delta r/\rho]. \quad (55)$$

The Goldschmidt correction factor for Al^{3+} changing from octahedral to tetrahedral coordination is 0.94. The difference in radii for this change is thus $0.06r_{octa}$. It should be noted that the anion radius is taken as a constant. The potential parameter correction factor for tetrahedrally coordinated Al^{3+} ions was used for all models in the potential. The Al^{3+} ions use the octahedral potentials for all sites other than the tetrahedral sites. The use of the two potential parameters for Al^{3+} is essential for these models to predict the expected phase stability.[17]

The calcium magnetoplumbite structure is shown in Figure 3.1, and the strontium magnetoplumbite structure is shown in Figure 3.2. The theoretical barium magnetoplumbite structure can be seen in Figure 3.3. Figure 3.4 and 3.5 show the structures of the Ba-poor barium β(I)-alumina and the Ba-rich barium β(II)-alumina, respectively. The main features of these structures were described in Section IB of this work.

Table V. Interatomic Potential Parameters for Ca^{2+}, Sr^{2+}, Ba^{2+}, Mg^{2+}, Mn^{2+}, Al^{3+}, Mn^{3+}, and O^{2-}

Interation	A (eV)	ρ (A)	C (eV A^{-6})
Ca^{2+} - O^{2-}	1228.90	0.33700	0.00
Sr^{2+} - O^{2-}	1400.00	0.35000	0.00
Ba^{2+} - O^{2-}	931.70	0.39490	0.00
Al^{3+}_{tetra} - O^{2-}	1334.31	0.30059	0.00
Al^{3+}_{octa} - O^{2-}	1474.40	0.30059	0.00
Mg^{2+} - O^{2-}	821.60	0.32420	0.00
Mn^{2+}- O^{2-}	715.80	0.34640	0.00
Mn^{3+}- O^{2-}	1257.90	0.32140	0.00
O^{2-} - O^{2-}	22764.20	0.14910	17.89

Table VI. Shell Model Parameters for Ca^{2+}, Sr^{2+}, Ba^{2+}, Mn^{2+}, and O^{2-}

Interaction	Shell Charge Y (e)	Spring Constant k (eV A^{-2})
Ca^{2+}(core) - Ca^{2+}(shell)	1.260	34.00
Sr^{2+}(core) - Sr^{2+}(shell)	1.330	21.53
Ba^{2+}(core) - Ba^{2+}(shell)	1.460	14.78
Mn^{2+} (core) - Mn^{2+} (shell)	3.000	81.20
O^{2-}(core) - O^{2-}(shell)	-2.207	27.29

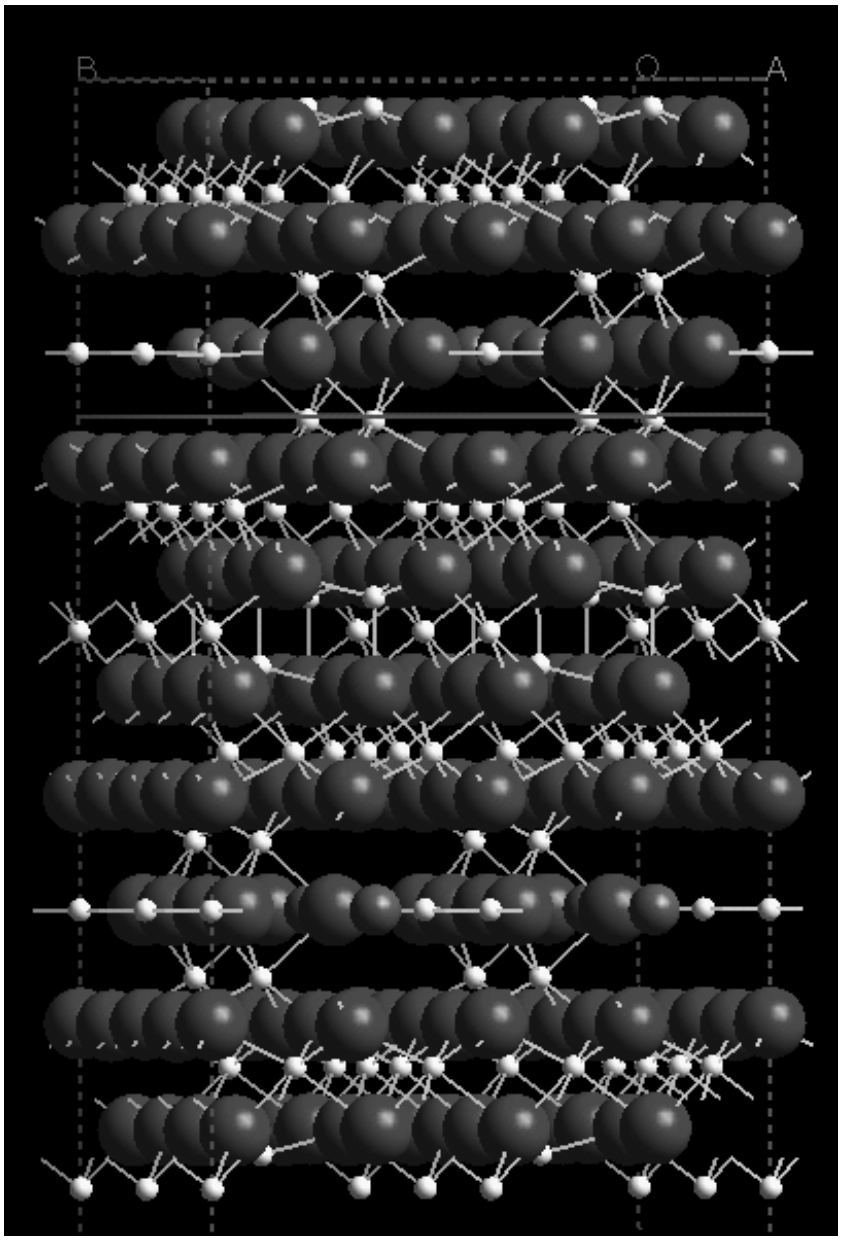

Figure 3.1. Calcium magnetoplumbite crystal structure.
Ions are color coded as follows: red - O^{2-}, white - Al^{3+}, and green - Ca^{2+}. The blue line represents the {001} lowest energy termination plane.

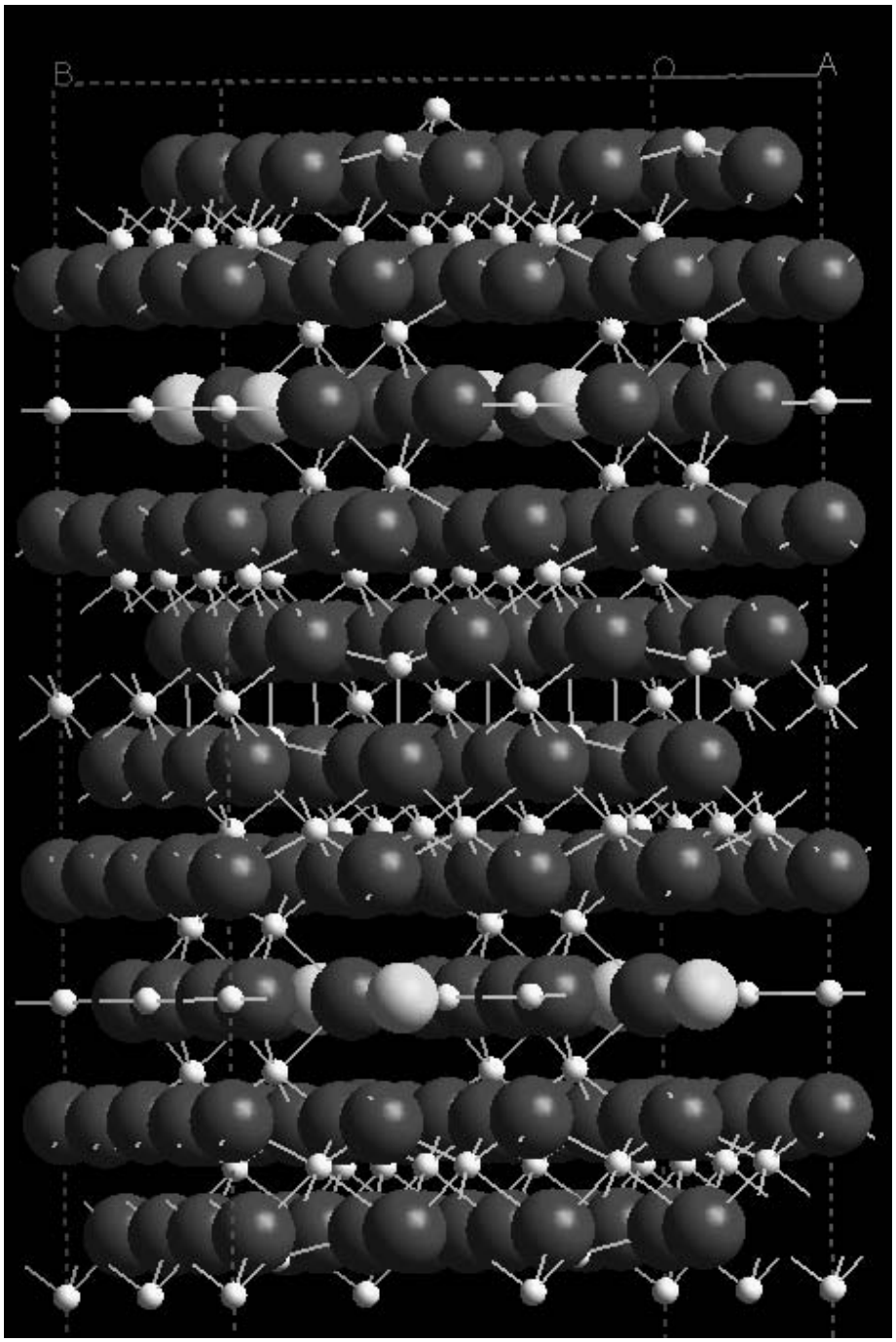

Figure 3.2. Strontium magnetoplumbite crystal structure.
Ions are color coded as follows: red - O^{2-}, white - Al^{3+}, and yellow - Sr^{2+}.

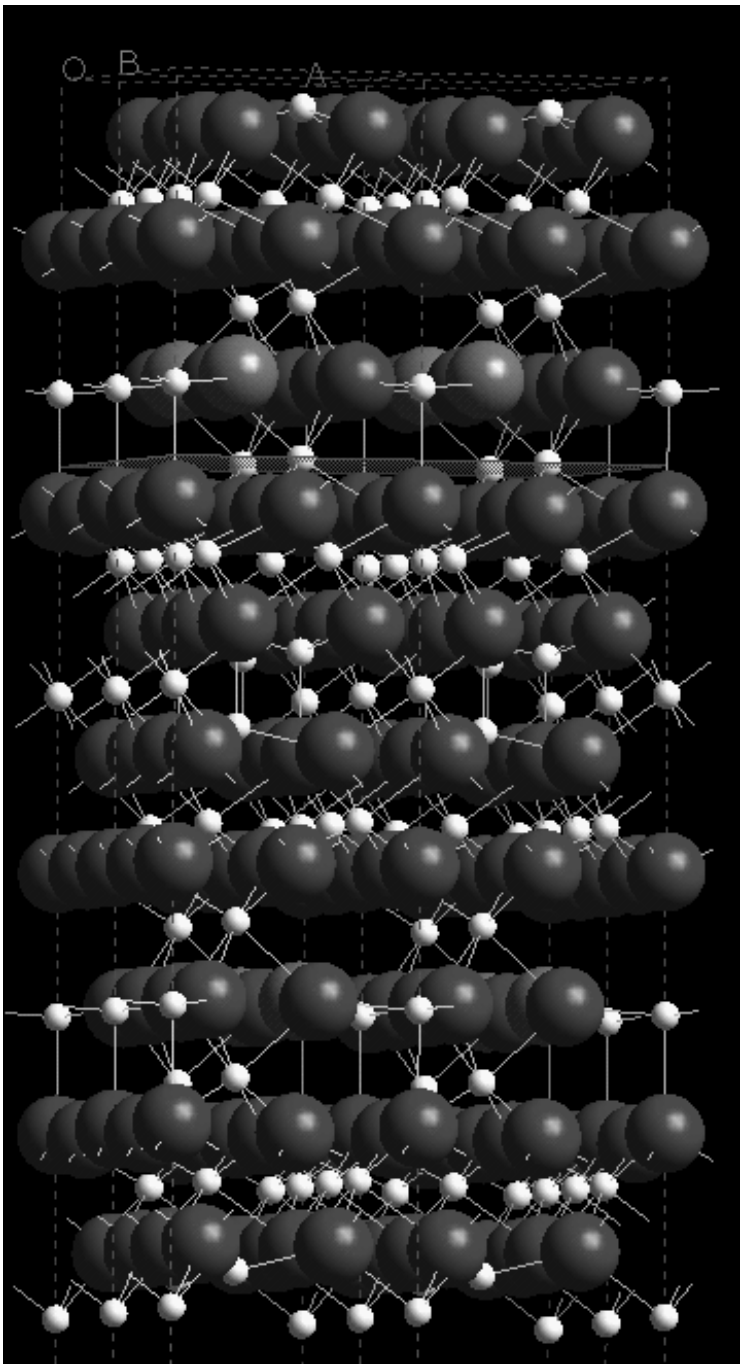

Figure 3.3. Barium magnetoplumbite crystal structure.
Ions are color coded as follows: red - O^{2-}, white - Al^{3+}, and blue - Ba^{2+}.
The blue line shows O^{2-} rumpling and the {001} lowest energy termination plane.

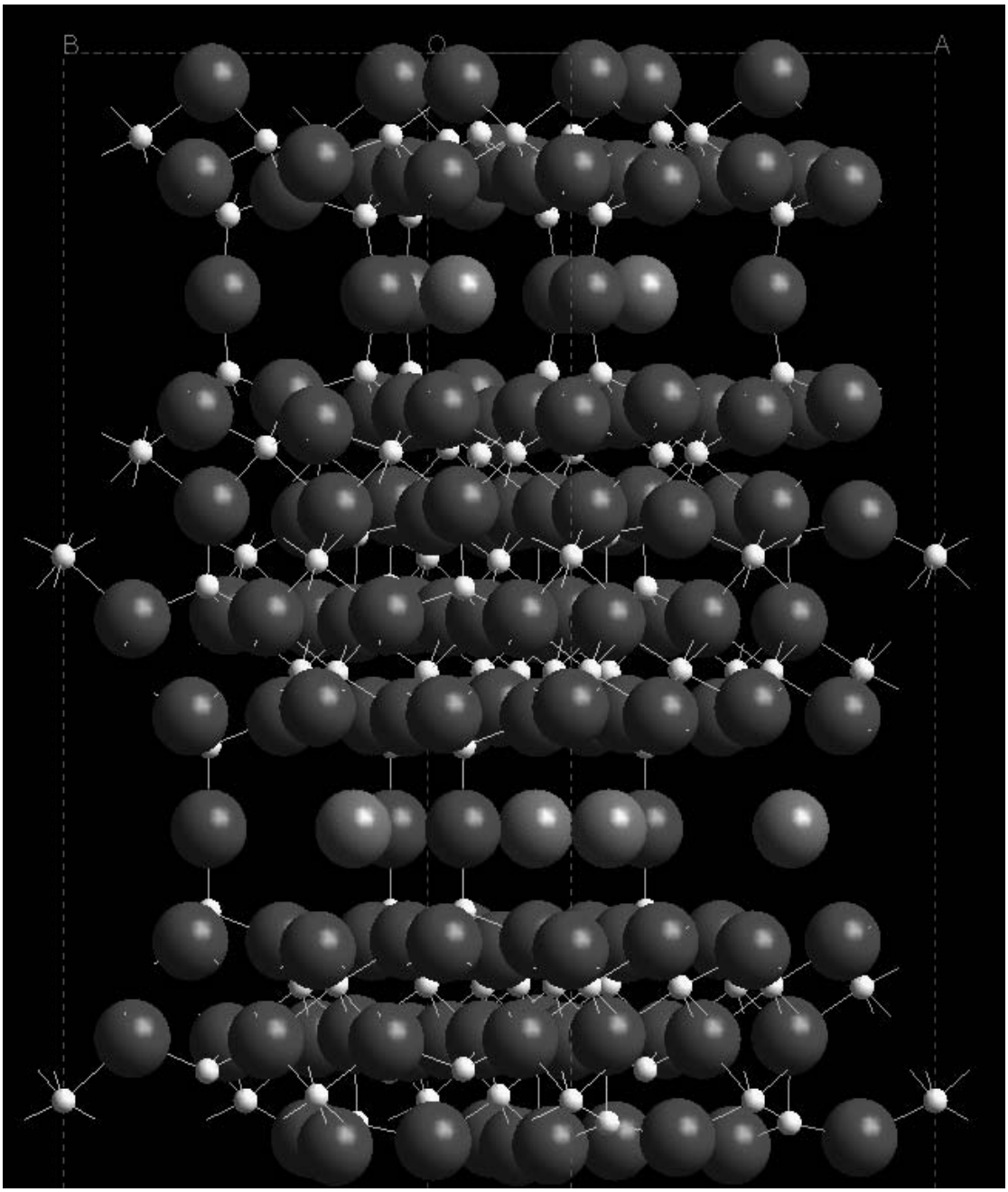

Figure 3.4. Barium β(I)-alumina crystal structure.
Ions are color coded as follows: red - O^{2-}, white - Al^{3+}, and blue - Ba^{2+}.

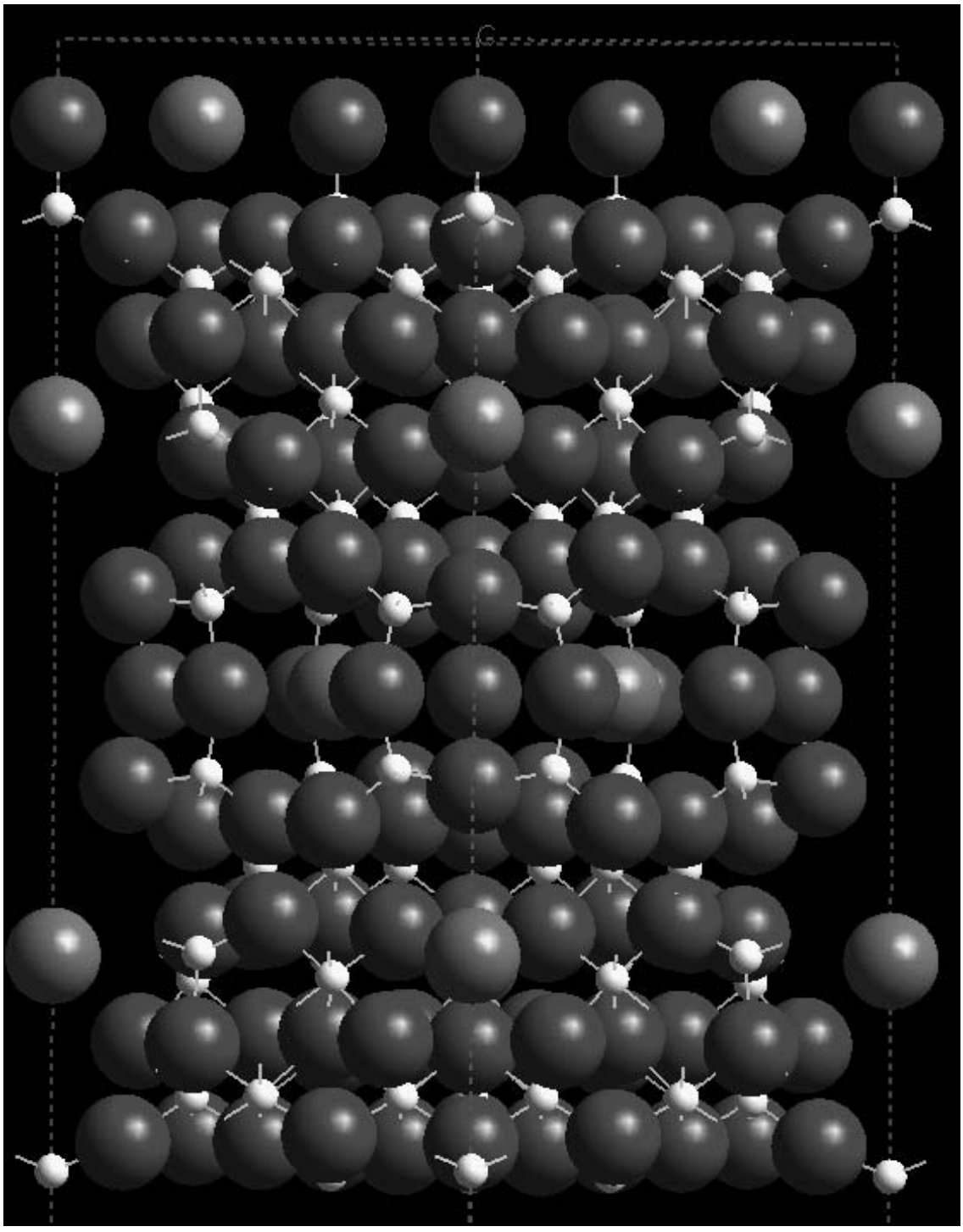

Figure 3.5. Barium β(II)-alumina crystal structure.
Ions are color coded as follows: red - O^{2-}, white - Al^{3+}, and blue - Ba^{2+}.

B. Effect of Chemistry and Structure on Dipole Momement

The surface energy of different crystals depends on the crystal face, crystal structure, and on the chemistry of the crystal. The {001} surfaces of NaCl have the lowest surface energy resulting in its cubic crystal shape.[55] The {001} surfaces of alumina have the lowest surface energy resulting in sometimes resulting in a platey morphology.[59] The different geometries of crystals, such as the cubic structure of NaCl and the platey nature of alumina, depend on the crystal structure. It should be noted that processing conditions can also influence crystal morphology, due to reaction kinetics and the relative location of the nucleation sites. MgO is isostructural with NaCl. The surface energies of their {001} faces have the same relative value compared with their other surfaces. The crystal shape is identical, but their measured surface energy values are different.[83] The chemistry of the structure does influence the surface energy values.

Calcium and strontium magnetoplumbite are isostructural. Barium magnetoplumbite, due to the rumpling of the oxygen layers surrounding the mirror plane, has a different space group than the calcium and strontium magnetoplumbites. This causes the barium magnetoplumbite to be thermodynamically unstable. The barium magnetoplumbite structure is therefore a theoretical structure. The surface energies for each of these crystals are thus not expected to be identical. However, it is expected that they will all have similar crystal geometries, with the possible exception of the theoretical barium magnetoplumbite system due to its lower symmetry. Even with this difference, it was expected that the lowest energy surface for each system would be the {001} basal plane due to experimental observations thus obtaining a platey geometry for each system.[90,91]

Both high aspect ratio platey and rod shaped crystals have been found experimentally for the calcium and strontium magnetoplumbite systems.[90,91] The suppression of grain growth of the {001} surface, which results in the rod-like morphology, is due to the rate limiting diffusion of the divalent cation.[90,92] Barium hexa-aluminate, which forms barium β(I)-alumina and barium β(II)-alumina, crystallizes into high aspect ratio platey crystals.[91,93,94] The ultimate morphology of the crystals depends on the method by which they are prepared. When reaction kinetics are not a factor in grain growth, each of these systems forms plately

crystals indicating that the {001} surface possesses the lowest surface energy. The results presented here agree with the expected crystal geometries. Both the chemistry and structure affects the calculated surface energies.

In determining the surface energies, as stated earlier, the first step is to find termination planes that have low dipole moments perpendicular to the surface. When this was done for the magnetoplumbite structures, the {001} basal plane was noticeably missing. Manual constructions of these termination planes were needed to model accurately the crystal's shape. This result was not completely unexpected since work on the basal plane of alumina showed large amounts of rumpling of the oxygen layer.[59] This indicated that the dipole moment was reduced by surface relaxations.

One result found in searching for low dipole termination planes was that the space group affects the number of low dipole moment termination planes for a given surface orientation. The first indication of the space group affecting the number of termination planes was the difference seen between the calcium and barium magnetoplumbite structures. This is due to the lower symmetry of the theoretical barium magnetoplumbite crystal. Calcium magnetoplumbite has one termination plane when the crystal is oriented to model the {012} surfaces. This low dipole termination plane is also present in the strontium magnetoplumbite structure. The {012} planes are notably absent from the barium magnetoplumbite calculations. The lowering of symmetry in the barium magnetoplumbite lattice was not expected to have such a significant affect on the geometry of the crystal, since the experimentally found crystal geometries were similar for the calcium and strontium magnetoplumbite and the barium β-aluminas. The calculated surface energies result in similar crystal geometries. The differences in the calculated results would be difficult to detect experimentally since any changes in crystal geometry would be rather minor due to the predominance of the {001} surface in these systems. The number of termination planes for the surfaces of each structure is given in Table VII. The calculated surface energies indicate that the resultant crystal morphologies would be plate-like. The lowering of symmetry for the barium magnetoplumbite structure appears to reduce the number of low dipole termination planes for the {012} and the {122} orientations. On the other hand,

increases can be seen for

Table VII. Number of Termination Planes per Symmetrically Equivalent Orientations for Calcium, Strontium, and Barium Magnetoplumbite

Surface	Calcium	Strontium	Barium
{100}	6	6	6
{110}	6	6	9
{120}	7	7	7
{112}	1	4	5
{012}	2	2	0
{122}	6	6	5

the {110} and {112} orientations.

It was found that the chemistry of the crystal also affects the number of termination planes. These results would not change the basic crystal geometries. The calcium and strontium magnetoplumbite have different numbers of termination planes for the {112} orientation. This is presumably due to the larger size of the Sr^{2+} ions which increases the unit cell size. Since the difference in size of these two cations is small, there is only two orientations where the larger cation, thus larger unit cell, increases the number of low dipole moment surfaces. The increases seen for the {110} and {112} orientations in the barium magnetoplumbite structure are also due to the larger size of the Ba^{2+} cation.

C. Calcium Magnetoplumbite Surfaces

1. Low Dipole Surfaces

The calcium magnetoplumbite system had over 120 low dipole and reconstructed {001} terminations that were modeled. The majority of the surface energy calculations were done on planes that initially have low dipole moments normal to the surface, i.e. termination planes generated by METADISE. Surfaces with non-zero dipole moments are expected to have divergent surface energies. The equilibrium positions of the atoms are based on the coordination of each atom within the system. The termination of the bulk leaves the surface atoms in lower coordinated positions (i.e. unsatisfied bonds). These unsatisfied bonds increase the potential energy of the atom's position.

Since the relaxation of the surface block also includes atoms that lie further into the bulk than those that occupy the top-most positions, their relaxation also influences how the surface atoms relax. The depth of the relaxed atomic positions for the divalent cation can greatly influence the surface energy as seen in the {100} surfaces.

2. {100} Surfaces

The {100} family of surfaces had 18 termination planes that exhibited low dipole moments. There were six terminations for each of the symmetrically equivalent (100), (010),

and (1_0) orientations. Table VIII includes the depth and relaxed surface energy of each of the modeled planes. Figure 3.6, oriented so that the c-axis is normal to the paper, shows the location of the termination planes for the {100} surfaces. Figures 3.7 and 3.8 show the {100} unrelaxed and relaxed surfaces, respectively. The relaxed depth of the divalent Ca^{2+} ions appears to be the dominant factor in the calculated relaxed surface energies.

In these surfaces, the Ca^{2+} ions prefer positions that leave them exposed. The large divalent Ca^{2+} cation has a smaller field strength than that of the smaller and higher charged Al^{3+} ions. The surface Al^{3+} ions have lower coordination numbers than the bulk Al^{3+} ions with their neighboring O^{2-} ions. The bulk Al^{3+} ions also have lower coordination numbers than the bulk Ca^{2+} ions with their neighboring O^{2-} ions. The loss of a single bonding O^{2-} ion increases the potential of the surface site for the Al^{3+} more than the loss of a single bonding O^{2-} ion does for the higher coordinated Ca^{2+} ion. Another factor in exposing the Ca^{2+} is based on size alone. The larger size of the Ca^{2+} ion does not allow for as much relaxation to occur when its position is not on the immediate surface. Al^{3+} relaxations are easier to accommodate in the lower positions of the surface block. The lower coordination of an exposed Ca^{2+} ion in a relaxed surface structure is not as critical as it would be for an exposed Al^{3+} ion. An exposed position on the surface for the Ca^{2+} includes the benefits of both cases. A third factor is the polarizability of the Ca^{2+} ion. The shell of the Ca^{2+} can relax more than the core of the Ca^{2+} ion. Dipole moments normal to the surface can be reduced by relaxation of the Ca^{2+} shell. The lowest energy surfaces for these planes have two exposed Ca^{2+} ions.

However, the coordination of the Ca^{2+} ion, although not as critical for the Al^{3+} ions, does play a role in the calculated surface energies and cannot be overlooked in examination of the results. The sixth termination plane for the (100), (010), and (1_0) orientations would be expected to have the second lowest surface energy configuration, if Ca^{2+} ion depth alone determined surface energies. This is not the case. The Ca^{2+} ions are exposed to the surface but their coordination is low enough that their positions cause a large increase in their site potentials, effectively eliminating the benefit of the lowering of energy due to the lower cation depth.

Table VIII. {100} Surface of Calcium Magnetoplumbite: Ca^{2+} Depth vs Surface Energy

Termination	(010)		(100)		(1_0)	
	γ (J/m^2)	Ca^{2+} Depth (A)	γ (J/m^2)	Ca^{2+} Depth (A)	γ (J/m^2)	Ca^{2+} Depth (A)
1st	2.780	2.59	3.16	3.06	3.23	2.86
2nd	2.93	2.29	2.86	1.98	5.44	2.19
3rd	2.91	2.26	2.73	2.32	2.91	2.26
4th	2.74	1.39	2.59	1.45	2.68	1.46
5th	2.39	0.65	2.39	0.65	2.58	0.66
6th	2.76	0.83	3.24	0.81	2.92	0.91

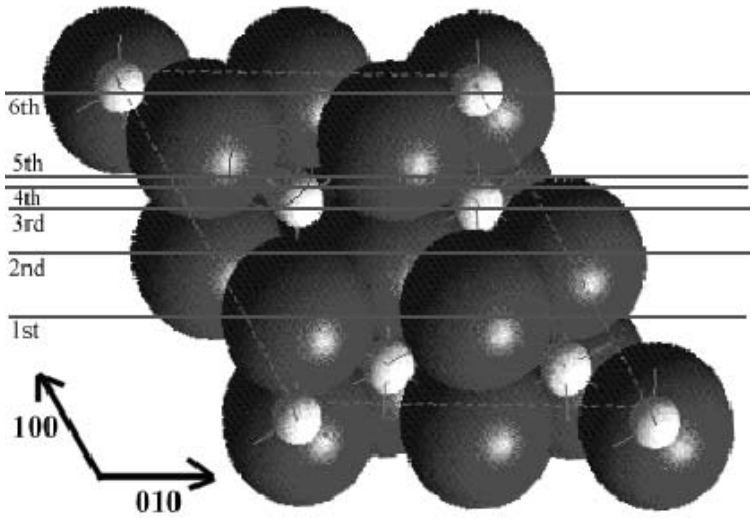

Figure 3.6. Location of terminations for the {100} magnetoplumbite surfaces.
The red atoms are oxygen, the white spheres are the aluminum atoms, and the blue circles are the positions of the divalent cations further down the c-axis. The c-axis is parallel to the normal to the paper. The blue lines represent the termination planes with the {100} exposed surface aligned so that the normal to the surface is pointing toward the bottom of the page.

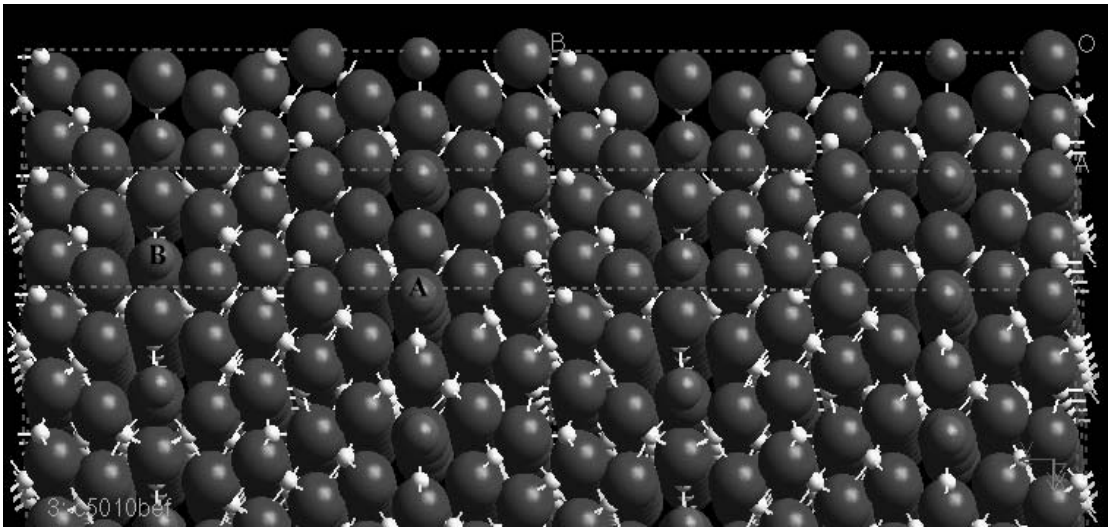

Figure 3.7. Unrelaxed {100} surface of calcium magnetoplumbite.
Ions are color coded as follows: red - O^{2-}, white - Al^{3+}, and green - Ca^{2+}. Surface image is of four blocks of unit cells of the modeled surface area. A is the top Ca^{2+} ion and B is the second Ca^{2+} ion.

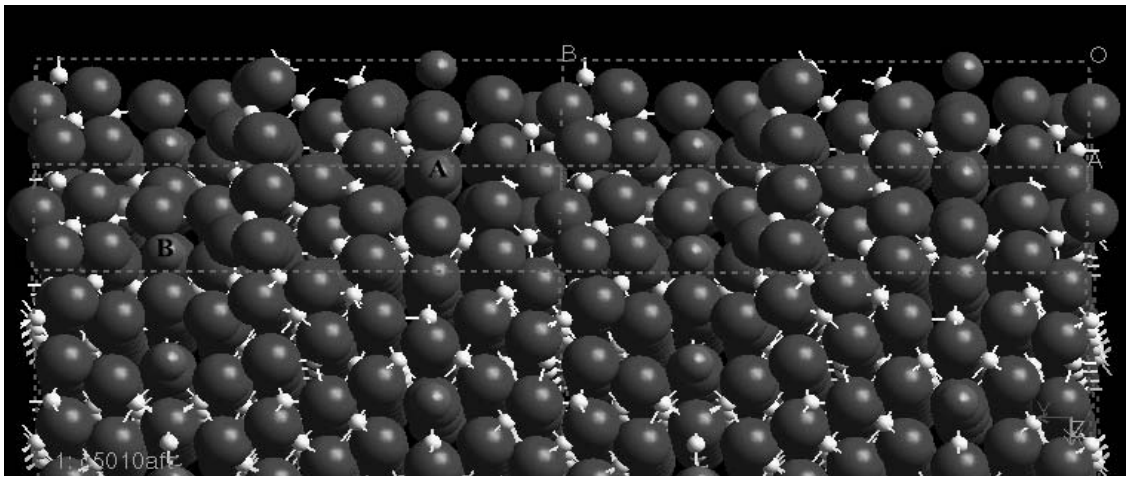

Figure 3.8. Relaxed {100} surface of calcium magnetoplumbite.
Ions are color coded as follows: red - O^{2-}, white - Al^{3+}, and green - Ca^{2+}. Surface image is of four blocks of unit cells of the modeled surface area. A is the top Ca^{2+} ion and B is the second Ca^{2+} ion.

One problem that should be evident upon examination of the calculated surface

energies is the lowest surface energy plane of the (1_0) surface. Although it was expected to have the same surface energy, due to symmetry of the lattice, as the other lowest energy planes of the (100) and (010) surfaces, its calculated value is higher. Two possibilities have been considered for this discrepancy. The first is that when the lattice is oriented to perform the calculation, rounding errors, inherent to the system being hexagonal and possible computer data storage errors, produce a surface that does not have exactly the same starting configuration. The surface lattice parameters are slightly different. The initial configuration for the (1_0) surface then relaxed to a metastable equilibrium configuration that has a higher surface energy.

The second possible explanation for the higher surface energy calculated for the (1_0) surface is that the "opposite" side of the lattice was modeled. The cleaving of a crystal causes two newly formed surfaces. This would suggest that the (100) surface is one of the newly created surfaces while the (1_0) is the second newly created surface. Since the calculated surface structure and energies of the (010) and (100) surfaces are identical, these should be the same newly created surface.

This possibility would require that the symmetry of the system was such that opposite sides of the newly created surfaces would relax differently. The dipole moments of the unrelaxed surfaces would seem to support this explanation. The (100) and (010) surfaces have a different sign for the calculated dipole moments normal to the surfaces than that of the (1_0) surface.

However, examination of other surfaces within the calcium magnetoplumbite lattice and the {100} family of surface of the strontium and barium magnetoplumbite lattices does not support this conclusion. The symmetry of the system also does not lend itself well to this hypothesis. The symmetry of the planes being modeled indicates that the (1_0) surface should still relax to the same equilibrium position and thus the same surface energy. Although this possibility is not without its merits, it is most likely that the starting configurations are so significantly different that a metastable structure for the (1_0) surface was found. The nearly zero values of the dipole moments normal to the surface make the difference in sign more likely due to slight differences in starting configurations that do not

have any real physical meaning.

The difference of the surface block energy between the (100) surface and the (1_0) surface is 1.45 eV. The repulsive energy in the (1_0) surface was found to be higher. This leads to the conclusion that in this configuration, atoms hinder relaxation of their neighbors resulting in a metastable configuration. In a real crystal, the area of the (1_0) surface would be identical to those of the symmetrically equivalent (100) and (010) surfaces. The calculated metastable surface would then relax to the equilibrium structure arrived at for the (100) and (010) surfaces.

This leads to two new questions that arise while performing these types of calculations. The difference in sign for the calculated dipole moment was troubling at first, if the break down of symmetry is not responsible for the difference in energies. The explanation for this most likely lies in the way the reoriented lattice is constructed. Since the dipoles calculated are essentially zero (on the order of 10^{-36} C m), a small change in the initial configuration of even a single ion could result in a change in sign of the calculated dipole.

The second question is whether a metastable equilibrium configuration has indeed been reached, instead of the global minimum. The starting configurations of the other two orientations, (100) and (010), also do not have identical configurations but yet they both relax to very nearly identical configurations. This is a very strong indication that it is the global minimum. Caution should thus be exercised when examining these results. It is possible that global minima are not reached for a given set of planes. The best indication that the global minima has been reached is by examining all the symmetrically equivalent surfaces. In the case of the {100} surfaces, two of the three sets of orientations relax to the same configuration and lowest energy which should be satisfactory to conclude that the global minima has been reached in those cases. The third orientation is a metastable equilibrium configuration caused by errors in the rotation of the lattice.

3. Other Low Dipole Surfaces

Table IX contains the calculated relaxed surface energies of the calcium

Table IX. Relaxed Surface Energies of Calcium Magnetoplumbite

Surface	γ (J/m^2)
{100}	2.39
{110}	2.64
{120}	2.74
{012}	2.31
{112}	3.08
{122}	2.67

magnetoplumbite system. Only the lowest relaxed surface energy planes of symmetrically equivalent surfaces have been included. One feature common to all of these surfaces is that the Al^{3+} ions relax into the surface structure. Only the Al^{3+} ions coordinated with O^{2-} ions that have relaxed to positions above the original surface are exposed. In most cases, the Ca^{2+} ion is exposed or close enough to the surface in their initial configuration to relax to an exposed position. The area of exposed surface per unit cell is also larger than for the {100} surfaces.

Dangling O^{2-} ions are considered to be ions that have relaxed to positions above the unrelaxed surface plane. These O^{2-} ions are associated with higher surface energies. The O^{2-} ions in these dangling positions increase the potential energy of the surface and lead to their relatively higher surface energies.

The {110} surface, shown in Figure 3.9, has two exposed Ca^{2+} ions (A and B). An O^{2-} ion (C) has relaxed to a position above the final surface but not above the unrelaxed surface. The first Ca^{2+} ion (A) is coordinated with the raised O^{2-} ion, which also has two neighboring Al^{3+} ions. The coordination of the O^{2-} ion with these cations partially satisfies its bonds; therefore, its position is stabilized. The first Ca^{2+} position is stabilized by the raised O^{2-} ion. The second Ca^{2+} ion (B) is situated in a highly coordinated position, coordinated with six O^{2-} ions on the same plane. The {110} surface has the third lowest surface energy of the low dipole surfaces. The stabilization of the raised O^{2-} ion probably decreases the surface energy as does the exposure of the two Ca^{2+} ions.

The {120} surface, see Figure 3.10, has two dangling O^{2-} ions, one (A) of which is coordinated with two Al^{3+} ions, the other (B) being coordinated by two Al^{3+} ions and a Ca^{2+} ion. This surface also has three exposed Ca^{2+} ions. The calculated surface energy is higher than that of the {110} surface. Each of the exposed Ca^{2+} ions is coordinated with four O^{2-} ions. Even though there are three exposed Ca^{2+} ions, the lack of a Ca^{2+} ion near the second dangling O^{2-} increases its site potential and thus the surface energy, compared to the {110} surface.

The lowest surface energy of low dipole surfaces of the calcium magnetoplumbite system is the {012} orientation, see Figure 3.11. This surface only has one exposed Ca^{2+} ion.

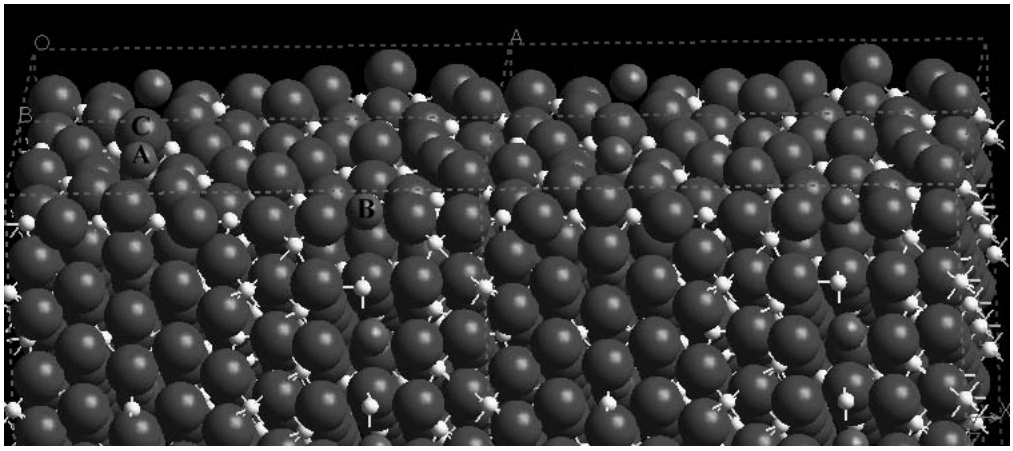

Figure 3.9. Relaxed {110} surface of calcium magnetoplumbite.
Ions are color coded as follows: red - O^{2-}, white - Al^{3+}, and green - Ca^{2+}. Surface image is of four blocks of unit cells of the modeled surface area. The Ca^{2+} ion (A) is coordinated with the O^{2-} ion (C) relaxed to a position above the original surface. The Ca^{2+} ion (B) is coordinated with six O^{2-} ions.

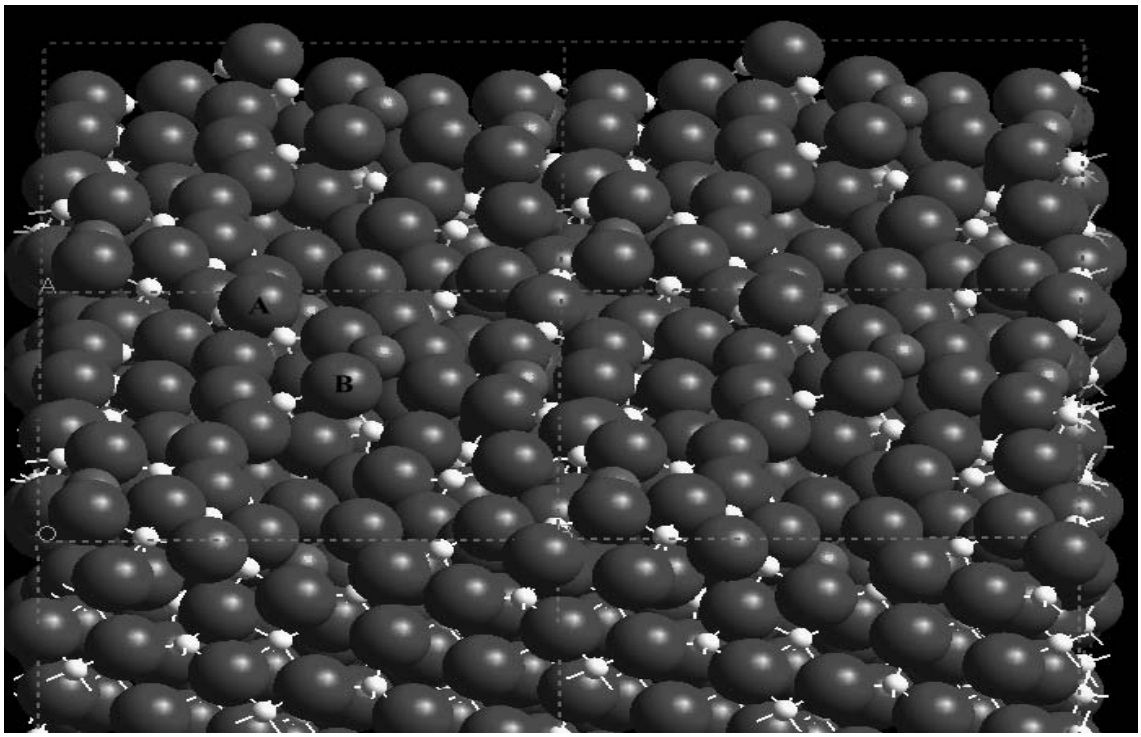

Figure 3.10. Relaxed {120} surface of calcium magnetoplumbite.
Ions are color coded as follows: red - O^{2-}, white - Al^{3+}, and green - Ca^{2+}. Surface image is of four blocks of unit cells of the modeled surface area. Dangling O^{2-} ion (A) is coordinated with a two Al^{3+} ions. Dangling O^{2-} ion (B) is coordinated with two Al^{3+} and one Ca^{2+} ion.

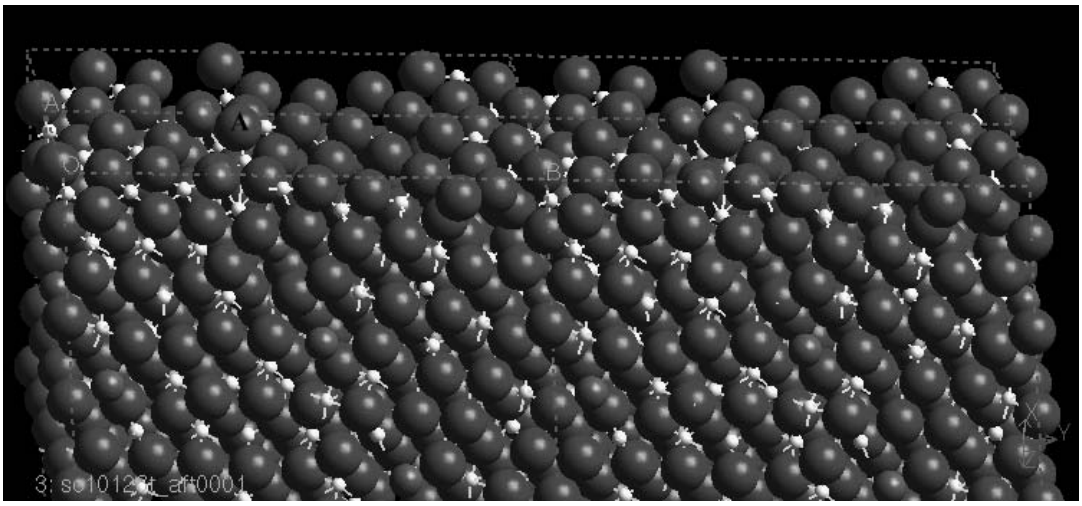

Figure 3.11. Relaxed {012} surface of calcium magnetoplumbite.
Ions are color coded as follows: red - O^{2-}, white - Al^{3+}, and green - Ca^{2+}. Surface image is of four blocks of unit cells of the modeled surface area. Ion A is a dangling O^{2-} ion coordinated with one Ca^{2+} and three Al^{3+} ions.

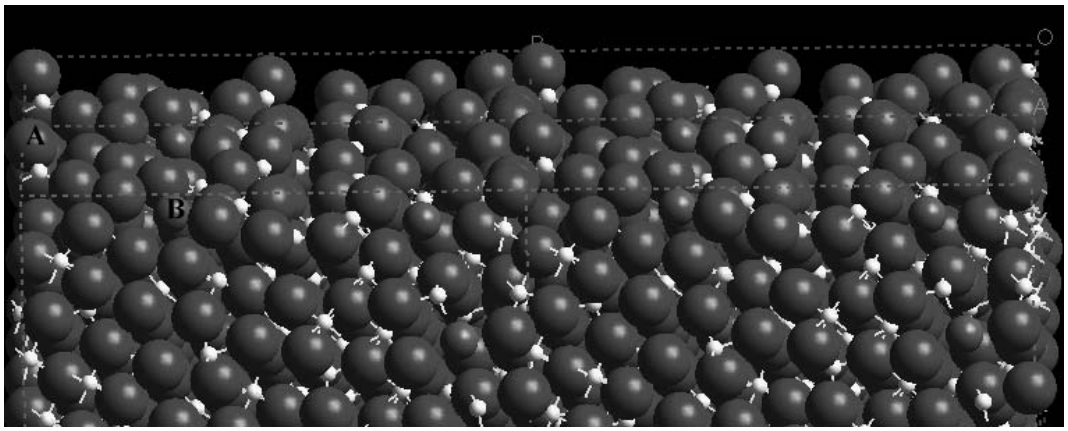

Figure 3.12. Relaxed {112} surface of calcium magnetoplumbite.
Ions are color coded as follows: red - O^{2-}, white - Al^{3+}, and green - Ca^{2+}. Surface image is of four blocks of unit cells of the modeled surface area. The O^{2-} ion (A) has relaxed to a position above the original surface. The Ca^{2+} ion (B) occupies an exposed position.

There is a dangling O^{2-} ion (A) which has a neighboring Ca^{2+} and three Al^{3+} ions. One would expect a higher surface energy than that calculated, due to the dangling O^{2-} ion and only one exposed Ca^{2+} ion. The explanation for this surface having such a relatively low surface energy is that there are three, instead of two, Al^{3+} ions coordinated with the dangling O^{2-} ion. The long and short-range potential, ignoring the polarization energy, between the three Al^{3+} ions and the dangling O^{2-} ion is -6.09 eV. Calculating the potential with only two Al^{3+} ions, based on the average distance of the three Al^{3+} ions, results in the higher potential of -4.06 eV. The addition of the third Al^{3+} ion further stabilizes the O^{2-} ion, so that the overall surface energy of this configuration is lower than those of the other low dipole surfaces.

The {112} surface, see Figure 3.12, has one dangling O^{2-} ion (A) and one exposed Ca^{2+} ion (B). The dangling O^{2-} ions is coordinated with two Al^{3+} ions. The combination of a dangling O^{2-} ion coordinated with only two Al^{3+} ions and one exposed Ca^{2+} ions leads to the high surface energy of this surface.

There are three dangling O^{2-} ions in the relaxed {122} surface, seen in Figure 3.13. There are two exposed Ca^{2+} ions. The first Ca^{2+} ion (A) has also relaxed to a position above the unrelaxed surface. There are three closely neighboring O^{2-} ions which act to stabilize the Ca^{2+} ion's (A) position. Two of the dangling O^{2-} ions (B and C) are stabilized by two neighboring Al^{3+} ions. The third (D) has both an Al^{3+} and a Ca^{2+} ion acting as stabilizers. The calculated lower surface energy for the {112} than the {120} surface is interesting because of the greater number of dangling O^{2-} ions and the lower number of exposed Ca^{2+} ions in the {112} surface. Examination of the calculated results shows that the repulsive energy term is higher in the {120} surface than the {122} surface. The smaller size of the surface area per unit cell of the {120} surface, 321.7 A^2, causes neighboring O^{2-} ions to relax to positions where the repulsive energy is higher than in the larger, 326.4 A^2, {122} surface.

These surfaces do not appear to be as sensitive to the number of Ca^{2+} being in an exposed surface position as they are in the {100} surfaces. The orientation of the crystal is such that the size of non-exposed Ca^{2+} ions does not hinder the relaxation in the mirror plane. The more important factor in determining the lowest surface energy is then the coordination of the exposed atoms and the relative amount of repulsion between neighboring

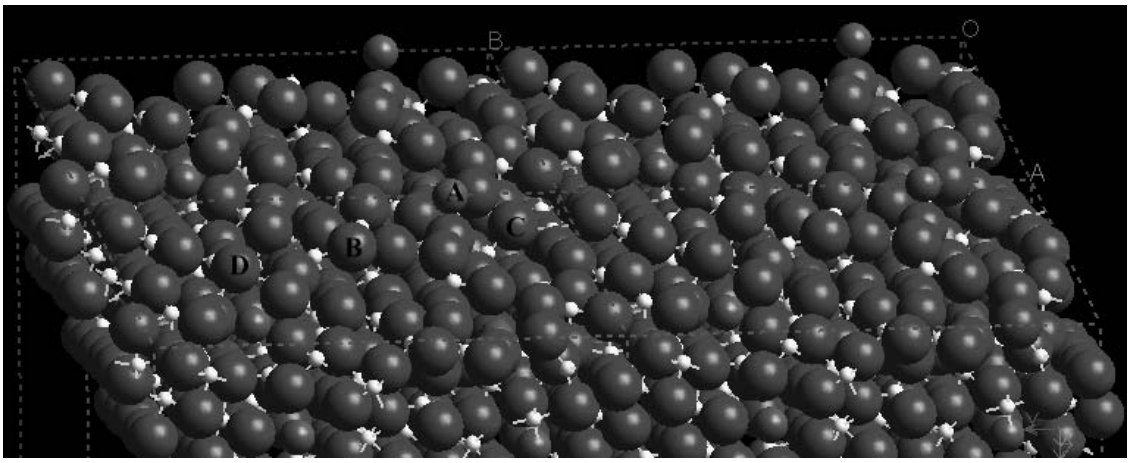

Figure 3.13. Relaxed {122} surface of calcium magnetoplumbite.
Ions are color coded as follows: red - O^{2-}, white - Al^{3+}, and green - Ca^{2+}. Surface image is of four blocks of unit cells of the modeled surface area. The Ca^{2+} ion (A) has relaxed to a position above the original surface. The dangling O^{2-} ions (B and C) are each coordinated with two Al^{3+} ions. The dangling Ca^{2+} ion (A) and an Al^{3+} ion are coordinated to the third dangling O^{2-} ion (D).

ions.

4. The {001} Surface

The calculated relaxed energies of the {001} terminations are given in Table X. It had been expected that the basal {001} plane would have the lowest surface energy due to observed fracture characteristics and crystal morphology. However, the lack of a set of low dipole moment terminations required that planes within this surface be manually constructed. The first attempt at determining the surface energy of the (001) surface used the "top" of the unit cell, as seen as the blue plane in Figure 3.1, as a starting point. This corresponds to a position within the spinel block. However, relaxed surface energy calculated, 7.03 J/m^2, was much higher than minimum energy surfaces of all the other orientations. The possible surface configurations were limited by the number of Al^{3+} ions needed on this plane in order to maintain charge neutrality.

The second location within the lattice that was examined was the mirror plane containing the calcium, oxygen and corner aluminum ions. The mirror plane was chosen because of the success of finding low energies for other surfaces that had the Ca^{2+} ion exposed. The calculated surface energy for this termination was still significantly higher than the other calculated surface orientations.

These first attempts yielded much higher surface energies than the other surfaces, indicating that another approach was necessary since experimental evidence indicated that the {001} surface has the lowest surface energy.[91] The charge neutrality requirement limited the available configurations of the surface. Surface reconstruction has been seen frequently in other systems, notably, the structurally related alumina system and metals.[67,95] The use of supercells allows for more configurations to be constructed while maintaining surface charge neutrality. A 2x2 supercell was used to model the (001) surface with a termination plane in the mid-spinel block. Several configurations were modeled. The calculated surface energy of 3.37 J/m^2 was still higher than all other surfaces in the calcium magnetoplumbite system, still in contrast to the expectations from experimental observations.[91] This indicated that the close packed intra-spinel O^{2-} plane was not the ideal

staring configuration. The construction

Table X. Surface Energies of the Relaxed Calcium Magnetoplumbite {001} Sufaces

Surface (2x2 unless noted)	γ (J/m^2)
Mid-Spinel Block (1x1)	7.03
Mid-Spinel Block	3.37
Mirror Configuration I	3.03
Mirror Configuration II	2.89
O^{2-} - Al^{3+} Layer Beneath Mirror Plane	1.96

of 2x2 supercell models with the mirror plane termination resulted in two configurations that had lower energies than those in the mid-spinel block. The lowest calculated surface energy for the mirror plane termination was 2.89 J/m^2. This value was still much higher than would be necessary for a platelet crystal morphology since surface energy of most other orientations was lower.

Later calculations on other systems, specifically the barium β(I)-alumina, indicated that there was another (001) termination plane that might yield a lower surface energy configuration than found so far. This was the O^{2-} and Al^{3+} layer just below the mirror plane. It is another O^{2-} layer with Al^{3+} ions also exposed. Again, a 2x2 supercell was used in calculating the surface energy. The calculated surface energy of 1.96 J/m^2 was lower than those found for the mirror plane termination. It was also lower than all the other surfaces in the calcium magnetoplumbite system. Three different locations within the lattice were used as starting points for the constructed surface calculations.

The surface relaxation of the newly calculated (001) surface showed two major features. The first is the relaxation of the highly charged and small Al^{3+} ions. They move to positions in the oxygen layer with no lateral relaxation. This results in a higher coordination of the Al^{3+} ions. The second feature is the rumpling of the exposed O^{2-} layer. The rumpling allows room to accommodate the relaxed Al^{3+} ions. This is similar to the calculated surface relaxation seen in α-Al_2O_3.[59] The combination of these relaxations removes the already low dipole moment perpendicular to the surface while increasing the coordination of both the Al^{3+} and O^{2-} ions. The unrelaxed and relaxed minimum (001) surface configurations can be seen in Figures 3.14 and 3.15. In each figure, a black line has been included to show the subtle rumpling of the O^{2-} ions. The top of the O^{2-} ions all lie on this line in the unrelaxed surface structure. In the relaxed surface structure, alternating O^{2-} ions are slightly raised and thus the top of these ions due not lie on the line.

D. Strontium Magnetoplumbite Surfaces

1. Low Dipole Moment Surfaces

The strontium magnetoplumbite system had 123 low dipole and reconstructed {001}

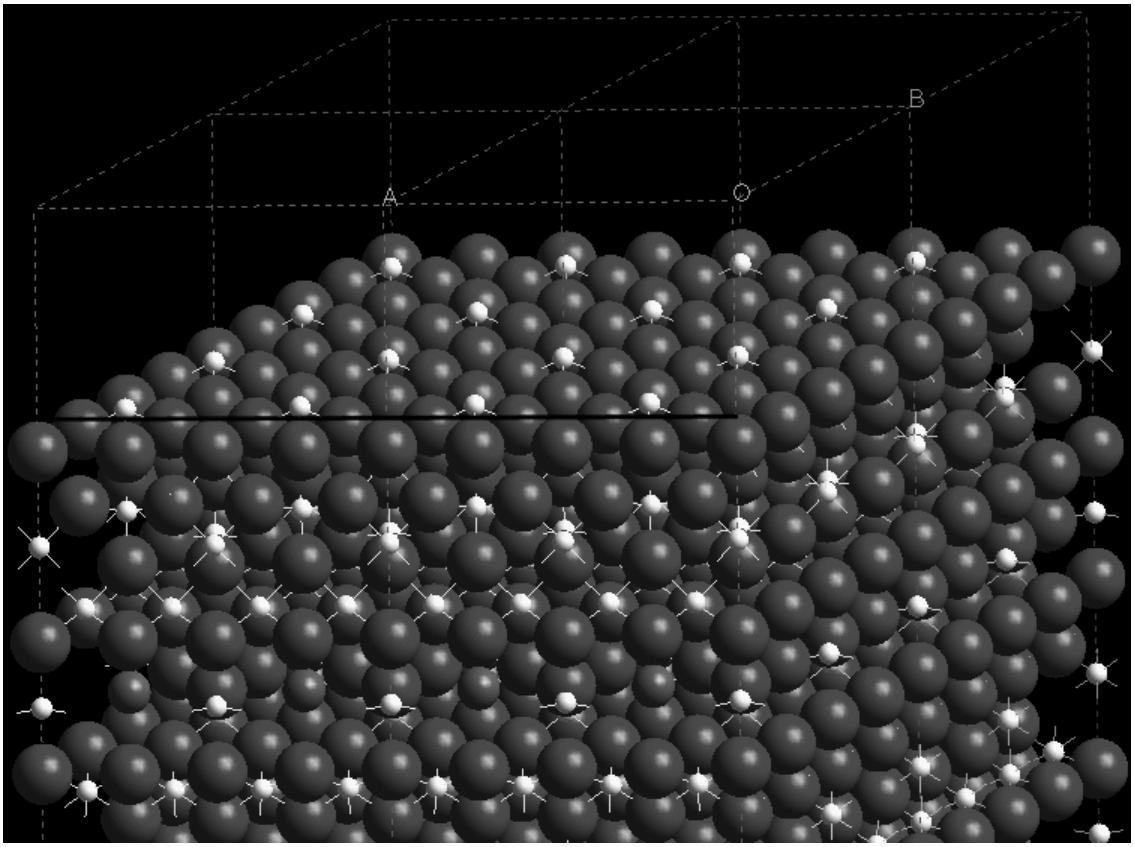

Figure 3.14: Unrelaxed {001} surface of calcium magnetoplumbite.
Ions are color coded as follows: red - O^{2-}, white - Al^{3+}, and green - Ca^{2+}. Surface image is of four blocks of unit cells of the modeled surface area. The black line shows the unrumpled O^{2-} layer.

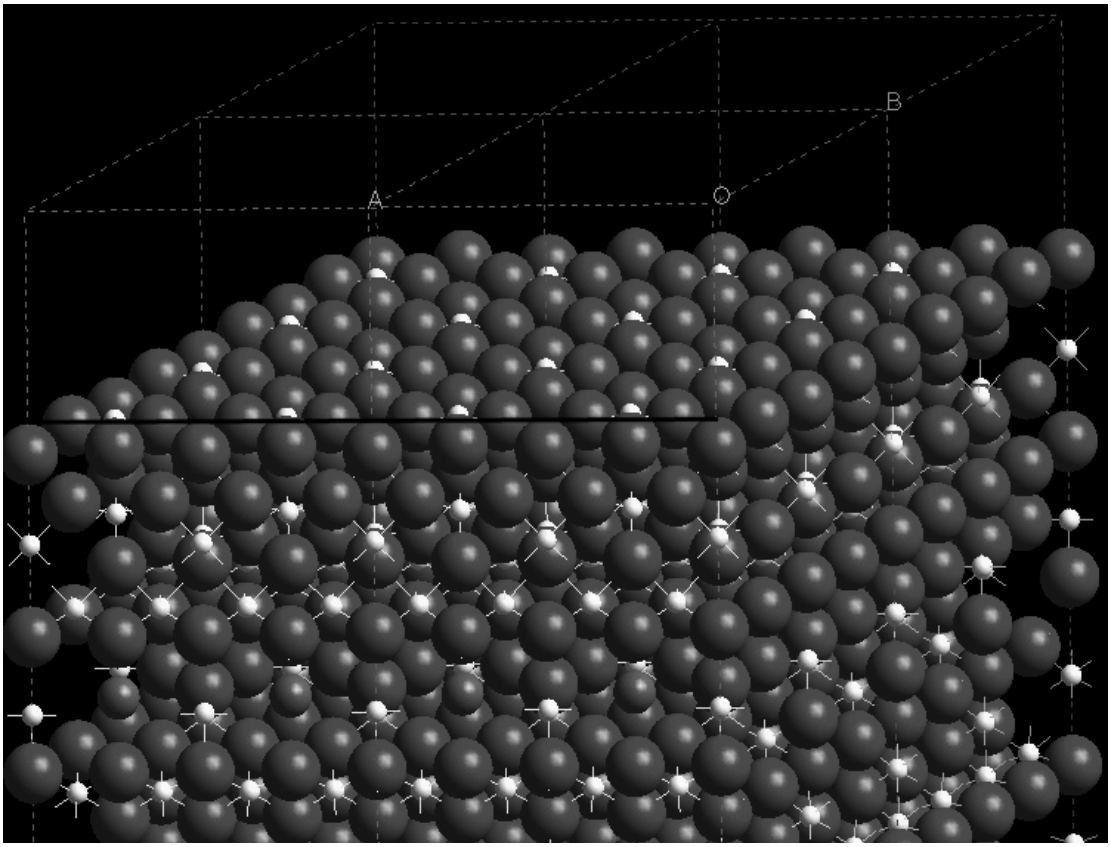

Figure 3.15. Relaxed {001} surface of calcium magnetoplumbite.
Ions are color coded as follows: red - O^{2-}, white - Al^{3+}, and green - Ca^{2+}. Surface image is of four blocks of unit cells of the modeled surface area. The black line shows the rumpled O^{2-} layer.

terminations that were modeled. The number of terminations modeled is different from the calcium magnetoplumbite system due to the larger size of the Sr^{2+} ion. The calculated results for strontium magnetoplumbite system are similar to those of the calcium magnetoplumbite system. The bulk of the surface energy calculations were done on planes that were initially found to have low dipole moments normal to the surface (i.e., termination planes generated by METADISE).

2. {100} Surfaces

Table XI contains the calculated values of the eighteen (010), (100), and (1_0) termination planes. The lowest energy surface also has two Sr^{2+} ions exposed as in the lowest energy {100} calcium magnetoplumbite surface. The first and second terminations of the {100} planes do not have any exposed Sr^{2+} ions, and these terminations possess relatively high surface energies, also as seen previously in the calcium magnetoplumbite {100} surfaces. Since the relaxation of the surface block also includes atoms that lie further into the bulk than those that occupy the top-most positions, their relaxation also influences how the surface atoms relax. The large size of the Sr^{2+} ion hinders relaxations when occupying sub-surface sites.

Figures 3.16 and 3.17 show the unrelaxed and relaxed configurations of the lowest energy surface. Figures 3.18 show the relaxed surface of the fifth termination of the (100) surface. The same problem that is seen in the calcium magnetoplumbite occurs in the strontium magnetoplumbite system. The calculation of the surface unit cells of these symmetrically equivalent orientations is not performed efficiently due to computer storage errors and rounding errors due to the hexagonal structure. As a result, the re-calculated lattice parameters and ion positions are not identical for the symmetrically equivalent planes. These changes do not allow the O^{2-} ions coordinated to the deeper Sr^{2-} ion (B) to relax to the lower equilibrium configuration, because of an increase in repulsive interactions between the neighboring O^{2-} ions. The difference in O^{2-} ion positions is more visible in the strontium magnetoplumbite surfaces than for the calcium magnetoplumbite system. The O^{2-} ions remain in positions that are aligned with the deeper Sr^{2+} ion (B) for the (100) and (1_0)

Table XI. {100} Surface of Strontium Magnetoplumbite: Sr^{2+} Depth vs Surface Energy

Termination	(010)		(100)		(1_0)	
	γ (J/m^2)	Sr^{2+} Depth (A)	γ (J/m^2)	Sr^{2+} Depth (A)	γ (J/m^2)	Sr^{2+} Depth (A)
1st	3.02	3.16	3.08	3.24	2.94	2.89
2nd	3.40	2.05	3.07	2.54	**2.59**	**1.70**
3rd	2.96	2.04	2.96	2.03	2.96	2.04
4th	2.70	1.22	2.76	1.22	2.89	1.41
5th	2.57	0.54	2.71	0.47	2.71	0.47
6th	3.51	0.94	4.12	1.18	3.42	0.80

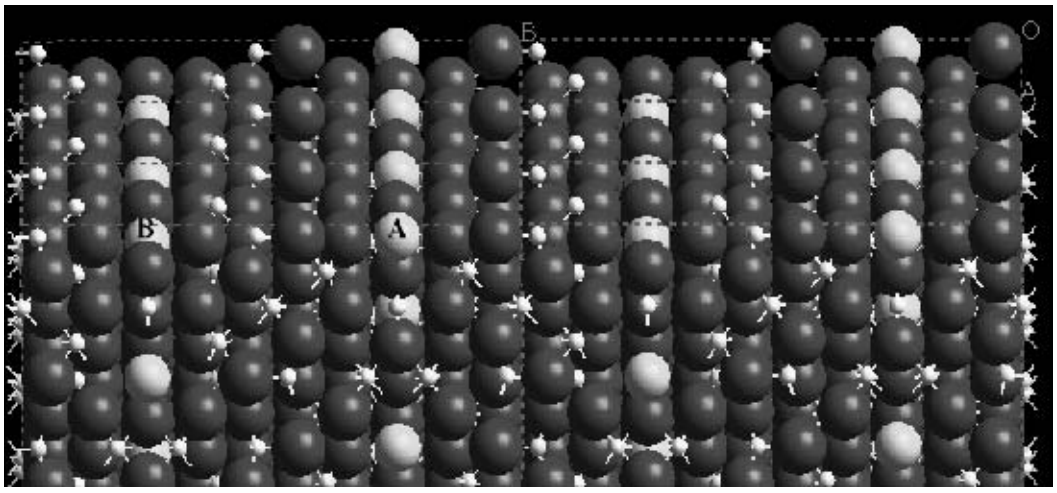

Figure 3.16. Unrelaxed {100} surface of strontium magnetoplumbite.
Ions are color coded as follows: red - O^{2-}, white - Al^{3+}, and yellow - Sr^{2+}. Surface image is of six blocks of unit cells of the modeled surface area. A being the top Sr^{2+} ion and B is the second Sr^{2+} ion.

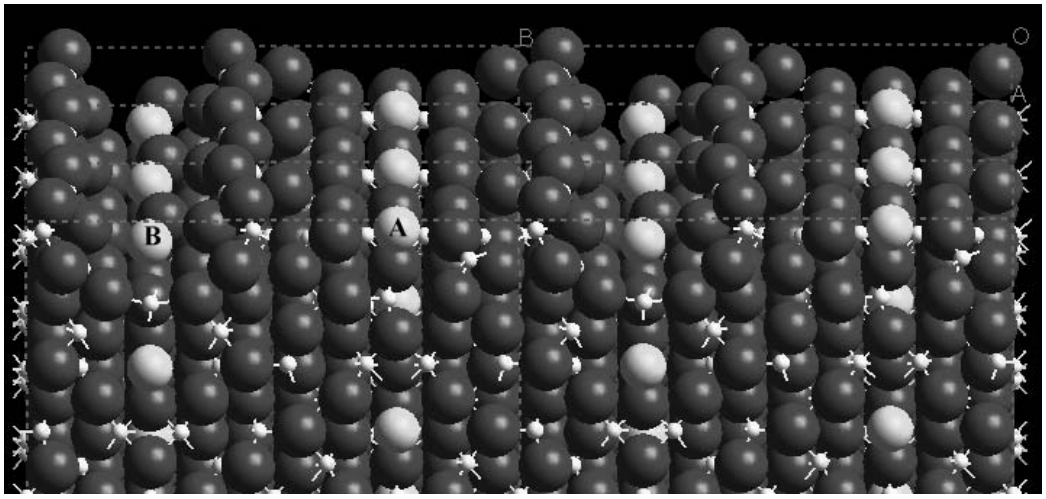

Figure 3.17. Relaxed {100} surface of strontium magnetoplumbite.
Ions are color coded as follows: red - O^{2-}, white - Al^{3+}, and yellow - Sr^{2+}. Surface image is of six blocks of unit cells of the modeled surface area. A being the top Sr^{2+} ion and B is the second Sr^{2+} ion.

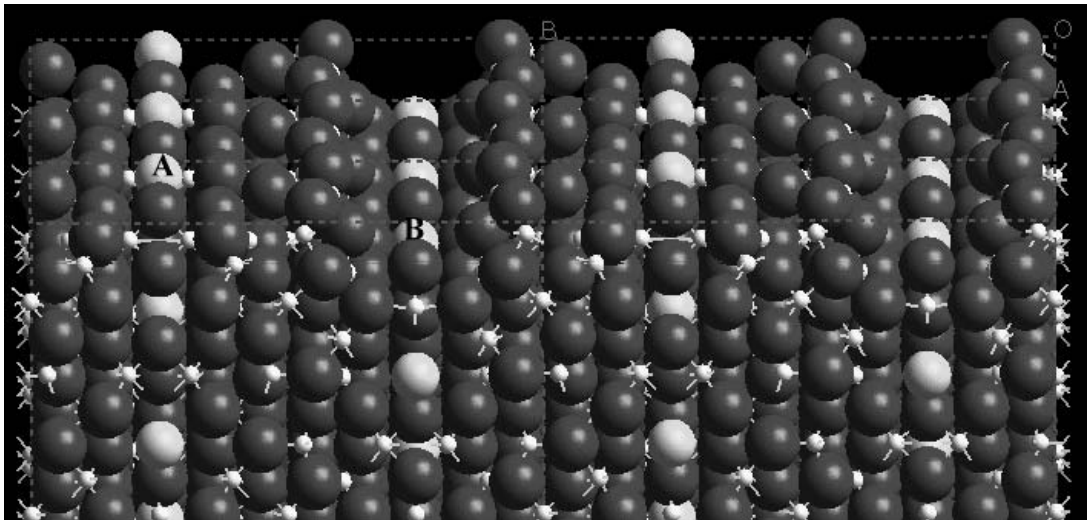

Figure 3.18. Relaxed 5th termination of the (100) surface of strontium magnetoplumbite. Ions are color coded as follows: red - O^{2-}, white - Al^{3+}, and yellow - Sr^{2+}. Surface image is of six blocks of unit cells of the modeled surface area. A is the top Sr^{2+} ion and B is the deeper Sr^{2+} ion.

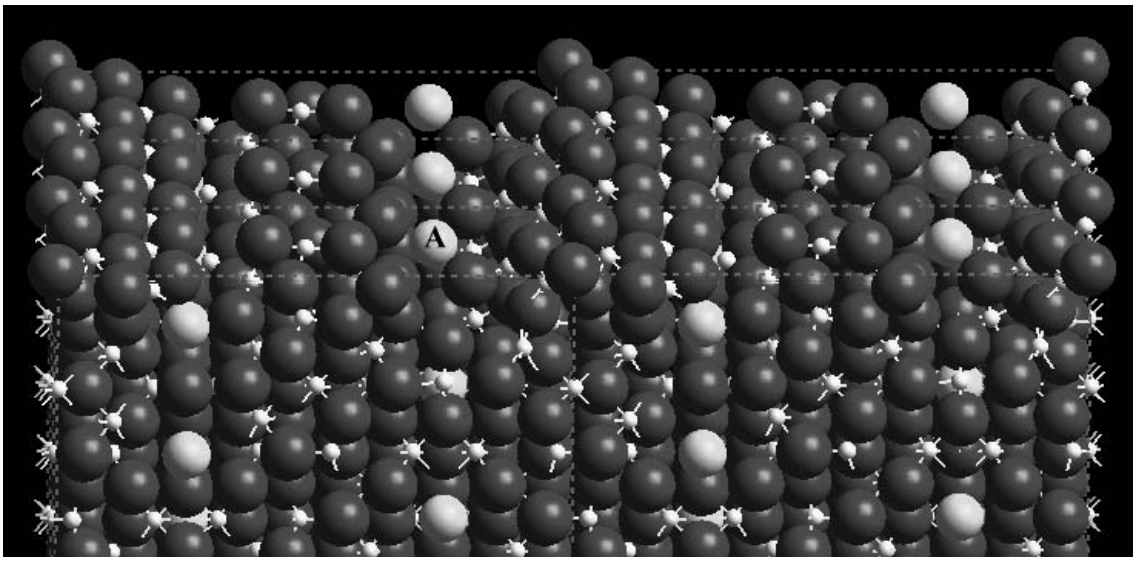

Figure 3.19. Relaxed 2nd termination of the $(1\bar{1}0)$ surface of strontium magnetoplumbite. Ions are color coded as follows: red - O^{2-}, white - Al^{3+}, and yellow - Sr^{2+}. Surface image is of six blocks of unit cells of the modeled surface area. There is only one exposed Sr^{2+} ion (A).

surfaces. In the (010) surface, these O^{2-} ions relax to positions out of line with the Sr^{2+} ion. There is also a relaxation normal to the surface. The O^{2-} ions are able to relax further into the bulk for the (010) surface than for the (100) and (1_0) surfaces. The higher energy (100) and (1_0) surfaces appear to be due to the O^{2-} and Sr^{2+} ions remaining in an orderly row such as seen in the unrelaxed (010), (100), and (1_0) starting configurations.

The larger size of the Sr^{2+} would seem to indicate that it should be easier to retain a higher coordination; thus exposing the Sr^{2+} cations should affect the surface energy more than it would for the Ca^{2+} ion. This is not the case, so it is likely that it is not the coordination of the Sr^{2+} ions that dictates which surface is the lowest energy configuration, but rather the higher polarizability of the Sr^{2+} ion. The higher polarizability allows a greater deformation of the Sr^{2+} ion, i.e. the creation of a larger dipole moment evident by the greater relaxation of the Sr^{2+} shell. The hindering of relaxation by the subsurface Sr^{2+} ion is overcome with the larger polarizability of the Sr^{2+} ion. This larger polarization, although more effective in exposed surface positions, allows for low energy configurations that do not have two exposed Sr^{2+} ions. An example of this can be seen in Figure 3.19 of the second (1_0) surface. This surface has essentially the same surface energy of 2.59 J/m^2 as the lowest {010} surface energy of 2.57 J/m^2, even though their relaxed surface structures are different.

There are two differences between these structures: the number of exposed Sr^{2+} ions and the positions of the aligned surface O^{2-} ions. In the (010) surface, there are two exposed Sr^{2+} ions. The first Sr^{2+} ion (A) lies in a plane of coordinating O^{2-} ions. The second Sr^{2+} ion (B) lies in a channel between two rows of raised O^{2-} ions. The (1_0) surface has only one exposed Sr^{2+} ion. Its position is similar to the second Sr^{2+} ion (B in Figure 3.18) in the (010) surface as it lies in a channel between two rows of raised O^{2-} ions. The O^{2-} ions in the channel relax to positions further apart than those in the (010) surface, moving out of alignment with neighboring O^{2-} ions and the exposed Sr^{2+} ion. The hindering of relaxation of atoms further in the surface block is offset by the larger distances between these surface O^{2-} ions, thus resulting in the lower than expected surface energy of the second (1_0) surface.

3. Other Low Dipole Surfaces

The surfaces with the lowest energy configurations of the strontium magnetoplumbite system are given in Table XII. The unit cell of the strontium magnetoplumbite is larger than that of the calcium magnetoplumbite system due to the size of the Sr^{2+} ion. This causes the surface area for the same orientations to be larger. The Al^{3+} ions become slightly more exposed, but still relax into the structure of the surface. The Sr^{2+} ions are exposed, or are very near the surface, in the initial unrelaxed structures.

The {110} surface structure, see Figure 3.20, has two exposed Sr^{2+} ions. The first Sr^{2+} ion (A) is coordinated by six O^{2-} ions lying in a plane below this Sr^{2+} ion. The second Sr^{2+} ion (B) is also coordinated with six O^{2-} ions. These O^{2-} ions lie in the same plane as the Sr^{2+} ion. The relatively high surface energy is due to the highly polarized environment of the first Sr^{2+} ion.

The {120} surface, see Figure 3.21, has four exposed Sr^{2+} ions (A, B, D, and E) and two dangling O^{2-} ions (F and G). The calculated surface energy is the highest of all of the low dipole surfaces. Two of the exposed Sr^{2+} ions (A and B) are coordinated to the same O^{2-} ion (C). They have positions that are in the same plane but are not aligned in a row. The third Sr^{2+} ion (D) occupies a slightly raised position and is coordinated by four O^{2-} ions. The fourth Sr^{2+} ion (E) is coordinated by a raised O^{2-} ion and a O^{2-} ion in common with the third Sr^{2+} ion. The fourth Sr^{2+} ion is also close to two Al^{3+} ions. Coulombic repulsion between the fourth Sr^{2+} ion and the two Al^{3+} ions increases the site potential of both the Sr^{2+} and the Al^{3+} cations. The neighboring dangling O^{2-} ion (F) is coordinated to these two Al^{3+} ions and the Sr^{2+} ion. The second dangling O^{2-} ion (G) is coordinated with three Al^{3+} ions. The combination of the higher site potential of the fourth Sr^{2+} ion and the two dangling O^{2-} ions leads to the relatively high surface energy.

Figure 3.22 shows the surface structure of the {012} orientation which has only one exposed Sr^{2+} ion (A). This surface has one O^{2-} ion (B) which relaxes to a slightly raised position. It is coordinated with three Al^{3+} ions and the exposed Sr^{2+} ion similar to its bulk coordination. The Sr^{2+} ion is coordinated with five O^{2-} ions. The neighboring O^{2-} ions form a cage around the bottom of the exposed Sr^{2+} ion. This cage lowers the site potential of the

Table XII. Relaxed Surface Energies of Strontium Magnetoplumbite

Surface	γ (J/m^2)
{100}	2.57
{110}	2.74
{120}	2.83
{012}	2.52
{112}	2.07
{122}	2.74

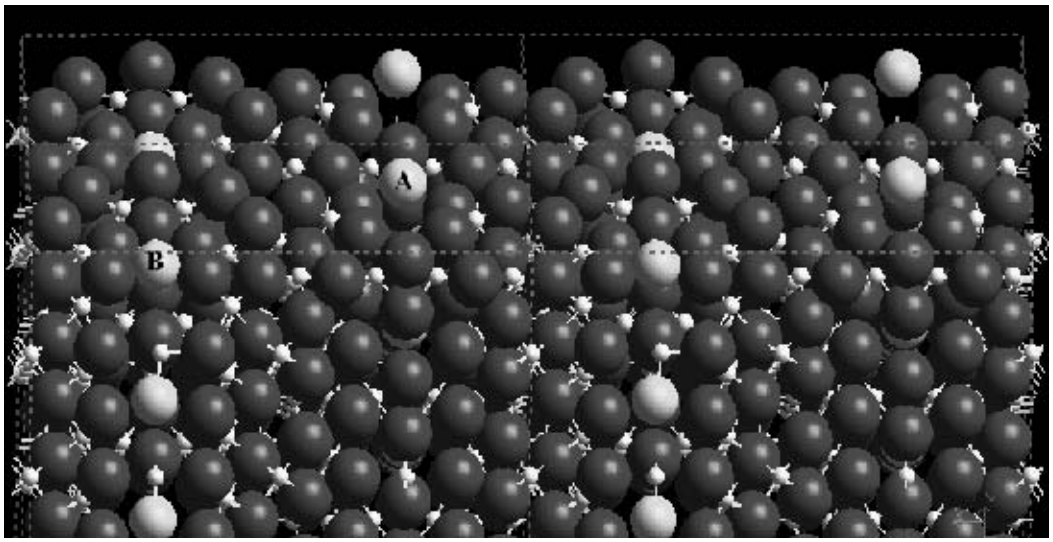

Figure 3.20. Relaxed {110} surface of strontium magnetoplumbite.
Ions are color coded as follows: red - O^{2-}, white - Al^{3+}, and yellow - Sr^{2+}. Surface image is of four blocks of unit cells of the modeled surface area. Both Sr^{2+} ions are coordinated with six O^{2-} ions. The first (A) has relaxed to a position above the original surface and its neighboring O^{2-} ions. The second (B) occupies a position nearly on the same plane as its neighboring O^{2-} ions.

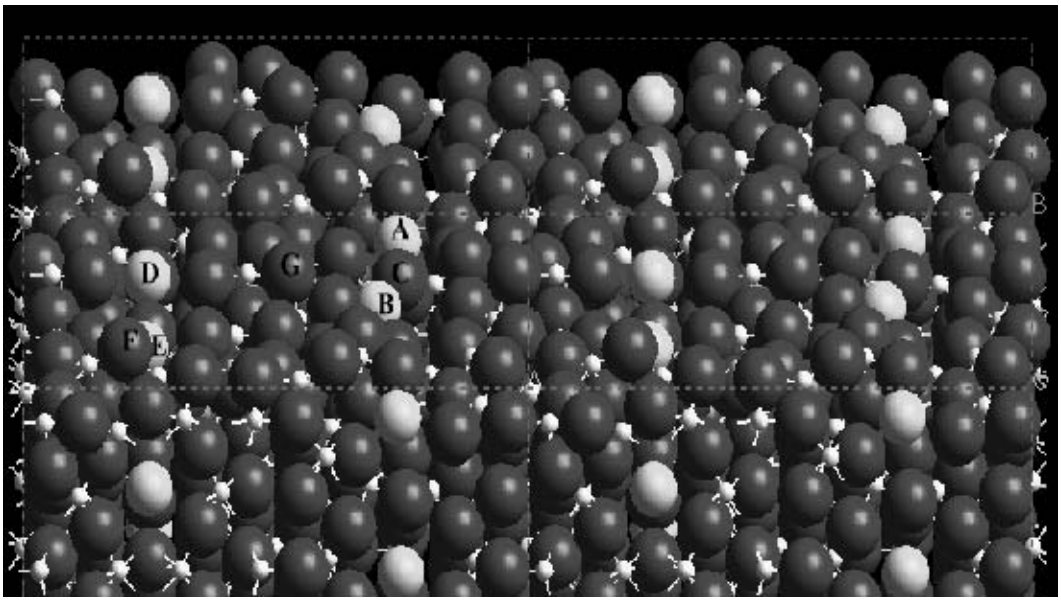

Figure 3.21. Relaxed {120} surface of strontium magnetoplumbite.
Ions are color coded as follows: red - O^{2-}, white - Al^{3+}, and yellow - Sr^{2+}. Surface image is of four blocks of unit cells of the modeled surface area. There are four exposed Sr^{2+} ions (A, B, D, and E). Two of the exposed Sr^{2+} ions (A and B) are coordinated with the same O^{2-} ion (C). There are two dangling O^{2-} ions (F and G). The first (F) is coordinated with two Al^{3+} ions and the fourth Sr^{2+} ion (E). The four Sr^{2+} ion also occupies a position very close to the two Al^{3+} ions. The second dangling O^{2-} ion is coordinated with three Al^{3+} ions. The third Sr^{2+} ion (D) occupies a slightly raised position and is coordinated by four O^{2-} ions.

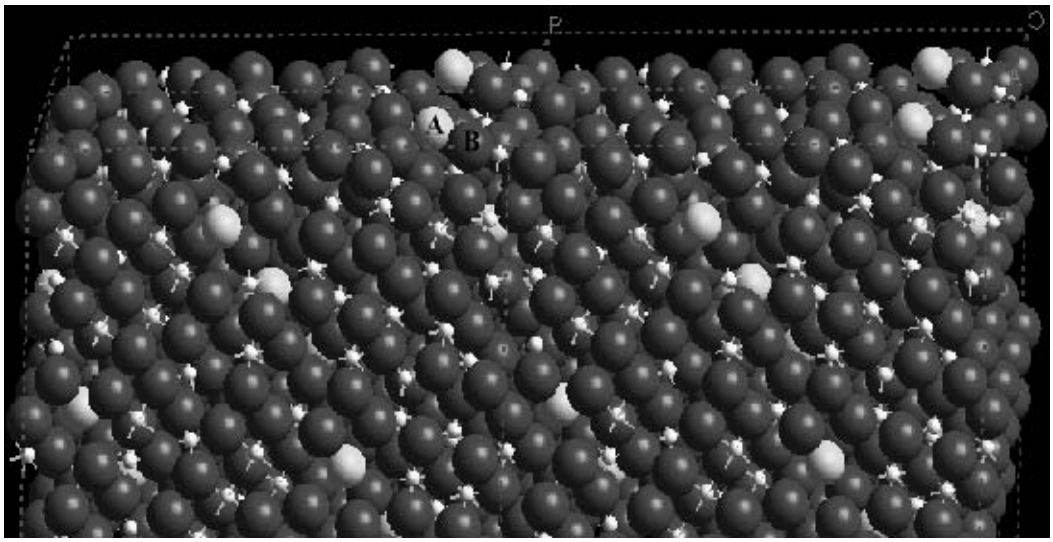

Figure 3.22. Relaxed {012} surface of strontium magnetoplumbite.
Ions are color coded as follows: red - O^{2-}, white - Al^{3+}, and yellow - Sr^{2+}. Surface image is of four blocks of unit cells of the modeled surface area. There is one exposed Sr^{2+} ion (A) and one O^{2-} ion (B) that has relaxed to a position just above the original surface.

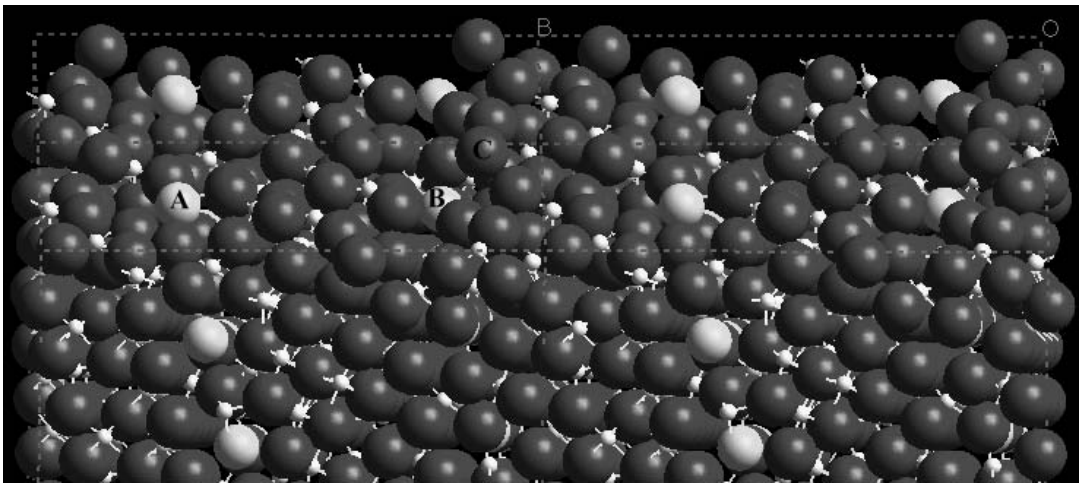

Figure 3.23. Relaxed {112} surface of strontium magnetoplumbite.
Ions are color coded as follows: red - O^{2-}, white - Al^{3+}, and yellow - Sr^{2+}. Surface image is of four blocks of unit cells of the modeled surface area. Both exposed Sr^{2+} ions (A and B) have six O^{2-} ion nearest neighbors. The is one dangling O^{2-} ion (C).

Sr^{2+} ion. The dangling O^{2-} ion and the exposed Sr^{2+} ion stabilize their respective positions which results in its relatively low surface energy.

The {112} surfaces, see Figure 3.23, has two exposed Sr^{2+} ions (A and B) and a dangling O^{2-} ion (C). The dangling O^{2-} ion is coordinated by a single Al^{3+} ion. The two exposed Sr^{2+} ions occupy highly coordinated positions. The first Sr^{2+} ion (A) is coordinated with six O^{2-} ions that lie below the Sr^{2+} ion. The second Sr^{2+} ion (B) is also coordinated with six O^{2-} ions. The O^{2-} ions form a cage that leaves it less exposed than the first Sr^{2+} ion. The second Sr^{2+} ion is also close to the dangling O^{2-} ion. This surface has the lowest surface energy of the non-basal plane orientations. The high coordination of the Sr^{2+} ions overcome any increases in surface energy due to the low coordinated dangling O^{2-} ion.

There are three exposed Sr^{2+} ions on the {122} relaxed surface, see Figure 3.24. There is a single Sr^{2+} ion (A) and two Sr^{2+} ions (B and C) grouped together. There are three dangling O^{2-} ions. The single Sr^{2+} occupies a highly coordinated position, in a cage, as seen in the {112} surface. The other two Sr^{2+} ions occupy second nearest neighboring sites and share coordination with a single O^{2-} ion. The dangling O^{2-} ions lie close to each other. Two of these O^{2-} ions (D and E) are coordinated with three Al^{3+} ions. The third (F) is coordinated with two Al^{3+} ions and the single Sr^{2+} ion. The relaxed position of the three dangling O^{2-} ions results in the high energy of this surface orientation even though there are three exposed Sr^{2+} ions.

Although the mirror plane is more crowded due to the larger size of the Sr^{2+} ion, the spinel-like blocks are more open than in calcium magnetoplumbite due to the larger unit cell. This more open structure allows for easier relaxation for the subsurface ions. The three highest energy surfaces of the strontium magnetoplumbite system are the {110}, {120}, and {122} orientations. The high energy of the {120} and {122} surfaces are related to the close proximity of the surface cations and the high number of dangling O^{2-} ions. The short distances between the cations increases the coulombic repulsive energy while the low coordination of the dangling O^{2-} ions decreases the coulombic attractive energy. The benefits of the high polarizability of the Sr^{2+} ion and the subsurface relaxation allowed by the exposure of the Sr^{2+} ions are lost due to this increase in the coulombic interaction

energy.

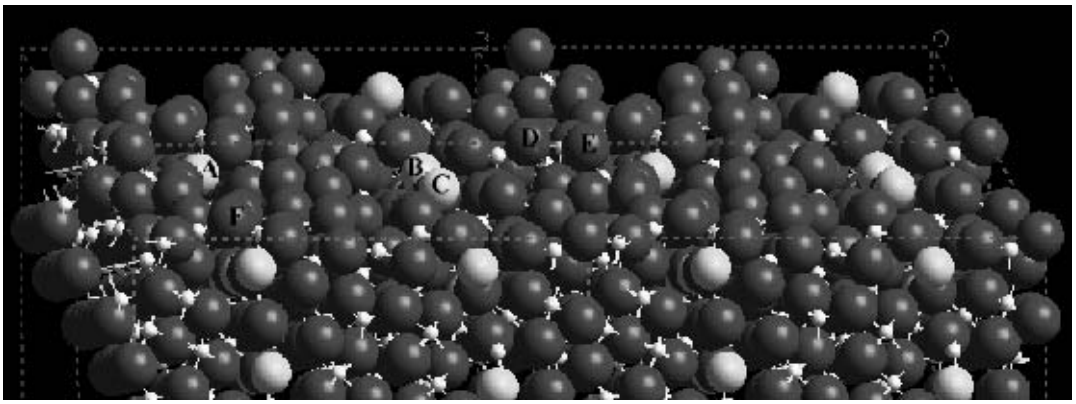

Figure 3.24. Relaxed {122} surface of strontium magnetoplumbite.
Ions are color coded as follows: red - O^{2-}, white - Al^{3+}, and yellow - Sr^{2+}. Surface image is of four blocks of unit cells of the modeled surface area. The first exposed Sr^{2+} ion occupies a highly coordinated position. The second and third Sr^{2+} ions are share a common O^{2-} ion. Two dangling O^{2-} ions (D and E) are coordinated with three Al^{3+} ions. The third (F) is coordinated with two Al^{3+} ions and the first Sr^{2+} ion (A).

This results in the high surface energies calculated for these two orientations.

The calculated surface energies of the {110} and {122} orientations are equal. The {122} surface has three dangling O^{2-} ions and three exposed Sr^{2+} ions. The {110} surface would be expected to have a lower calculated surface energy. There are no dangling O^{2-} ions but there is a Sr^{2+} ion (A) which sits above its coordinating O^{2-} ions. The high surface energy is due to the positions of the top Sr^{2+} (A) and O^{2-} ions.

In the strontium magnetoplumbite system, the exposure of Sr^{2+} ions plays a lesser role in determining which surfaces have low calculated surface energies. This is due to the more open spinel block structure which allows more subsurface relaxation to occur than in calcium magnetoplumbite. The coordination of the Sr^{2+} and the O^{2-} ions becomes the most important factor in the surface energy of an orientation.

4. {001} Surfaces

The calculated relaxed surface energies of the {001} terminations are given in Table XIII. As with the calcium magnetoplumbite system, it was expected that the basal {001} plane would have the lowest surface energy because of observed fracture characteristics and crystal morphology. The lack of low dipole moments required that planes within this surface be manually constructed.

The "top" of the lattice of a single unit cell was used as a starting point in first attempt in calculating the {001} surface energy. This corresponds to a position within the spinel block. However, the calculated relaxed surface energy, 8.33 J/m^2, was much higher than the minimum energies of all the other surfaces. The low calculated energies of surfaces with exposed cations in both the calcium and strontium systems led to examination of the mirror plane. These calculation also yielded very high surface energies.

A 2x2 supercell was then adopted to allow more configurations while maintaining charge neutrality. This is because there are a greater number of ion positions to leave or remove from the exposed surface. The mid-spinel block termination resulted in a calculated energy of 4.12 J/m^2. The success of the calculations on the calcium magnetoplumbite system suggested that the O^{2-} and Al^{3+} layer just below the mirror plane might result in a

lower

Table XIII. Surface Energies of the Relaxed Strontium Magnetoplumbite {001} Sufaces

Surface (2x2 unless noted)	γ (J/m^2)
Mid-Spinel Block (1x1)	8.33
Mid-Spinel Block	4.12
Mirror Configuration I	2.89
Mirror Configuration II	2.05
O^{2-} - Al^{3+} Layer Beneath Mirror Plane	1.70

surface energy configuration. The calculated surface energies were indeed lower than those found when the mirror plane was the termination plane configuration.

The lowest calculated energy structure of the strontium magnetoplumbite {001} surface was found to exhibit a similar relaxation to that found in the calcium magnetoplumbite system. Two main features are observed. The first is the relaxation of the highly charged and small Al^{3+} ions. They relax to positions into the oxygen layer with no lateral relaxation. This results in a higher coordination of the Al^{3+} ions and lowers the dipole moment associated with their positions above the O^{2-} layer. The second feature is the rumpling of the exposed O^{2-} layer. The rumpling allows additional room to accommodate the relaxed Al^{3+} ions. The combination of these relaxations reduces the already low dipole moments normal to the surface while increasing the coordination of both the Al^{3+} and O^{2-} ions. The unrelaxed and relaxed minimum energy {001} surface configurations can be seen in Figures 3.25 and 3.26. In each figure, a black line has been included to show the subtle rumpling of the O^{2-} ions. The top of the O^{2-} ions all lie on this line in the unrelaxed surface structure. In the relaxed surface structure, alternating O^{2-} ions are slightly raised, and thus the top of these ions do not lie on the line.

E. Barium Magnetoplumbite Surfaces

1. Low Dipole Moment Surfaces

The theoretical barium magnetoplumbite had 113 low dipole and reconstructed terminations that were modeled. The calculated results for barium magnetoplumbite system surfaces are similar to those of the calcium and strontium magnetoplumbite systems. The bulk of the surface energy calculations were done on planes that initially have low dipole moments normal to the surface (i.e. termination planes generated by METADISE).

2. {100} Surfaces

Table XIV contains the surface energy of the eighteen {100} surfaces as a function of Ba^{2+} depth. The depth of the Ba^{2+} ions below the surface is again the dominant factor in surface structure of these orientations. The unrelaxed and relaxed minimum energy

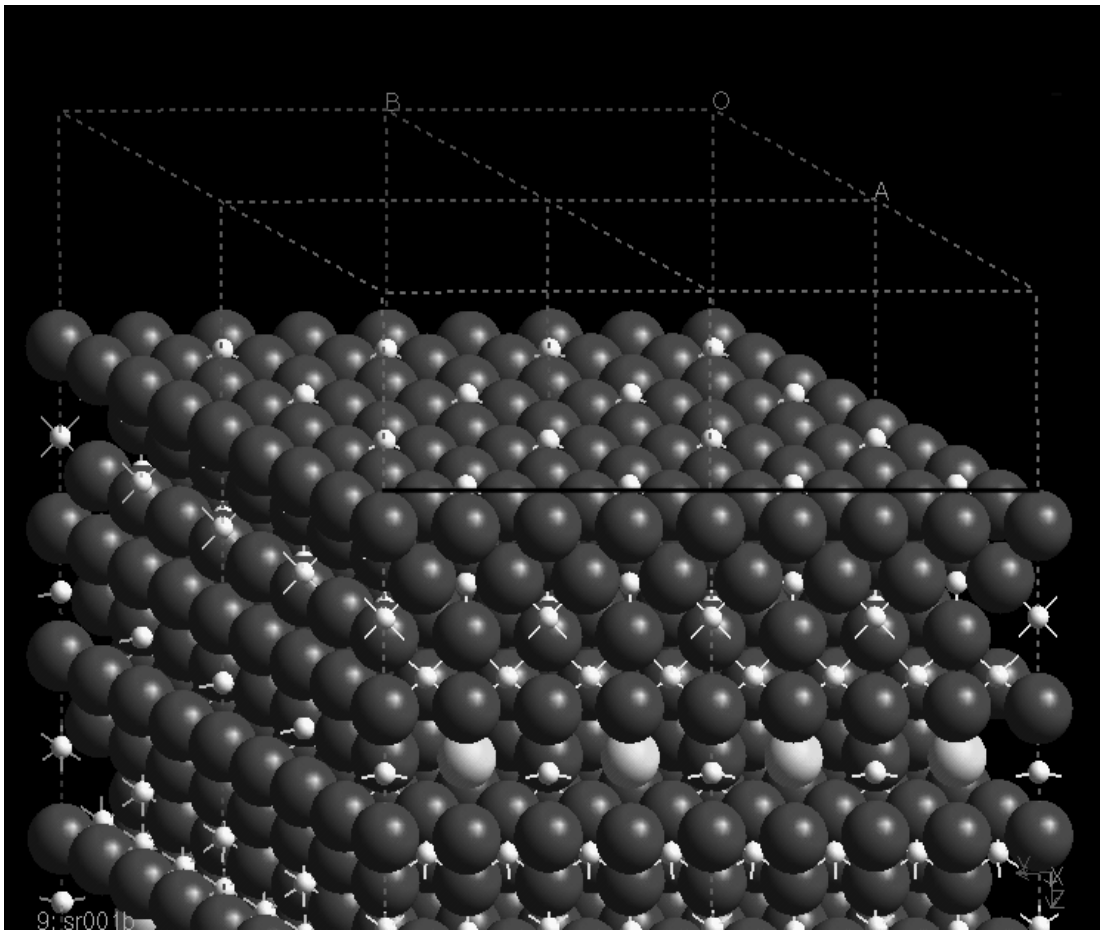

Figure 3.25. Unrelaxed {001} surface of strontium magnetoplumbite.
Ions are color coded as follows: red - O^{2-}, white - Al^{3+}, and yellow - Sr^{2+}. Surface image is of four blocks of unit cells of the modeled surface area. The black line shows the unrumpled O^{2-} layer.

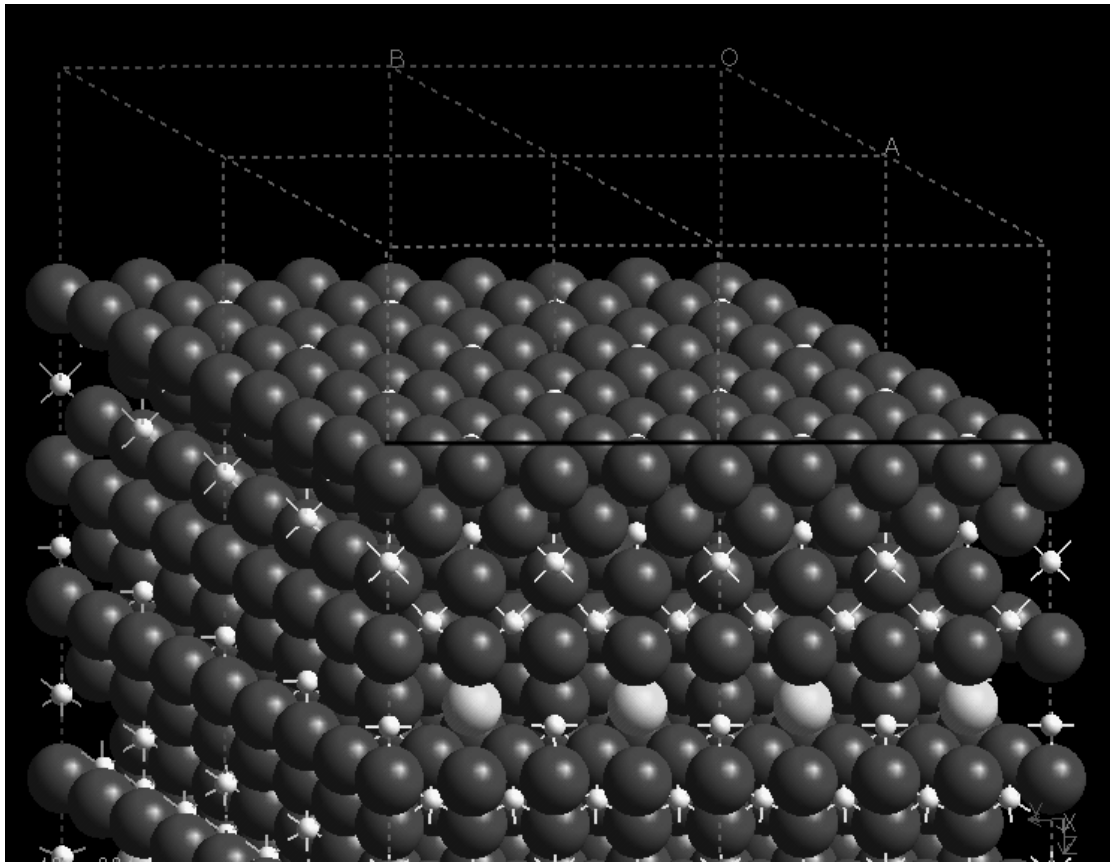

Figure 3.26. Relaxed {001} surface of strontium magnetoplumbite.
Ions are color coded as follows: red - O^{2-}, white - Al^{3+}, and yellow - Sr^{2+}. Surface image is of four blocks of unit cells of the modeled surface area. The black line shows the rumpled O^{2-} layer.

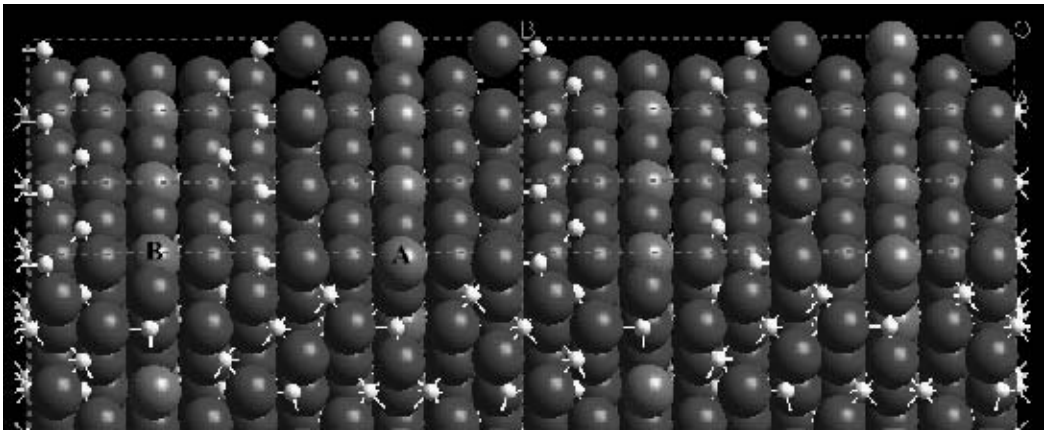

Figure 3.27. Unrelaxed {100} surface of barium magnetoplumbite.
Ions are color coded as follows: red - O^{2-}, white - Al^{3+}, and blue - Ba^{2+}. Surface image is of six blocks of unit cells of the modeled surface area. A is the top Ba^{2+} ion and B is the second exposed Ba^{2+} ion.

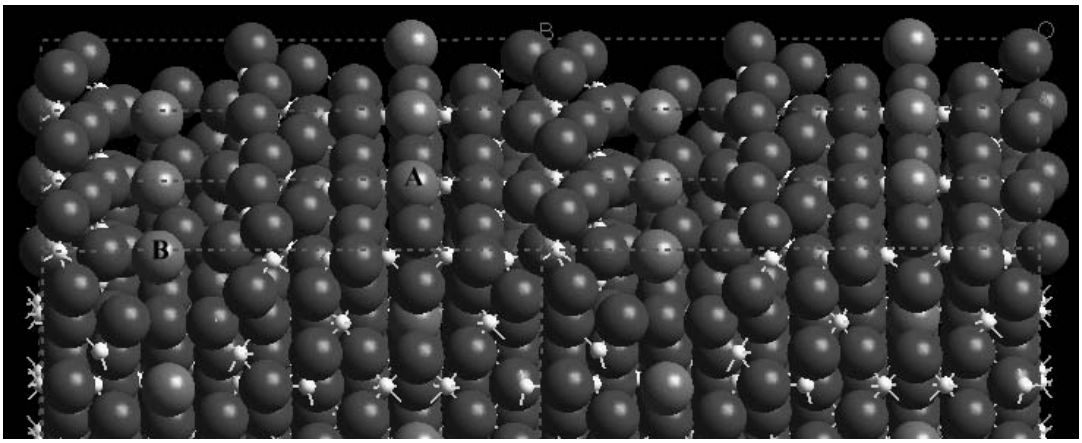

Figure 3.28. Relaxed {100} surface of barium magnetoplumbite.
Ions are color coded as follows: red - O^{2-}, white - Al^{3+}, and blue - Ba^{2+}. Surface image is of six blocks of unit cells of the modeled surface area. A is the top Ba^{2+} ion and B is the second exposed Ba^{2+} ion.

Table XIV. {100} Surface of Barium Magnetoplumbite: Ba^{2+} Depth vs Surface Energy

Termination	(010)		(100)		(1_0)	
	γ (J/m^2)	Ba^{2+} Depth (A)	γ (J/m^2)	Ba^{2+} Depth (A)	γ (J/m^2)	Ba^{2+} Depth (A)
1st	2.65	0.95	2.63	0.00	7.46	2.10
2nd	2.95	2.44	3.34	2.36	3.34	2.36
3rd	2.77	0.65	4.86	2.10	2.78	1.18
4th	2.59	0.97	2.59	0.97	2.81	1.05
5th	2.09	0.31	2.09	0.31	2.09	0.31
6th	2.18	1.07	2.18	1.07	2.18	1.07

configurations of the {100} surface of barium magnetoplumbite are shown in Figures 3.27 and 3.28.

The lowest energy surface has two exposed Ba^{2+} ions, similar to the calcium and strontium magnetoplumbite systems. The relaxed surface structure is closer to the {100} strontium magnetoplumbite lowest energy surface than the strontium magnetoplumbite is to the calcium magnetoplumbite {100} surface. The calcium, strontium, and barium magnetoplumbite {100} surfaces have the first cation (A) in a position that forms a row of alternating cations and anions. The cations relax to position just above the alternating O^{2-} ions. The difference between the calcium magnetoplumbite surface and the strontium and barium magnetoplumbite surfaces is due to the second cation (B). In the strontium and barium magnetoplumbite systems, the second cation position is situated in a channel with O^{2-} ions forming the sides. The cations do not form a straight row. The calcium magnetoplumbite does not have this channel. The differences observed in the calcium magnetoplumbite must be due to the smaller size of the Ca^{2+} ion which needs less relaxation of the O^{2-} ions to accommodate its position.

Figure 3.29 illustrates the relaxed structure of the second (010) surface. The position of the first Ba^{2+} ion (A) is at a depth of -0.14 A. Although this surface has the top Ba^{2+} relaxed to an exposed position, it still exhibits significantly higher surface energy than the fifth {100} termination planes. There are two possibilities for this high surface energy. The first is that the Ba^{2+} ion has relaxed to a position above the original surface, although the Ba^{2+} ion is in a highly coordinated position since the neighboring O^{2-} ions also have relaxed to positions above the original surface. This reason therefore is probably not the cause of the high surface energy. The second possibility is that the lower Ba^{2+} ion has prevented atoms closer to the surface from relaxing completely. This leaves the small and highly charged Al^{3+} ions exposed. This exposure results in the high surface energy for this configuration.

The last plane to be discussed is the second termination of the (1_0) orientation. This has the highest surface energy of the {100} surfaces. This is because of relaxation that results in no exposed Ba^{2+} ions. This surface is the only one out of the eighteen in these orientations that does not have at least one exposed Ba^{2+} ion.

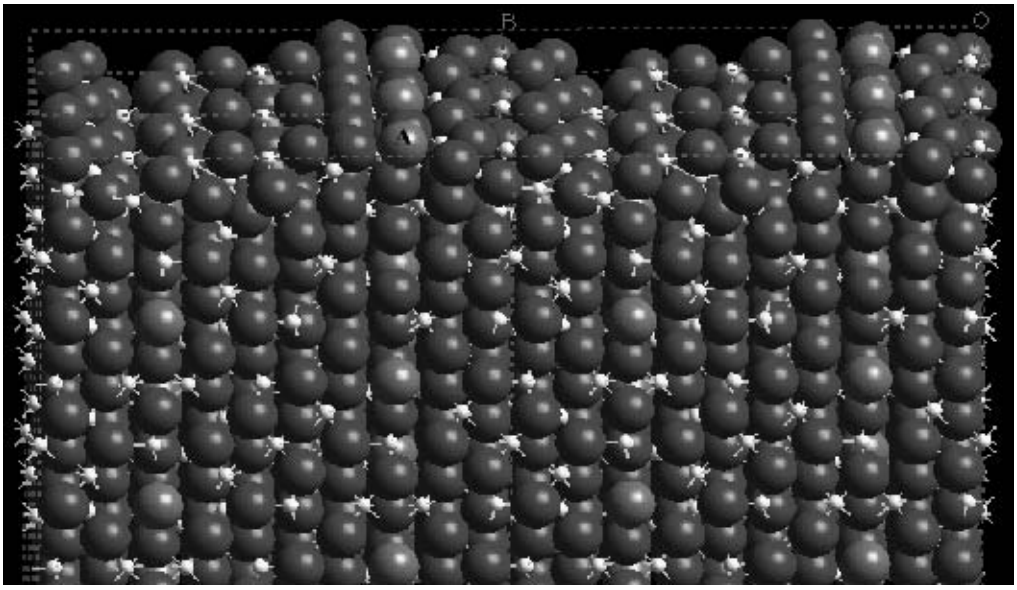

Figure 3.29. Relaxed 2nd termination of the (010) surface of barium magnetoplumbite. Ions are color coded as follows: red - O^{2-}, white - Al^{3+}, and blue - Ba^{2+}. Surface image is of six blocks of unit cells of the modeled surface area. The exposed Ba^{2+} ion (A) has relaxed to a position above the original surface.

Coordination of the Ba^{2+} ion is seen to influence the surface energy of the termination plane. It does not, however, play as large a role as the relaxation of Ba^{2+} ions to exposed surface positions. The large size of the Ba^{2+} ion does two things for these surfaces. The first is similar to the conclusion reached in the calcium magnetoplumbite system, that is to say that the locations of the subsurface Ba^{2+} ions do not allow a great deal of relaxation to occur for neighboring atoms. The second role that its size plays is in the increase in the polarizability of the Ba^{2+} ion. This ease of distortion of the "electron cloud" allows more relaxation to occur. This, coupled with its size, allows it to interact with neighboring atoms at longer distances so that the coordination is not the most important factor in determining the surface energy of a structure.

3. Other Low Dipole Moment Surfaces

Table XV contains the calculated lowest surface energy for the barium magnetoplumbite system for each of the low dipole orientations. The Al^{3+} surface ions relax to highly coordinated positions into the surface structure. This is a common feature in all the Magnetoplumbite surface structures. The starting configurations for these surfaces also have Ba^{2+} ions either at the surface or near enough to relax to exposed positions.

The relaxed {110} surface structure, shown in Figure 3.30, has two exposed Ba^{2+} ions (A and B) in highly coordinated positions, each with six neighboring O^{2-} ions that form a cage that lies beneath the Ba^{2+} ions. There are no dangling O^{2-} ions relaxing to sites that lie above the rest of the surface. Both exposed Ba^{2+} ions also have an Al^{3+} ion as a nearest neighbor. The coulombic interaction between the cations increases the site potential of both ions and causes the relatively high surface energy.

There are two exposed Ba^{2+} ions in the {120} surface structure shown in Figure 3.31. One exposed Ba^{2+} ion (A) occupies a site in a raised position. It is coordinated by five neighboring O^{2-} ions. The second Ba^{2+} ion (B) rests in a ring of O^{2-} ions that lie nearly parallel to the surface with a dangling O^{2-} ion (C) almost covering its position. This dangling O^{2-} ion is coordinated to three Al^{3+} ions. Two nearby O^{2-} ions (D and E) have also relaxed to sites above the original surface. These two anions are coordinated by two Al^{3+} ions. The high surface energy of this orientation is most likely due to the position of these three O^{2-}

Table XV. Relaxed Surface Energies of Barium Magnetoplumbite

Surface	γ (J/m^2)
{100}	2.09
{110}	2.58
{120}	2.62
{112}	2.26
{122}	2.40

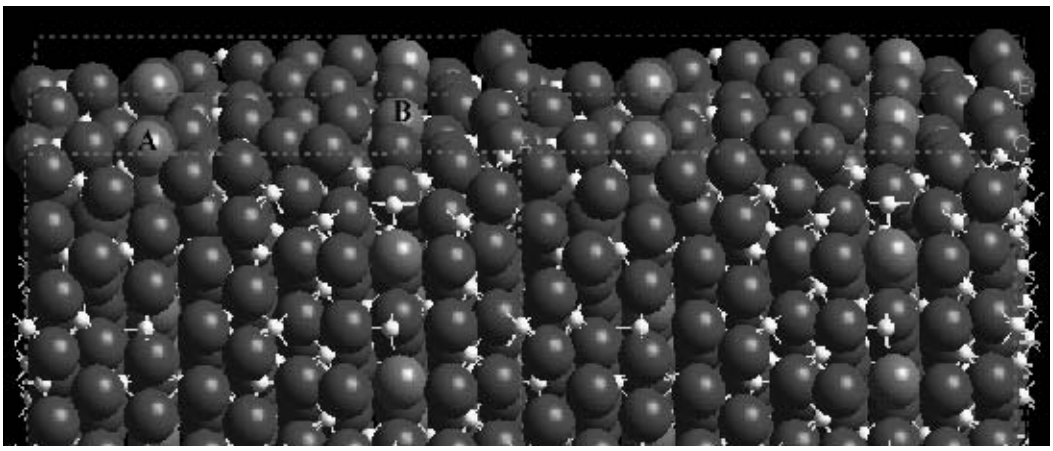

Figure 3.30. Relaxed {110} surface of barium magnetoplumbite.
Ions are color coded as follows: red - O^{2-}, white - Al^{3+}, and blue - Ba^{2+}. Surface image is of four blocks of unit cells of the modeled surface area. Both exposed Ba^{2+} ions (A and B) are coordinated with six O^{2-} ions and have a Al^{3+} ion nearest neighbor.

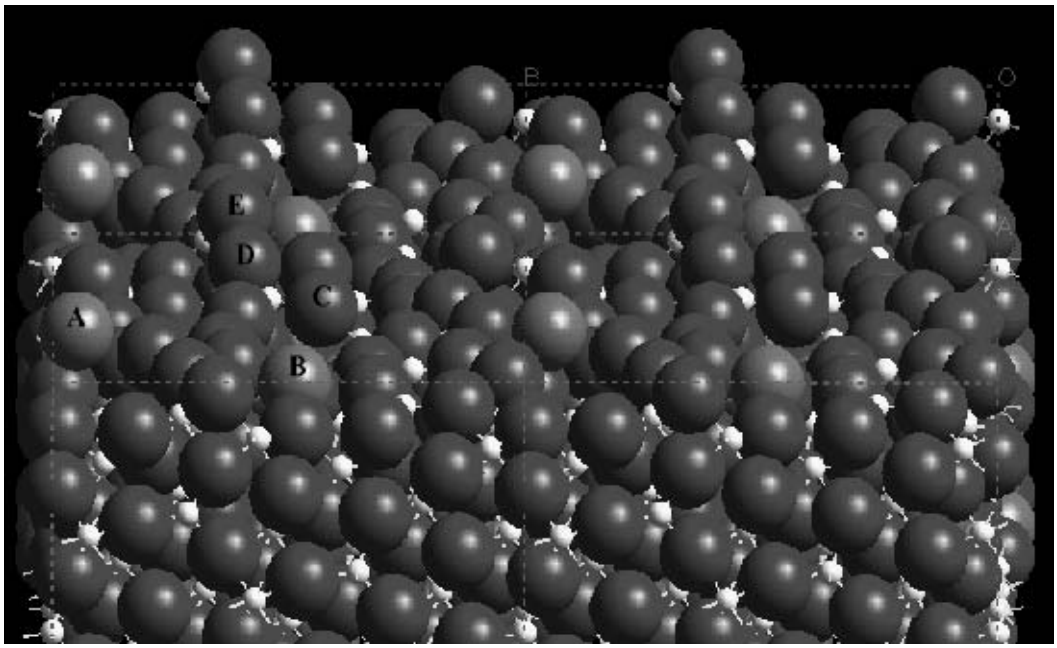

Figure 3.31. Relaxed {120} surface of barium magnetoplumbite.Ions are color coded as follows: red - O^{2-}, white - Al^{3+}, and blue - Ba^{2+}. Surface image is of four blocks of unit cells of the modeled surface area. The first exposed Ba^{2+} ion (A) relaxed to a position above the original surface. The second exposed Ba^{2+} ion (B) lies in a ring of O^{2-} ions and is covered by the first dangling O^{2-} ion (C). The other two dangling O^{2-} ions (D and E) are coordinated by two Al^{3+} ions.

ions. In addition to being above the rest of the surface, they also are in close proximity to each other. The repulsive energy between these positions, and the low coordination of two of these O^{2-} ions, increases the surface energy of this termination plane.

Figure 3.32 shows the {112} surface. It has two exposed Ba^{2+} ions. This surface is smooth and thus no O^{2-} ions occupy positions above the original plane of the surface. This surface also has a smaller exposure of the Al^{3+} ions than other orientations in this system. Both Ba^{2+} ions have neighboring O^{2-} ions that stabilize their exposed positions. This surface has the lowest surface energy of the low dipole surfaces, excluding the {100} orientation.

The {122} surface structure, see Figure 3.33, has three exposed Ba^{2+} ions. One (A) has seven neighboring O^{2-} ions. The other two (B and C) are nearest neighbors. All three Ba^{2+} ions have relaxed to positions above the unrelaxed surface plane. Several O^{2-} ions (D) have also relaxed to positions above the original surface. The decrease in surface energy due to the exposure of the Ba^{2+} ions is lost by dangling O^{2-} ions and the repulsive Coulombic forces between the neighboring Ba^{2+} ions.

The low dipole surfaces in the barium magnetoplumbite system have at least two exposed Ba^{2+} ions. The polarizability of the ion and the reduction in allowed relaxation of neighboring atoms when the Ba^{2+} ions occupy subsurface positions creates the lowest energy surfaces when the Ba^{2+} ions are exposed. The coordination of the Ba^{2+} remains high even in their exposed surface positions. The coordination of the O^{2-} ions influences the surface energy of the surface but to a lesser degree than the exposure of Ba^{2+} ions.

4. {001} Surfaces

The calculated relaxed surface energies of the (001) terminations are given in Table XVI. The possible surface configurations were limited by the number of Al^{3+} ions on this plane. The surface energy calculation of the (001) surface in the mid-spinel block results in a surface energy of 9.21 J/m^2. Two different mirror plane configurations containing an exposed Ba^{2+} ion were attempted using a single unit cell. The first mirror plane configuration was calculated to have a surface energy of 3.93 J/m^2. As in the calcium and strontium magnetoplumbite systems, the relaxed surface energies calculated were much

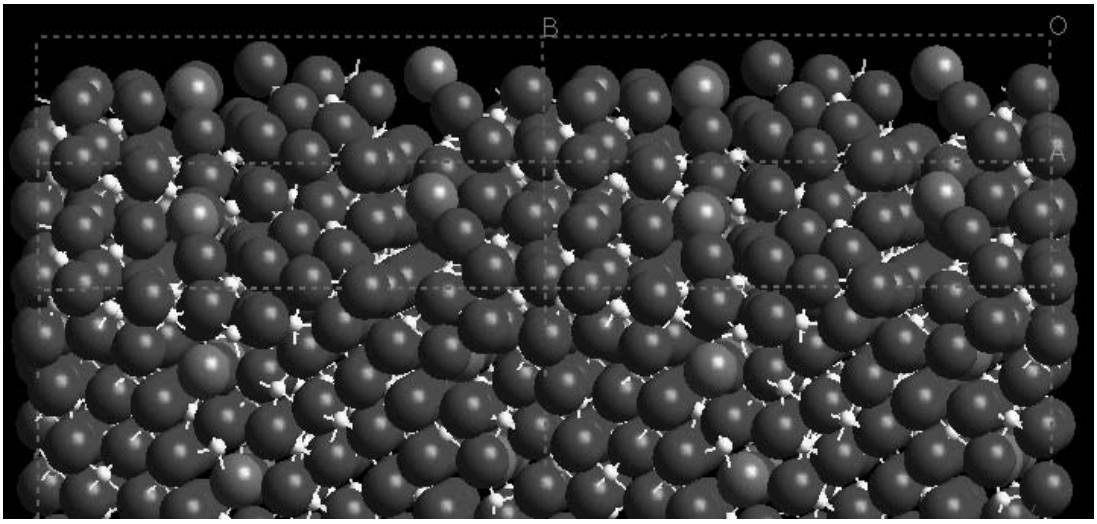

higher than

Figure 3.32. Relaxed {112} surface of barium magnetoplumbite.
Ions are color coded as follows: red - O^{2-}, white - Al^{3+}, and blue - Ba^{2+}. Surface image is of four blocks of unit cells of the modeled surface area.

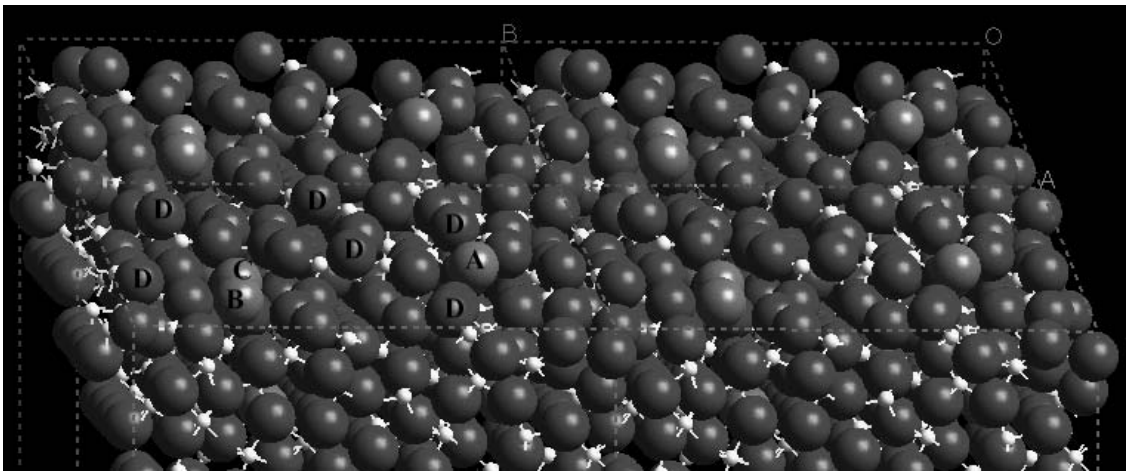

Figure 3.33. Relaxed {122} surface of barium magnetoplumbite.
Ions are color coded as follows: red - O^{2-}, white - Al^{3+}, and blue - Ba^{2+}. Surface image is of four blocks of unit cells of the modeled surface area. There are three exposed Ba^{2+} ions (A, B, and C). There are six O^{2-} ions (D) that relaxed to positions above the original surface. The first exposed Ba^{2+} ion (A) is coordinated to seven neighboring O^{2-} ions. The second and third exposed Ba^{2+} ions (B and C) relax to position of nearest neighbors.

Table XVI. Surface Energies of the Relaxed Barium Magnetoplumbite {001} Sufaces

Surface (2x2 unless noted)	**γ (J/m^2)**
Mid-Spinel Block (1x1)	9.21
Mid-Spinel Block	4.74
Mirror Configuration I	3.93
Mirror Configuration II	2.11
O^{2-} - Al^{3+} Layer Beneath Mirror Plane	1.03

minimum energy surfaces of all the other surfaces. The second configuration within the mirror plane was calculated to be 2.11 J/m^2, although this did not result in the lowest surface energy configuration.

A 2x2 supercell was used to allow for a greater number of possible configurations while maintaining the charge neutrality of the surface. This is because there are a greater number of ion positions to leave or remove from the exposed surface. The calculated surface energies of the mid-spinel block, 4.12 J/m^2, was higher than all of the low dipole moment surfaces. The later successes of the calculations on the calcium and strontium magnetoplumbite systems indicated that the O^{2-} and Al^{3+} layer just below the mirror plane ought to be the lowest surface energy configuration. The unrelaxed and relaxed minimum energy {001} surface configurations can be seen in Figures 3.34 and 3.35. A black line is included in these figures to indicate the rumpling of the O^{2-} ions.

The relaxations seen for this termination plane result in two main features. The first is the relaxation of the highly charged and small Al^{3+} ions. They relax to positions into the oxygen layer with no lateral relaxation. This results in a higher coordination of the Al^{3+} ions. The second feature is the change in the rumpling of the exposed O^{2-} layer. As noted earlier in this work, the large size of the Ba^{2+} ion causes rumpling in the bulk magnetoplumbite structure that lowers the symmetry and ultimately causes barium hexa-aluminate to adopt the two β-Alumina structures. The rumpling in the relaxed surface creates room to accommodate the relaxation of the Al^{3+} ions. In addition to a slight increase in the rumpling, O^{2-} ions neighboring the exposed Al^{3+} ions change the nature of rumpling. These O^{2-} ions, in the unrelaxed structure, occupy positions that are below their neighboring O^{2-} ions. In the relaxed structure, they occupy position above their neighboring O^{2-} ions.

F. Comparison of Magnetoplumbite Surfaces

A list of the relaxed surface energies of the magnetoplumbite systems is compiled in Table XVII. The general trend for these systems is that the calcium magnetoplumbite has a lower relaxed surface energy for a given orientation than the strontium magnetoplumbite surface. The increase in the size of the cation was first thought to be the cause of the

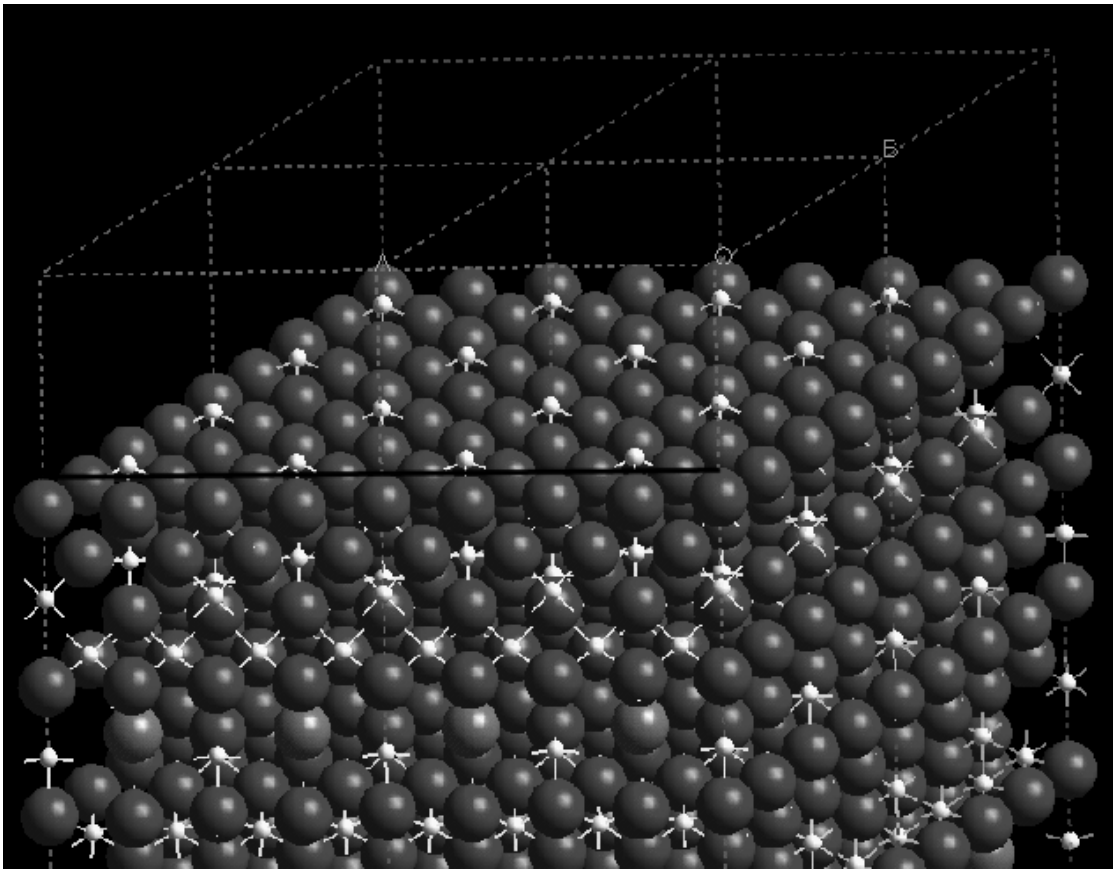

Figure 3.34. Unrelaxed {001} surface of barium magnetoplumbite.
Ions are color coded as follows: red - O^{2-}, white - Al^{3+}, and blue - Ba^{2+}. Surface image is of four blocks of unit cells of the modeled surface area. The black line shows the rumpling of the O^{2-} layer.

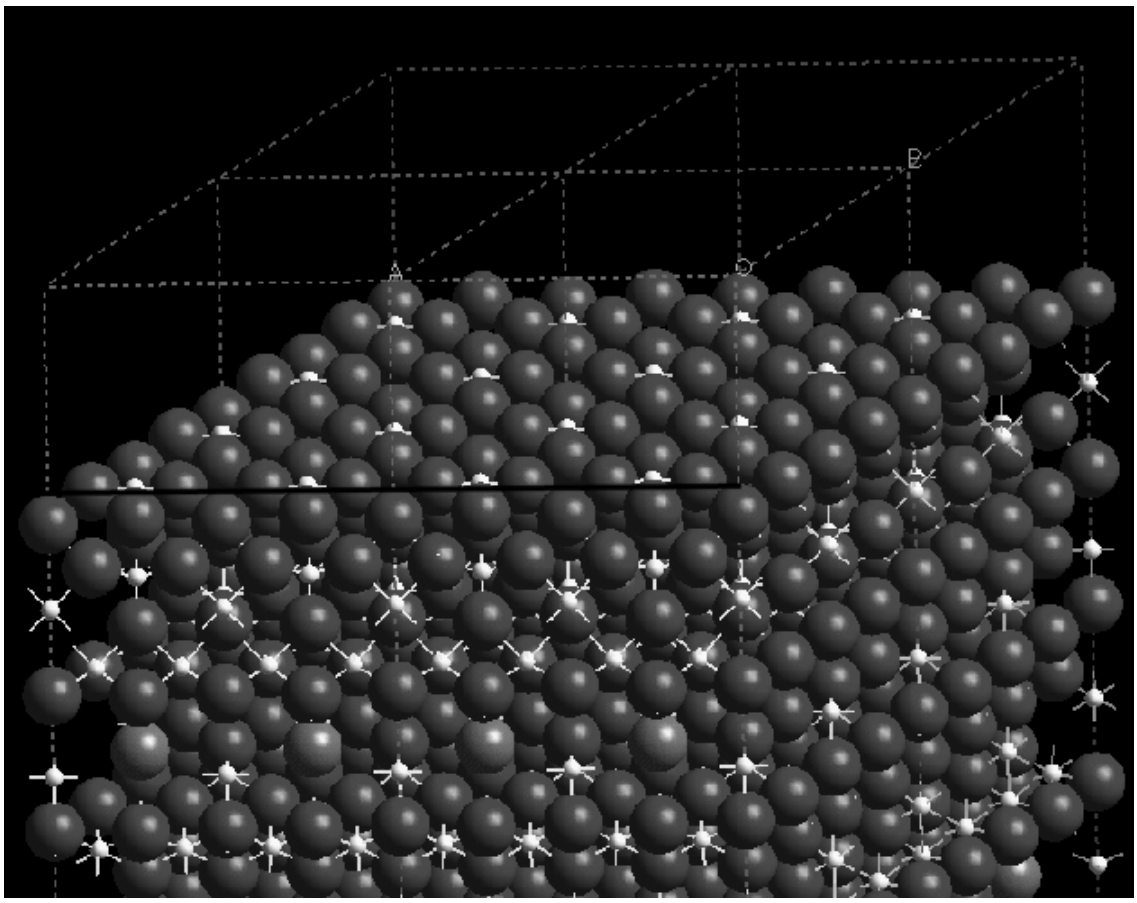

Figure 3.35. Relaxed {001} surface of barium magnetoplumbite.
Ions are color coded as follows: red - O^{2-}, white - Al^{3+}, and blue - Ba^{2+}. Surface image is of four blocks of unit cells of the modeled surface area. The black line shows the rumpling of the O^{2-} layer.

Table XVII. Calculated Surface Energies of Alkaline Earth Magnetoplumbites

Surface	Ca (J/m^2)	Sr (J/m^2)	Ba (J/m^2)
{100}	2.39	2.57	2.09
{110}	2.64	2.74	2.58
{120}	2.74	2.83	2.62
{012}	2.31	2.52	n/a
{112}	3.08	2.07	2.26
{122}	2.67	2.74	2.40
{001}	1.96	1.70	1.03

increase in the surface energy. This would indicate that the largest cation, Ba^{2+}, would result in the highest surface energy for a given orientation. This was not found to be the case. The theoretical barium magnetoplumbite structure has the lowest relaxed surface energy for a given orientation. The lower calculated values for the barium magnetoplumbite system seem to diminish the smaller cation, lower surface energy argument.

There still is the trend, where the smaller cation results in a lower surface energy for an orientation, exhibited by the calcium and strontium magnetoplumbite systems. There are two explanations that would lead to the conclusion that a larger ion would result in a lower surface energy. The first relates to the effect of the cation size on the size of the unit cell. An increase in the cation size results in a larger unit cell. This suggests that relaxation would be easier for the surface and subsurface ions in the larger cell. The second factor is that as the size of an ion increases, its polarizability also increases. The higher polarizability of the Sr^{2+} ion would seem to indicate that if the size of the atom is the cause for a difference in surface energy, it would be to the benefit of the larger ion. These two points seem at first to discount the size as the reason for the increase in surface energy for a given orientation.

The decrease in the surface energy for the barium magnetoplumbite is due to its larger size. The Ba^{2+} ion is too large for the mirror plane in this system. This causes the O^{2-} ions in the neighboring layers to rumple. This alters the bonding environment of ions on the termination planes. The rumpling in the bulk structure causes distortion of tetrahedral, octahedral, and dodecahedron sites near the mirror/conduction plane containing the Ba^{2+} ions of this system. The barium magnetoplumbite relaxed surface structures are closer to the rumpled bulk structure than in the relaxed calcium and strontium magnetoplumbite surfaces. Since the surface energy is the difference in energy between the structure of the surface atoms and the bulk structure, a smaller energy difference results in a lower surface energy. This leads to the barium magnetoplumbite surfaces having the lowest energies of these systems.

In the calcium and strontium magnetoplumbite systems, neither cation is large enough to distort the magnetoplumbite structure. The bulk structures of the calcium and strontium magnetoplumbite systems are essentially the same, both without the distortion of

the bulk structure. There are two ways in which the larger cation increases the surface energy. The larger unit cell has a higher surface area. Although more relaxation can occur, the surface structure is less dense for a given orientation as the cation size increases. This results in an increase in the surface energy. The second reason for the increase in the surface energy for the larger cation is due to the size of the mirror plane. In the mirror plane, the larger cation occupies more space thus making relaxation more difficult in the region of the mirror plane. These two factors result in the increase of the surface energy with increasing cation size. Although the Ba^{2+} is the largest of the cations, it does not reduce relaxation in the mirror plane. The barium magnetoplumbite structure has the rumpled O^{2-} layer. This rumpling opens up the mirror structure, allowing more relaxation to occur.

The {010}, {110}, {120}, {012}, and the {122} surfaces are the orientations where the calcium magnetoplumbite has the lower surface energy. In these orientations, the smaller cation size allows for atoms on and near the surface to relax to a greater extent while maintaining a dense surface structure. The dense surface structure hinders relaxation but increases the coordination of the surface atoms. The higher polarizability of the Sr^{2+} ion only reduces the site potential of the Sr^{2+} ion and its neighboring anions. It does not reduce the site potential of the other surface atoms. The less dense surface structure ultimately results in the higher surface energy found in the strontium magnetoplumbite system.

The subsurface relaxations also affect the surface energy. The smaller size of the cation allows the relaxation to occur more easily below the surface. This allows the divalent cation to reach the surface and the Al^{3+} ions on the surface to relax farther into the bulk. This effect of divalent size on surface energy is more important for surfaces with mirror planes perpendicular to the surface, i.e., the {100}, {110}, and {120} surfaces.

The only non-basal orientation where the strontium magnetoplumbite system has a lower surface energy than the calcium magnetoplumbite system is the {112} surface. Both systems have dangling O^{2-} ions but there is no exposed cation for the calcium magnetoplumbite surface. There is only one termination per symmetrically equivalent surface with low dipole moments for the {112} family of surfaces in the calcium magnetoplumbite system while there are four terminations in the strontium magnetoplumbite

system. The initial configuration of the low energy termination for the strontium magnetoplumbite system is not present in the calcium magnetoplumbite system. The larger unit cell size of the strontium magnetoplumbite system creates this additional low dipole moment termination plane. Attempts to model the termination corresponding to the same initial configuration in the calcium magnetoplumbite system resulted in a non-convergent energy calculation due to a high dipole moment.

In the {012} orientation, the larger size of the Sr^{2+} ion only allows one Sr^{2+} ion to relax to an exposed surface position. However, the second Ca^{2+} ion is also able to relax to the exposed surface position and thus a lower surface energy results. Based on results from the other orientations, it would be expected that in the {122} surface, the calcium magnetoplumbite surface energy would higher than that of the strontium magnetoplumbite surface since there are three exposed Sr^{2+} ions and only two exposed Ca^{2+} ions. The reduction in energy due to the extra exposed Sr^{2+} ion is lost because of the increase in coulombic energy between the neighboring Sr^{2+} and Al^{3+} ions.

The relaxed surface energy of the {001} surface decreases with increasing size of the divalent cation. Although the mirror plane is more crowded for strontium magnetoplumbite than for calcium magnetoplumbite, the relaxation that occurs is mostly normal to the surface. The larger cation thus permits greater relaxation to occur into and out of the more open spinel block. This allows the exposed Al^{3+} ions to relax to positions deeper in the structure, increasing its coordination; thus, the surface energy is lowered.

The calculated surface energies indicate that these crystals will exhibit plate-like geometries. These results also indicate that the geometries between systems will not be identical. The second lowest surface energy for the strontium magnetoplumbite system is the {112} orientation. The second lowest surface energy for the calcium magnetoplumbite system is the {012} orientation with the third lowest being the {100} surface. The {100} orientation is the fourth lowest in the strontium magnetoplumbite system. The barium magnetoplumbite system has {100} termination planes as the second lowest surface energy. This indicates that there will be subtle differences in their observed crystal geometries when processing conditions and reaction kinetics do not limit crystal growth.

G. Barium β(I)-Alumina Surfaces

There were 117 low dipole moment terminations modeled for the barium β(I)-alumina system. Unlike for the magnetoplumbite systems, all surface structure and energy calculations were performed on termination planes that have initially very low dipole moments, i.e. unrelaxed surfaces generated by METADISE. These include the {001} surfaces for the barium β(I)-alumina, since they did not require manual construction. Table XVIII lists all the calculated surface energies for the barium β(I)-alumina system.

1. Surfaces Other Than the {001} Surface

The major difference between the β-alumina and the magnetoplumbite phases is the difference in the mirror plane structure. This difference causes major differences in the calculated surface energies. The more open nature of the mirror plane region of the barium β(I)-alumina does not require that the divalent cation in the mirror plane must be small to accommodate relaxation of atoms closer to the surface.

The {100} termination plane, see Figure 3.36, does not have any exposed Ba^{2+} ions. Only the coordination of the surface atoms influences the surface energy, not the exposure of the Ba^{2+} ion, as is the case for the barium magnetoplumbite system. This, as stated above, is because of the more open nature of the mirror plane. The subsurface Ba^{2+} ions do not hinder relaxation. There are four O^{2-} ions (A) that have relaxed to positions above the unrelaxed surface plane. These are coordinated to two Al^{3+} ions each. There also are three dangling O^{2-} ions that are very close together. The repulsive forces between the ions increases the surface energy. It should be noted that these models allows the O^{2-} ions to be highly polarizable, although not quite as much as with the Ba^{2+} ion. The degree to which an ion can be polarized is reflected in the value of the spring constant, i.e., 27.29 eVA^2 for the O^{2-} ion and 14.78 eVA^2 for the Ba^{2+} ion. A lower value indicates a higher polarizability. The termination plane consisting of only O^{2-} and Al^{3+} ions can reduce its polarization energy by shifts in the O^{2-} shells and the ease in which Al^{3+} relax into the O^{2-} layers because of its small size. This combination of factors leads to a relatively low surface energy.

The lowest {110} surface energy configuration, as shown in Figure 3.37, consists of

Table XVIII. Relaxed Lowest Surface Energies of Barium β(I) Alumina

Surface	**γ (J/m^2)**
{010}	2.18
{110}	2.31
{101}	2.62
{201}	1.65
{102}	2.22
{111}	2.47
{112}	2.41
{001}	1.48

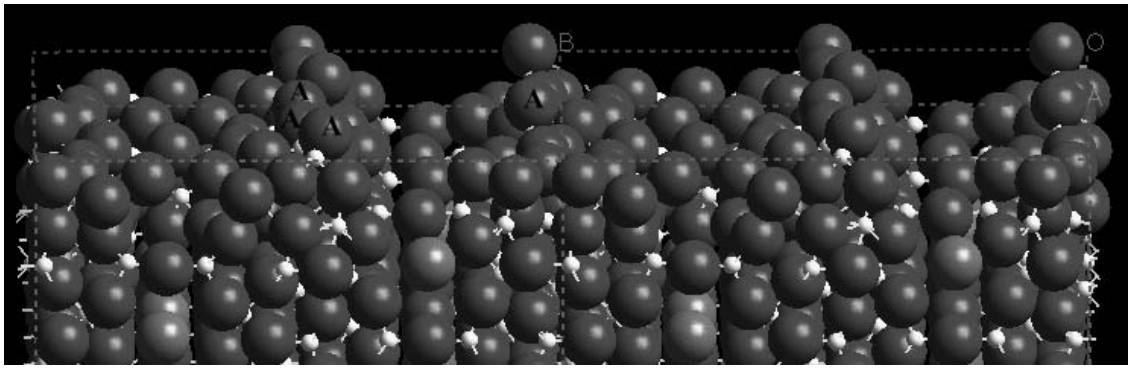

Figure 3.36. Relaxed {100} surface of barium β(I)-alumina.
Ions are color coded as follows: red - O^{2-}, white - Al^{3+}, and blue - Ba^{2+}. Surface image is of four blocks of unit cells of the modeled surface area. This surface structure has four dangling O^{2-} ions (A) that are each coordinated by two Al^{3+} ions. Three of these dangling O^{2-} ions occupies positions that are very close together.

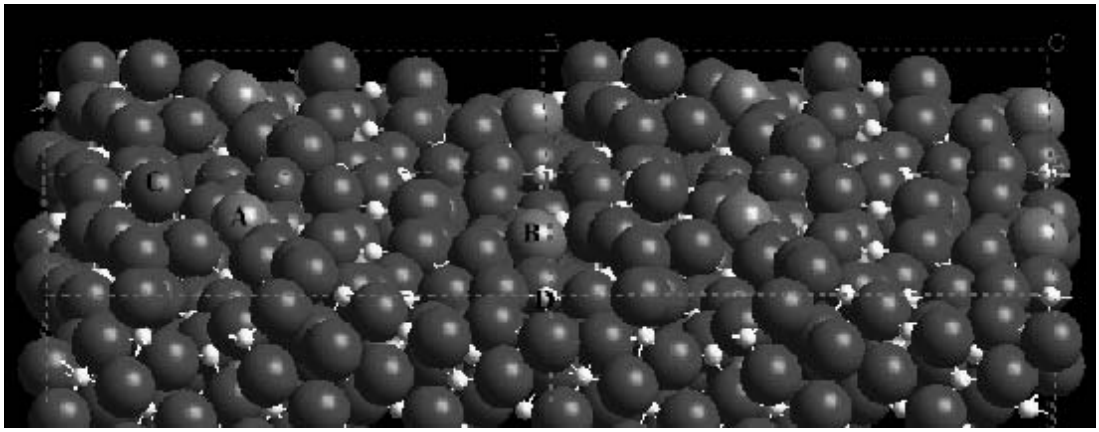

Figure 3.37. Relaxed {110} surface of barium β(I)-alumina.
Ions are color coded as follows: red - O^{2-}, white - Al^{3+}, and blue - Ba^{2+}. Surface image is of four blocks of unit cells of the modeled surface area. There are two exposed Ba^{2+} ions (A and B) occupy highly coordinated positions. There is one dangling O^{2-} ion (C) and one dangling Al^{3+} ion (D).

two exposed Ba^{2+} ions (A and B). These ions are highly coordinated by several O^{2-} nearest neighbors. There is one dangling O^{2-} ion (C) coordinated to three Al^{3+} ions. There is an Al^{3+} ion (D), at the corner of the surface cell, that occupies an exposed surface position. Although it has four nearest neighboring O^{2-} ions, this position, due to the high charge and small size of the Al^{3+} ion, leads to an increase in its site potential. This causes an increase in the surface energy of this orientation. The highly coordinated Ba^{2+} and O^{2-} ions on the surface keep the surface energy at a moderate value.

The {101} surface, see Figure 3.38, and the {201} surface, see Figure 3.39, orientations do not have exposed Ba^{2+} ions. They have very different surface energies, with the {201} surface having a much lower value than that of the {101} surface. The most obvious difference in the structures is in the arrangement of the rows of O^{2-} ions. In the {101} surface structure, the O^{2-} ions remain in two straight rows with a bridging Al^{3+} ion between them. In the {201} surface structure, these similar rows of O^{2-} ions have relaxed to a zig zag type pattern. A black line in each of these figures show the alignment of the O^{2-} ions. The {201} surface does not have the bridging Al^{3+} ions on the plane containing the rows of O^{2-} ions as in the {101} surface structure. This allows the O^{2-} ions in the {201} orientation to relax without having the polarization and repulsive energy terms increase dramatically. This relaxation of the O^{2-} ions lowers the resultant surface energy of the {201} orientation, to the second lowest overall value.

The {102}, {111}, and {112} surfaces have similar structures, as shown in Figures 3.40 - 3.42, respectively. One difference is the number of exposed Ba^{2+} ions. There are four exposed Ba^{2+} ions (A) in the {102} structure, two exposed Ba^{2+} ions (A) in the {111} surface structure, and three exposed Ba^{2+} ions (A) in the {112} surface structure. Each of these exposed Ba^{2+} ions occupy highly coordinated positions. The need for subsurface relaxation, seen in the magnetoplumbite structures, is not necessary for low surface energies in the barium β(I)-alumina system, due to the different mirror plane configuration. However, the number of exposed Ba^{2+} ions does influence the surface energy of the termination plane. Increasing the number of Ba^{2+} ions decreases the surface energy of similar structures due to the high polarizability of the Ba^{2+} ions. A higher polarizable ion requires less energy to

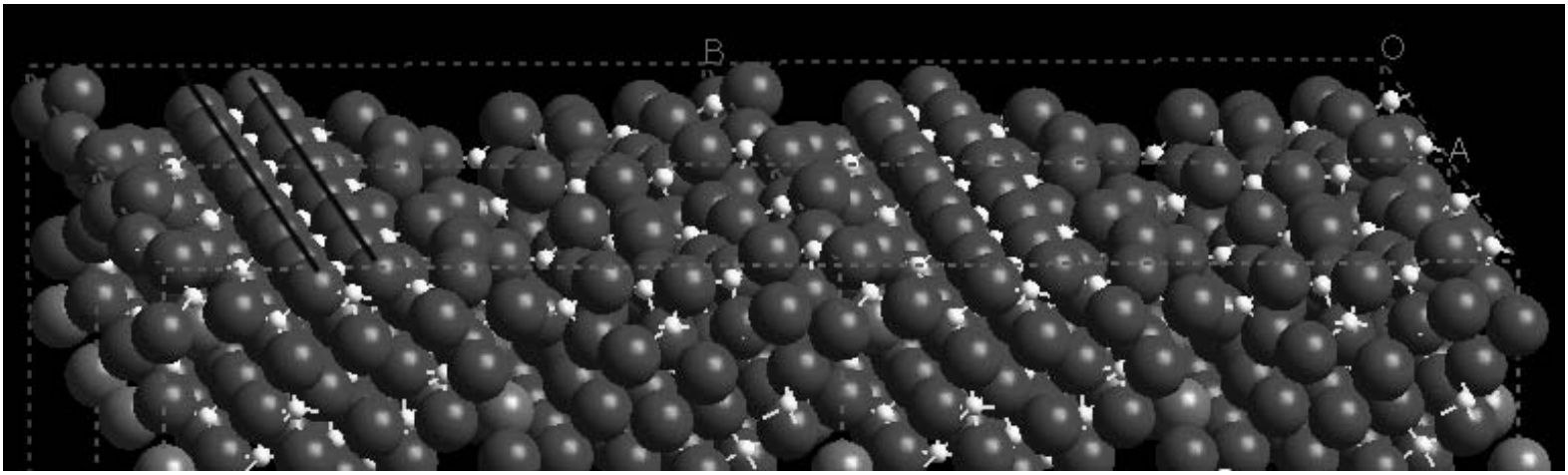

Figure 3.38. Relaxed {101} surface of barium β(I)-alumina.
Ions are color coded as follows: red - O^{2-}, white - Al^{3+}, and blue - Ba^{2+}. Surface image is of four blocks of unit cells of the modeled surface area. This surface has one row of aligned O^{2-} ions with bridging Al^{3+} ions between a slightly less aligned row of O^{2-} ions shown by the black lines. There are no exposed Ba^{2+} ions for this surface.

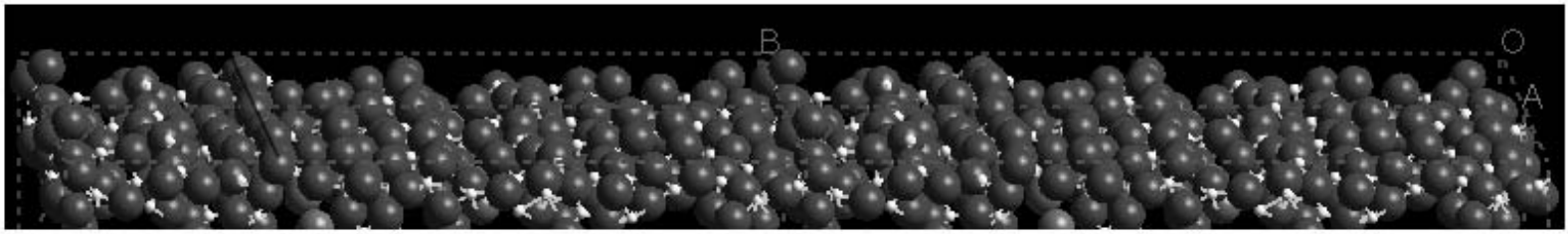

Figure 3.39. Relaxed {201} surface of barium β(I)-alumina.
Ions are color coded as follows: red - O^{2-}, white - Al^{3+}, and blue - Ba^{2+}. Surface image is of four blocks of unit cells of the modeled surface area. This surface has rows of O^{2-} ions that relax to a zig-zag pattern as shown by the black line. There are no exposed Ba^{2+} ions.

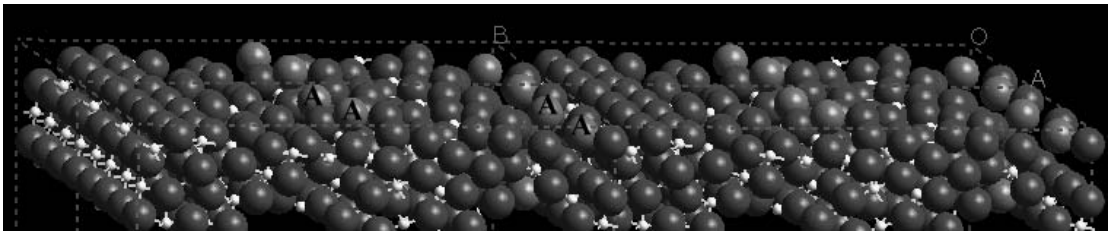

Figure 3.40. Relaxed {102} surface of barium β(I)-alumina.
Ions are color coded as follows: red - O^{2-}, white - Al^{3+}, and blue - Ba^{2+}. Surface image is of four blocks of unit cells of the modeled surface area. There are four exposed Ba^{2+} ions (A) in this relaxed surface.

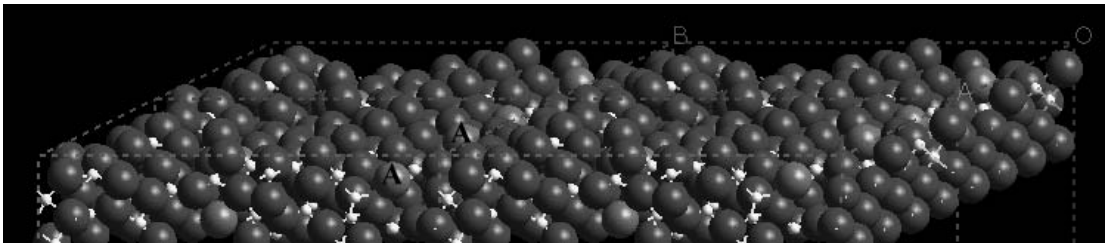

Figure 3.41. Relaxed {111} surface of barium β(I)-alumina.
Ions are color coded as follows: red - O^{2-}, white - Al^{3+}, and blue - Ba^{2+}. Surface image is of four blocks of unit cells of the modeled surface area. There are two exposed Ba^{2+} ions (A) in this relaxed surface.

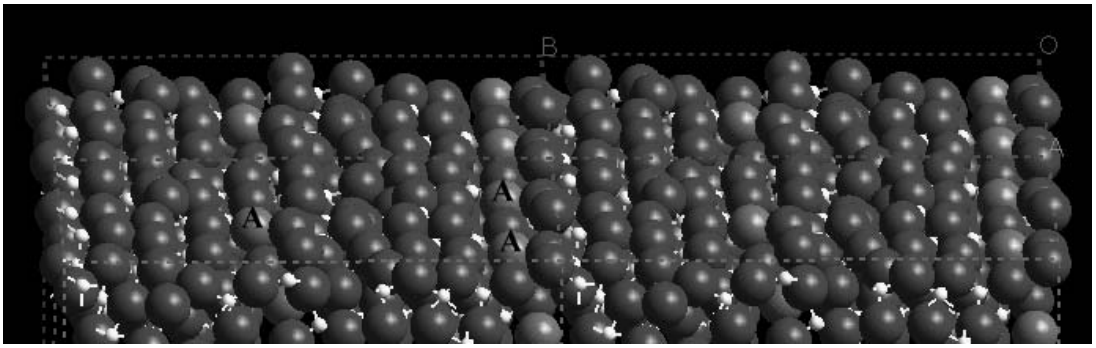

Figure 3.42. Relaxed {112} surface of barium β(I)-alumina.
Ions are color coded as follows: red - O^{2-}, white - Al^{3+}, and blue - Ba^{2+}. Surface image is of four blocks of unit cells of the modeled surface area. There are three exposed Ba^{2+} ions (A) in this relaxed surface.

result in the same degree of polarization than for a lower polarizable ion. The polarizability of the Ba^{2+} ion is greater than that of the O^{2-} ions. This greater polarizability decreases the polarization energy of the surface and thus reduces the surface energy.

The {112} termination plane has the same type of disorder in the rows of O^{2-} ions as seen in the {201} surface structure. This does not lower the surface energy substantially though. The {102} and {111} surfaces both keep the O^{2-} in horizontal lines along the surface as indicated by a black line in the figures, but for the {102} surface, the O^{2-} ions have an alternating relaxation in and out of the surface plane. This relaxation, along with the number of exposed Ba^{2+} ions, lowers the calculated surface energy for this orientation.

The relaxation of Ba^{2+} ions to the surface is not necessary to ensure that a surface will have a low energy. Given similar structures, though, an increase in the number of exposed Ba^{2+} ions decreases the polarization energy of the surface and therefore the surface energy. The main influence of the surface energy of these orientations is due to the O^{2-} ion position. Surfaces with constraints on the relaxation of the rows of O^{2-} ions show an increase in surface energies.

2. {001} Surface

The lowest surface energy for the {001} surfaces is for the termination at the O^{2-} and Al^{3+} layer below the mirror plane containing the barium vacancy and Reidinger defect. The relaxation for the {001} surface is similar to that of the magnetoplumbite systems. The unrelaxed and relaxed surface structures can be seen in Figures 3.43 and 3.44, respectively. The Al^{3+} ions relax to positions lower in the bulk structure. In the unrelaxed structure, there is some rumpling of the exposed O^{2-} layer, as seen in the barium magnetoplumbite {001} surface. The O^{2-} layer immediately below the conduction plane shows a small increase in rumpling to accommodate the relaxed Al^{3+} ions, although it is not evident by visual examination. This increases the coordination of the Al^{3+} ions and reduces the polarization energy of the surface. The similarity of the surface structure to the bulk structure results in a small difference in the surface and bulk energies. This small difference leads to a very low surface energy structure with a calculated value of 1.48 J/m^2. This was also seen in the

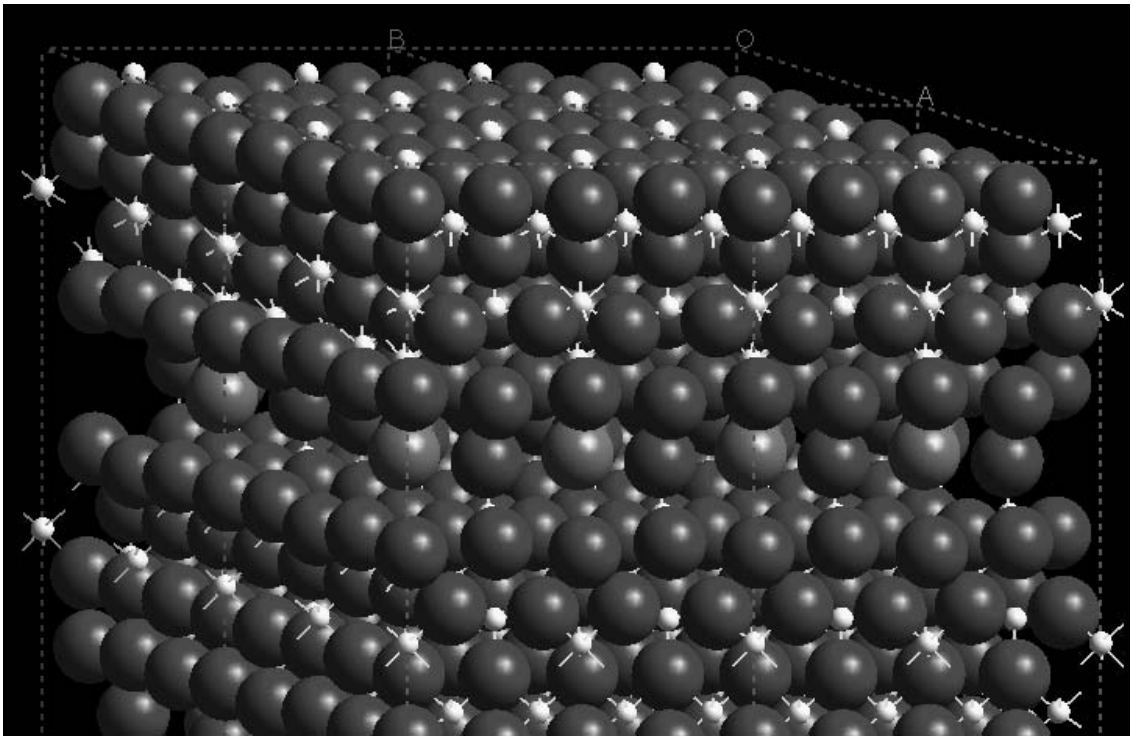

Figure 3.43. Unrelaxed {001} surface of barium β(I)-alumina.
Ions are color coded as follows: red - O^{2-}, white - Al^{3+}, and blue - Ba^{2+}. Surface image is of four blcoks of unit cells of the modeled surface area. The unrelaxed surface shows rumpling in the O^{2-} layer.

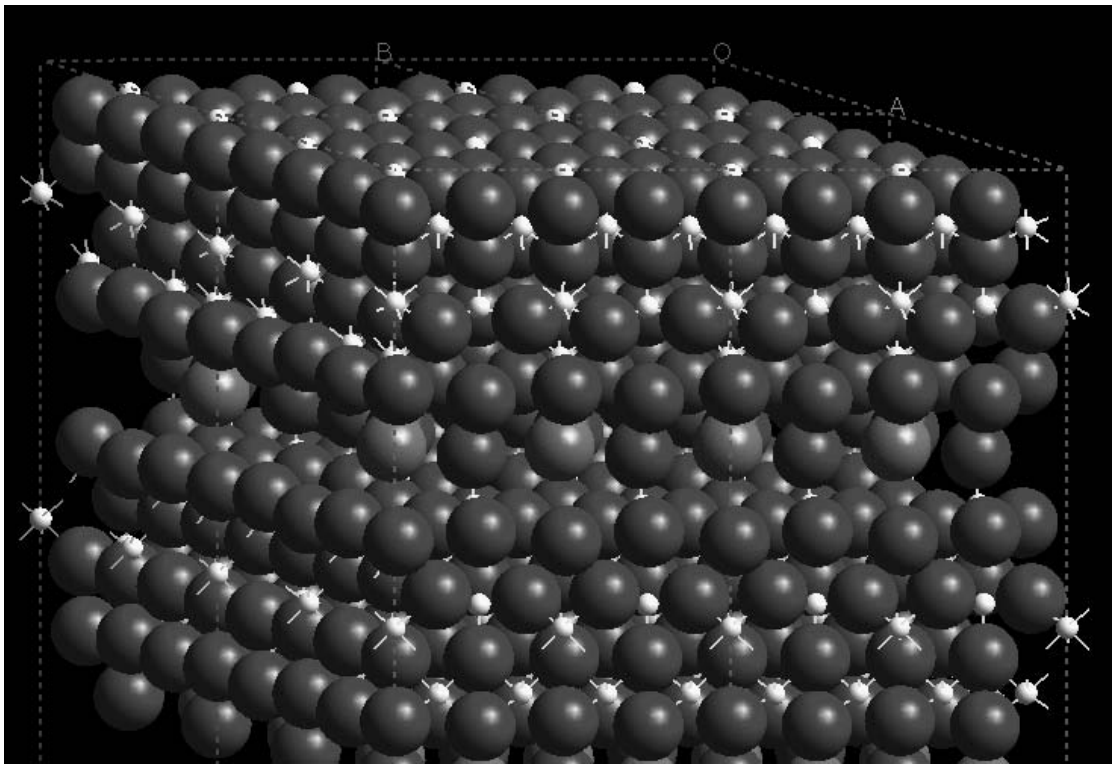

Figure 3.44. Relaxed {001} surface of barium β(I)-alumina.
Ions are color coded as follows: red - O^{2-}, white - Al^{3+}, and blue - Ba^{2+}. Surface image is of four blcoks of unit cells of the modeled surface area. The O^{2-} layer has a slight increase in rumpling although it is not evident by visual examination.

barium magnetoplumbite system.

We note that the calculation of the lowest surface energy {001} surface in the barium β(I)-alumina led to lower surface energy calculations for the magnetoplumbite systems.

H. Barium β(II)-Alumina Surfaces

There were 841 terminations modeled for the barium β(II)-alumina system. As in the barium β(I)-alumina surfaces, all surface structure and energy calculations were performed on termination planes that have initially very low dipole moments normal to the surface, as generated by METADISE. This includes the {001} surface. One problem encountered in the barium β(II)-alumina system was that for a large number of surfaces, the calculation of the surface energy did not converge because of dipole moments being created normal to the surface or for which the calculations terminated because of excessive polarization.

1. Surfaces Other Than The {001} Surface

Table XIX contains the lowest calculated surface energy for each of the orientations in the barium β(II)-alumina system. The major difference between the β-alumina phases and the magnetoplumbite systems is in the mirror plane structure. This causes large differences in the calculated surface energies. The more open nature of the mirror plane does not require that the divalent cation in the mirror plane be small to accommodate relaxation of atoms closer to the surface. This structure does, however, have a Ba^{2+} ion located in the spinel block. The "defect" is accommodated by the removal of two O^{2-} ions and a Al^{3+} ion. This gives more room around the mid-spinel Ba^{2+} ion for atoms to relax.

The excess Ba^{2+} ions and their positions in the lattice (i.e., the Ba^{2+} ion in the spinel block) results in an exposed Ba^{2+} ion on virtually all termination planes. This means that the coordination of the surface atoms and the polarization energy, due to the open nature of the structure, are the major factors in determining which surfaces will have the lowest energies.

The {100} surface can be seen in Figure 3.45. There are two exposed Ba^{2+} ions but no dangling O^{2-} ions. One Ba^{2+} ion (A) has five coordinating O^{2-} ions in a plane nearly parallel to the surface. The other exposed Ba^{2+} ion (B) is located in the mirror plane which is

Table XIX. Relaxed Lowest Surface Energies of Barium β(II) Alumina

Surface	**γ (J/m^2)**
{010}	2.14
{110}	1.97
{120}	2.88
{101}	1.65
{201}	2.15
{102}	2.32
{121}	2.82
{111}	2.81
{112}	2.06
{122}	3.04
{001}	1.25

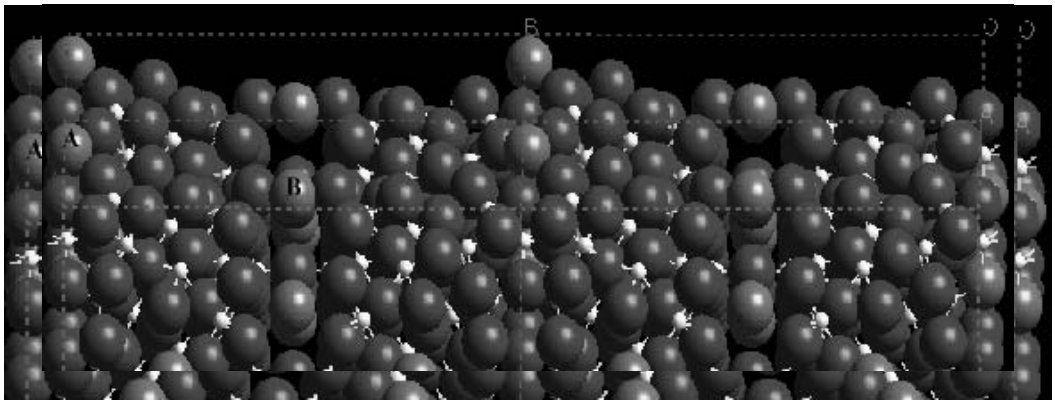

Figure 3.45. Relaxed {100} surface of barium β(II)-alumina.
Ions are color coded as follows: red - O^{2-}, white - Al^{3+}, and blue - Ba^{2+}. Surface image is of four blocks of unit cells of the modeled surface area. There are no dangling O^{2-} ions and two exposed Ba^{2+} ions (A and B). The first (A) is coordinated with five O^{2-} ions in a plane nearly parallel to the surface. The second (B) is located in the mirror plane that is perpendicular to the surface.

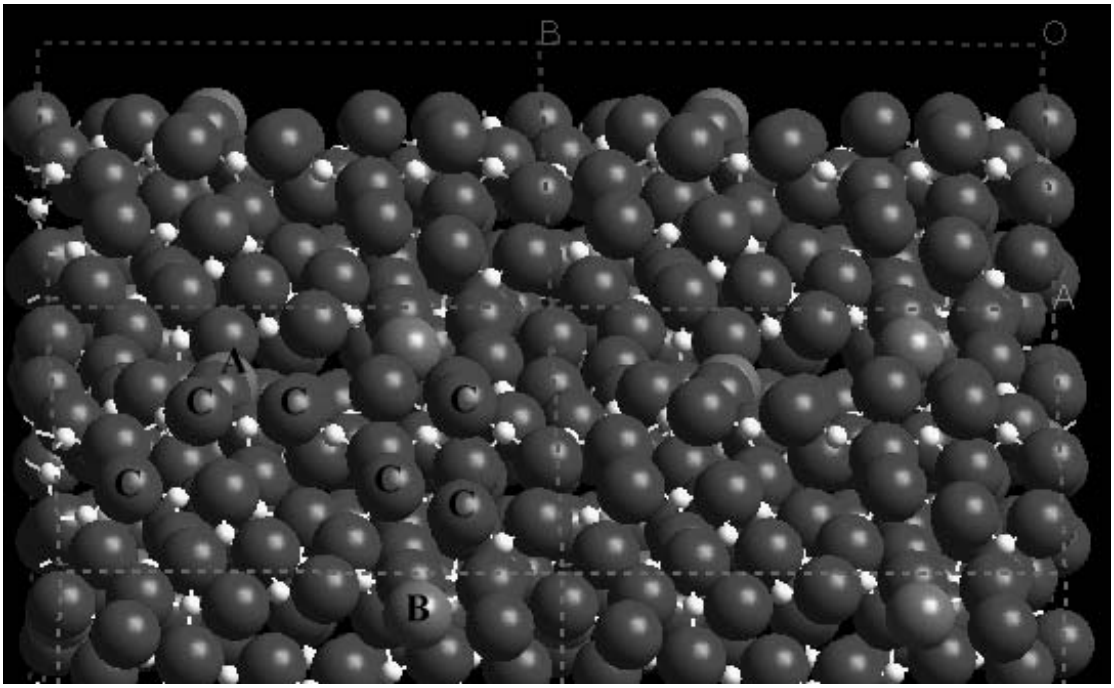

Figure 3.46. Relaxed {110} surface of barium β(II)-alumina.
Ions are color coded as follows: red - O^{2-}, white - Al^{3+}, and blue - Ba^{2+}. Surface image is of four blocks of unit cells of the modeled surface area. There are two exposed Ba^{2+} ions (A and B) and six dangling O^{2-} ions (C). The first Ba^{2+} ion (A) occupies a highly coordinated position. The second Ba^{2+} ion (B) is coordinated by five O^{2-} ions with a six that is slightly further away. Each of the dangling O^{2-} ions are coordinated with two Al^{3+} ions.

perpendicular to the surface. This mirror plane has a very open structure which leads to a highly polarized configuration.

Figure 3.46 shows the {110} surface, which has two surface Ba^{2+} ions (A and B) and several dangling O^{2-} ions (C). One of the surface Ba^{2+} ions (A) occupies a relaxed position that is highly coordinated with its neighboring O^{2-} ions. The second Ba^{2+} ion (B) has five O^{2-} close neighbors and a sixth that is further away. Each dangling O^{2-} ion has two Al^{3+} ions coordinated to it.

Figure 3.47 is of the {120} surface. There are five exposed Ba^{2+} ions. Three (A, B, and C) are coordinated to five O^{2-} lying nearly in the same plane as the Ba^{2+} ions. Another Ba^{2+} ion (D) has six O^{2-} neighbors. This Ba^{2+} ion has relaxed to a position above the unrelaxed surface plane. The final Ba^{2+} ion (E) has four neighboring O^{2-} ions in a plane slightly lower than the Ba^{2+} ion position. There is also an open region containing O^{2-} and Al^{3+} ions. This open region allows a highly polarized structure. This highly polarized structure increases the polarization energy resulting in its high surface energy value.

The {101} surface structure can be seen in Figure 3.48. The first feature of this surface that can be seen is the open structure containing the single exposed Ba^{2+} ion. It has several nearest neighboring O^{2-} ions layered almost perpendicular to the surface. This is the layer below the conduction plane. There appears to be very little relaxation occurring in this O^{2-} layer. There also several exposed Al^{3+} ions. Each of these Al^{3+} ions is coordinated with three O^{2-} ions. The resultant surface energy is substantially lower than would be expected due to the high number of exposed Al^{3+} ions.

Figure 3.49 shows the relaxed {201} surface structure. This surface has six exposed Ba^{2+} ions. Overall, this structure has the lowest surface atom density. A low surface density causes an increase in the polarization energy. The Ba^{2+} ion has a higher polarizability than the O^{2-} ion. The high number of these surface Ba^{2+} ions reduces the total polarization energy, relative to a surface with only O^{2-} and Al^{3+} ions, so that the calculated surface energy is of a intermediate value of 2.15 J/m^2.

The {102} surface, see Figure 3.50, is similar in structure to the {100} and {101} surfaces. Each of these structures has an open channel where the conduction plane meets the

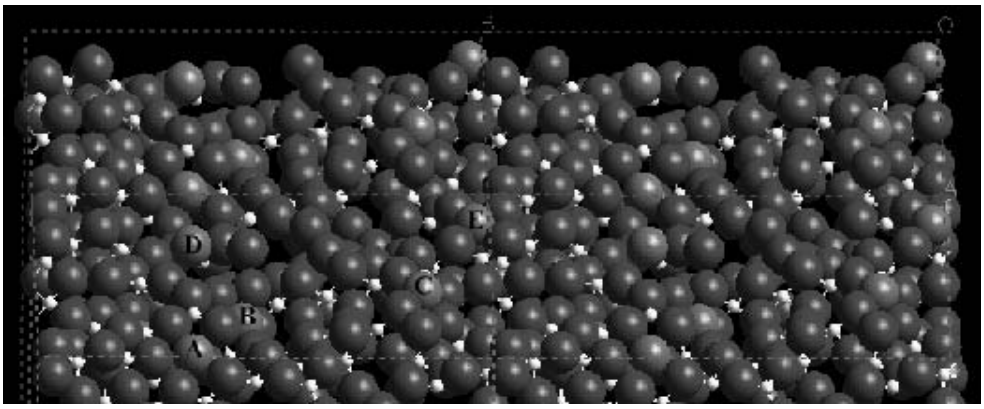

Figure 3.47. Relaxed {120} surface of barium β(II)-alumina.
Ions are color coded as follows: red - O^{2-}, white - Al^{3+}, and blue - Ba^{2+}. Surface image is of four blocks of unit cells of the modeled surface area. Three of the five exposed Ba^{2+} ions (A, B, and C) are coordinated to five O^{2-} ions lying nearly in the same plane as the Ba^{2+} ions. The fourth Ba^{2+} ion (D) has six neighboring O^{2-} ions and has relaxed to a position above the original surface. The fifth Ba^{2+} ion (E) is coordinated to four O^{2-} ions in a plane slightly below the Ba^{2+} ion.

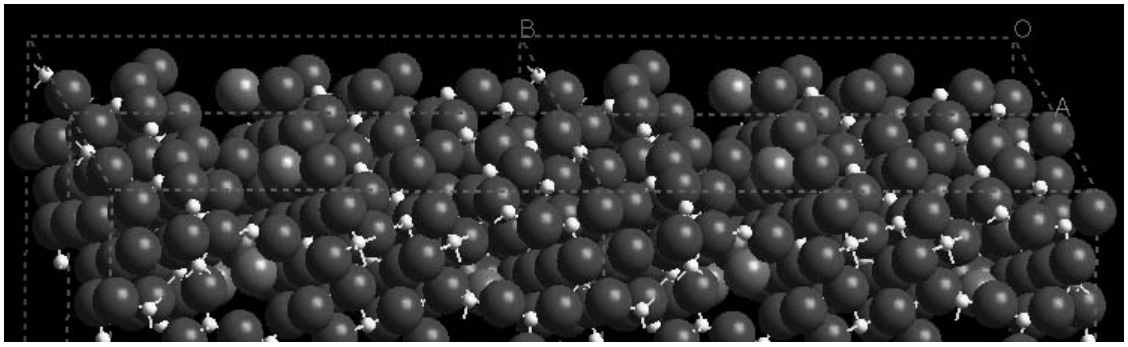

Figure 3.48. Relaxed {101} surface of barium β(II)-alumina.
Ions are color coded as follows: red - O^{2-}, white - Al^{3+}, and blue - Ba^{2+}. Surface image is of four blocks of unit cells of the modeled surface area. There is one exposed Ba^{2+} ion in a position to one side of an open channel. There are several exposed Al^{3+} ions.

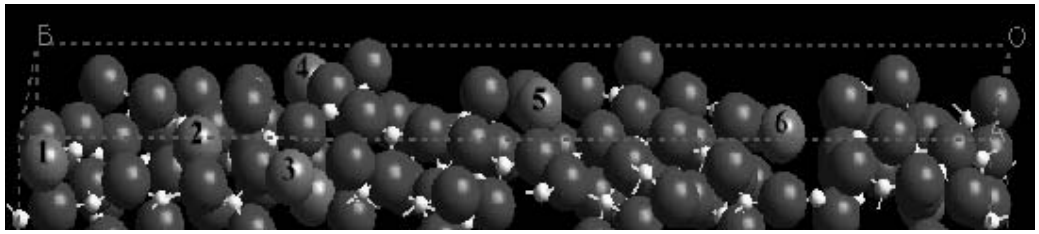

Figure 3.49. Relaxed {201} surface of barium β(II)-alumina.
Ions are color coded as follows: red - O^{2-}, white - Al^{3+}, and blue - Ba^{2+}. Surface image is of one unit cells of the modeled surface area. There are six exposed Ba^{2+} ions. This surface structure has a low surface ion density.

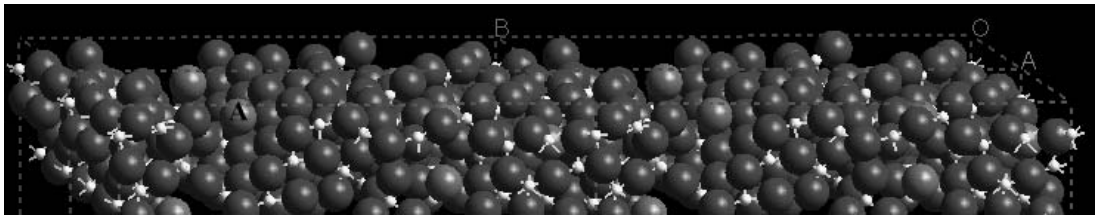

Figure 3.50. Relaxed {102} surface of barium β(II)-alumina.
Ions are color coded as follows: red - O^{2-}, white - Al^{3+}, and blue - Ba^{2+}. Surface image is of four blocks of unit cells of the modeled surface area. There is one exposed Ba^{2+} ion (A) for this surface that lies in an open channel.

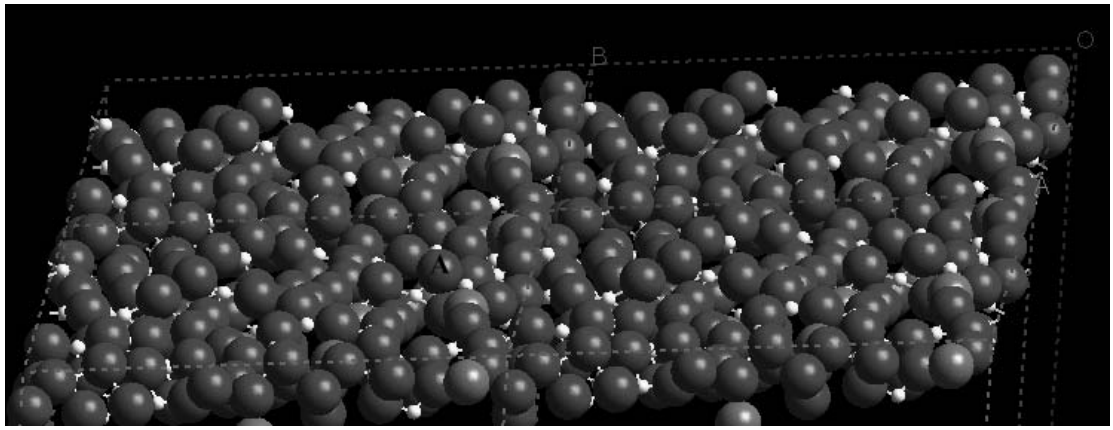

Figure 3.51. Relaxed {121} surface of barium β(II)-alumina.
Ions are color coded as follows: red - O^{2-}, white - Al^{3+}, and blue - Ba^{2+}. Surface image is of four blocks of unit cells of the modeled surface area. There is one dangling O^{2-} ion (A). Although there are none of the Ba^{2+} ions are exposed, there are five very near the surface, each covered by O^{2-} ions.

surface. The {102} has one exposed Ba^{2+} ion (A) in this channel. The distance between this Ba^{2+} ion and its neighboring O^{2-} ions is larger than the distance in the {101} surface for the corresponding arrangement of atoms. The coulombic energy is proportional to one over the square of the distance between ions. The larger distances between the oppositely charged ions increases the coulombic energy relative to the {101} structure and thus a higher surface energy for this orientation.

The calculated surface energies for the {102} and {100} surfaces are fairly close, 2.32 J/m^2 and 2.14 J/m^2 respectively. The mirror plane lies at a 45 degree angle to the surface in the {102} orientation. In the {100} orientation, the mirror plane is perpendicular to the surface and there is an additional exposed Ba^{2+} ion (B). The orientation relative to the normal to the surface of the mirror plane in the {100} surface allows for additional relaxation of the Ba^{2+} ion toward the surface. This additional relaxation and exposed Ba^{2+} ion in the {100} result in the surface structure of the {102} orientation having a higher surface energy relative to the {100} orientation.

The {121} surface structure is shown in Figure 3.51. There are five Ba^{2+} ions near the surface. Each is almost completely surrounded by several neighboring O^{2-} ions. These Ba^{2+} ions also have Al^{3+} ions that are relatively close. There is one dangling O^{2-} ion (A) coordinated with one Al^{3+} ion. The dangling O^{2-} ion and the increase in coulombic energy between the neighboring Ba^{2+} and Al^{3+} ions results in the high surface energy of 2.82 J/m^2.

Figure 3.52 shows the {111} surface structure. This relaxed surface has one exposed Ba^{2+} ion which is coordinated to four O^{2-} ions that lie in the surface plane. The surface has a close-packed O^{2-} layer. The high surface density and the coordination of the exposed Ba^{2+} ion was expected to result in a low surface energy for this structure. This is not the case. After a more detailed examination of the calculation, it was determined that the high surface energy is due to repulsive forces between neighboring O^{2-} ions.

The {112} surface, see Figure 3.53, has three exposed Ba^{2+} ions, one dangling Al^{3+} ion (A), and no dangling O^{2-} ions. There is a channel as in the {102} and {101} surfaces. The channel in the {112} orientation is more obvious, by visual examination, than in either of the {102} and {101} surfaces. The O^{2-} ions in the channel are staggered, coordinated with

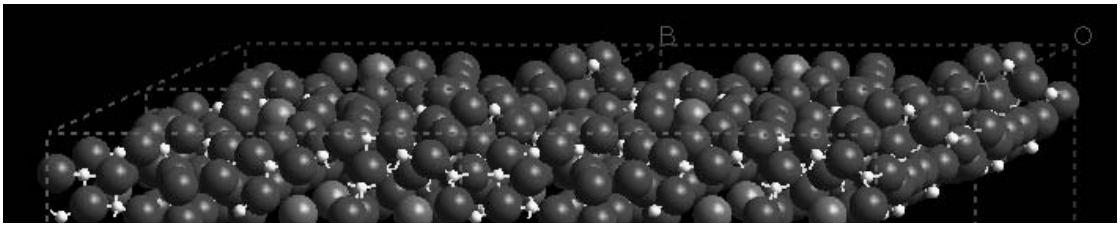

Figure 3.52. Relaxed {111} Surface of Barium β(II)-Alumina.
Ions are color coded as follows: red - O^{2-}, white - Al^{3+}, and blue - Ba^{2+}. Surface image is of four blocks of unit cells of the modeled surface area. There is one exposed Ba^{2+} ion coordinated to four O^{2-} ions. This surface has a dense packing of the O^{2-} ions.

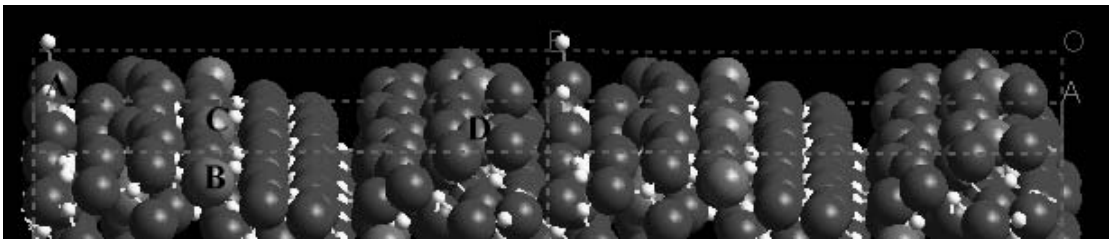

Figure 3.53. Relaxed {112} surface of barium β(II)-alumina.
Ions are color coded as follows: red - O^{2-}, white - Al^{3+}, and blue - Ba^{2+}. Surface image is of four blocks of unit cells of the modeled surface area. There is one dangling Al^{3+} ion (A) and three exposed Ba^{2+} ions (B, C, and D). Two of the exposed Ba^{2+} ions (B and C) lie in a line containing staggered O^{2-} ions. The third Ba^{2+} ion is coordinated by five O^{2-} ions.

bridging Al^{3+} ions. Two of the exposed Ba^{2+} ions (B and C) lie in a line containing the staggered O^{2-} ions than run parallel to the channel. These positions are coordinated to six exposed O^{2-} ions. The third exposed Ba^{2+} ion (D) is coordinated to five O^{2-} ions. There are also Al^{3+} ions that occupy positions fairly close to all three of the Ba^{2+} ions. This surface has a relatively low calculated surface energy, 2.06 J/m^2.

Figure 3.54 is of the {122} surface structure. There are six exposed Ba^{2+} ions in this structure. Four of the exposed Ba^{2+} ions (A, B, C, and D) have only three coordinated O^{2-} in the surface plane. One Ba^{2+} ion (E) is coordinated by only two O^{2-} ions. The last Ba^{2+} ion (F) has five neighboring O^{2-} ions that lie in a plane below it. There are also six dangling O^{2-} ions (G). The low coordination of the exposed Ba^{2+} ions and the very high number of dangling O^{2-} ions results in the highest calculated surface energy for the barium β(II)-alumina structure.

The {122}, {120}, {121}, and {111} surfaces have the highest calculated surface energy values. The {122} orientation has low coordinated Ba^{2+} ions and a high number of dangling O^{2-} ions. The {120} surface has one low coordinated, dangling Ba^{2+} ion and a low density of ions on the surface. The high surface energy of these two surfaces was expected by visual examination of the surface images. The high surface energies of the {111} and {121} surfaces were not obvious from visual examination. In the {111} surface, the surface is close-packed and the exposed Ba^{2+} ion occupies a highly coordination position. The {111} surface owes it high surface energy to high repulsive energy between closely neighboring O^{2-} ions. The {121} has one dangling O^{2-} ion but its high surface energy is due to the short distances between the like-charged Ba^{2+} and Al^{3+} ions which increases the coulombic energy of this surface.

The {101} orientation has the lowest, calculated non-basal surface energy. The {112} orientation has the third lowest non-basal calculated surface energy. These two surfaces have channels in which the exposed Ba^{2+} ions are situated and are the result of the open mirror plane structure of barium β(II)-alumina. The channels allow a greater degree of relaxation for the surface atoms. The relaxed structures also have a high degree of atom density without a high degree of repulsion energy between neighboring O^{2-} ions. These two

factors lead to

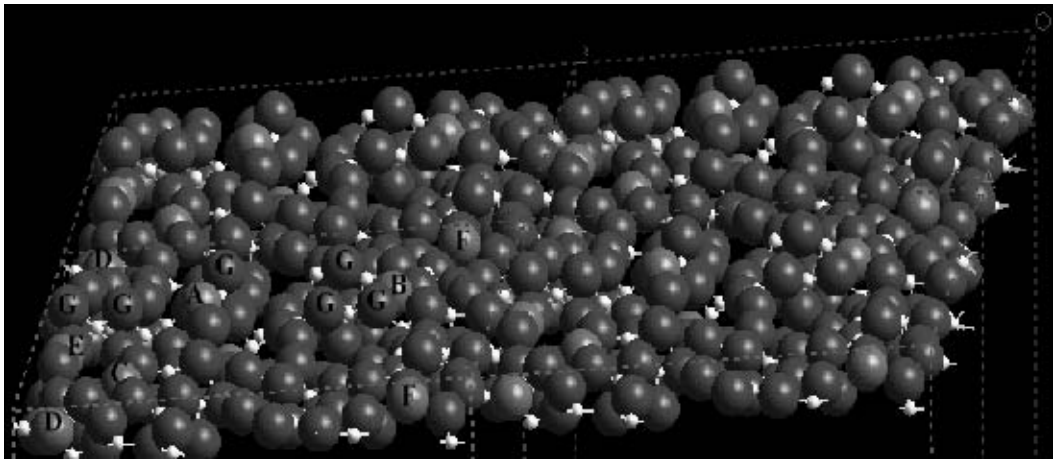

Figure 3.54. Relaxed {122} surface of barium β(II)-alumina.
Ions are color coded as follows: red - O^{2-}, white - Al^{3+}, and blue - Ba^{2+}. Surface image is of four blocks of unit cells of the modeled surface area. Four of the six exposed Ba^{2+} ions (A, B, C, and D) have only three coordinated O^{2-} ions. The fifth Ba^{2+} ion (E) is coordinated by only two O^{2-} ions. The sixth Ba^{2+} ion (F) has five neighboring O^{2-} ions that lie in a plane below it. There are also six dangling O^{2-} ions (G).

the low calculated surface energy for these orientations. The higher surface energy of the {112} orientation is due to the dangling Al^{3+} ion.

The relaxed {102} and {100} surfaces also have channels as in the {101} and {112} orientations. The channel on the {100} surface is perpendicular to the surface and does not allow the same degree of relaxation that is possible in the {101} and {112} orientations. The higher surface energy for the {102} orientation is not due to constrainment of relaxation. The relaxed {102} surface does allow more relaxation for atoms on the surface. The exposed Ba^{2+} ion in the channel of the {102} surface has longer bonds than in the other channeled surfaces. These longer bond distances increase the surface energy of this surface.

The density of the surface atoms is an important factor in the calculated surface energy for a given orientation. The {201} orientation is a good example. This orientation has a very low density in the relaxed structure. The decrease in surface energy due to the ease of relaxation is lost due to the lower coordination of the surface atoms. A dense surface structure can also cause an increase in repulsive forces if neighboring atoms are overly constrained, as seen in the {111} surface. The {110} surface strikes a balance between these two extremes. This surface has a high surface density without the constraints on relaxation. This surface has the second lowest calculated non-basal surface energy.

The dipole moments created by the atoms' positions in this open lattice caused some problems during the surface energy calculations. On many surfaces, excessive polarization occurred causing the calculation to terminate. These usually occurred with O^{2-} ions but were not limited to just that ion type. Relaxation increased the dipole moment normal to the surface in some terminations. These calculations resulted in divergent energies which terminated the calculation.

2. {001} Surface

The lowest surface energy for the {001} surfaces is located at the O^{2-} and Al^{3+} plane below the mirror plane. The resultant surface energy calculation is identical for the plane below either mirror plane. The charge compensating defects in the mirror plane and the mid-spinel block thus do not influence the surface energy of the O^{2-} and Al^{3+} layer. The

relaxation is similar to that seen in the barium β(I)-alumina and magnetoplumbite systems. The unrelaxed and relaxed surface structures can be seen in Figures 3.55 and 3.56, respectively. In the unrelaxed surface structure, as found in the barium magnetoplumbite and barium β(I)-alumina {001} surfaces, there is rumpling in the O^{2-} layer. However, in this system, the rumpling is imperceptible by visual examination. Neighboring O^{2-} ions relax in and out of the bulk less than 0.05 A from their unrelaxed positions. The Al^{3+} ions relax to positions lower in the bulk structure, and the rumpling in the O^{2-} layer immediately below increases to accommodate the relaxed Al^{3+} ions. This increase in rumpling is also not evident by visual examination. This increases the coordination of the Al^{3+} ions and reduces the polarization energy of the surface. The change in structure between the bulk and relaxed surface results in a small energy difference and thus a low surface energy value as found in the barium magnetoplumbite and barium β(I)-alumina {001} surfaces. This results in the lowest surface energy structure for the barium β(II)-alumina system.

I. Comparison of Surfaces of the Barium Phases

Table XX lists the calculated surface energies of the barium hexa-aluminates. One initial focus of this study was to determine if the barium magnetoplumbite phase could be stabilized by its surface energy in very small crystals, i.e., prevent the system from phase separating into the two barium β-alumina structures. The {001} surface is the lowest surface energy orientation for each of the three phases. This surface will be the dominant factor in the question of phase stability since this will be the largest surface of the crystal. There is a significantly lower calculated value for the barium magnetoplumbite crystal (1.03 J/m^2) than that of the barium β(I)-alumina crystal (1.48 J/m^2) and the barium β(II)-alumina crystal (1.25 J/m^2).

The phase separation of barium magnetoplumbite into the two beta phases is given by:

$$5.8\ Ba_2Al_{24}O_{38} \rightarrow Ba_6Al_{88}O_{138}\ [\beta(I)] + 0.8\ Ba_7Al_{64}O_{103}\ [\beta(II)].$$

The calculated enthalpy of this reaction is -1.79 eV.[22] The lowering of the surface energy of the barium magnetoplumbite must then overcome this reaction enthalpy by having crystals

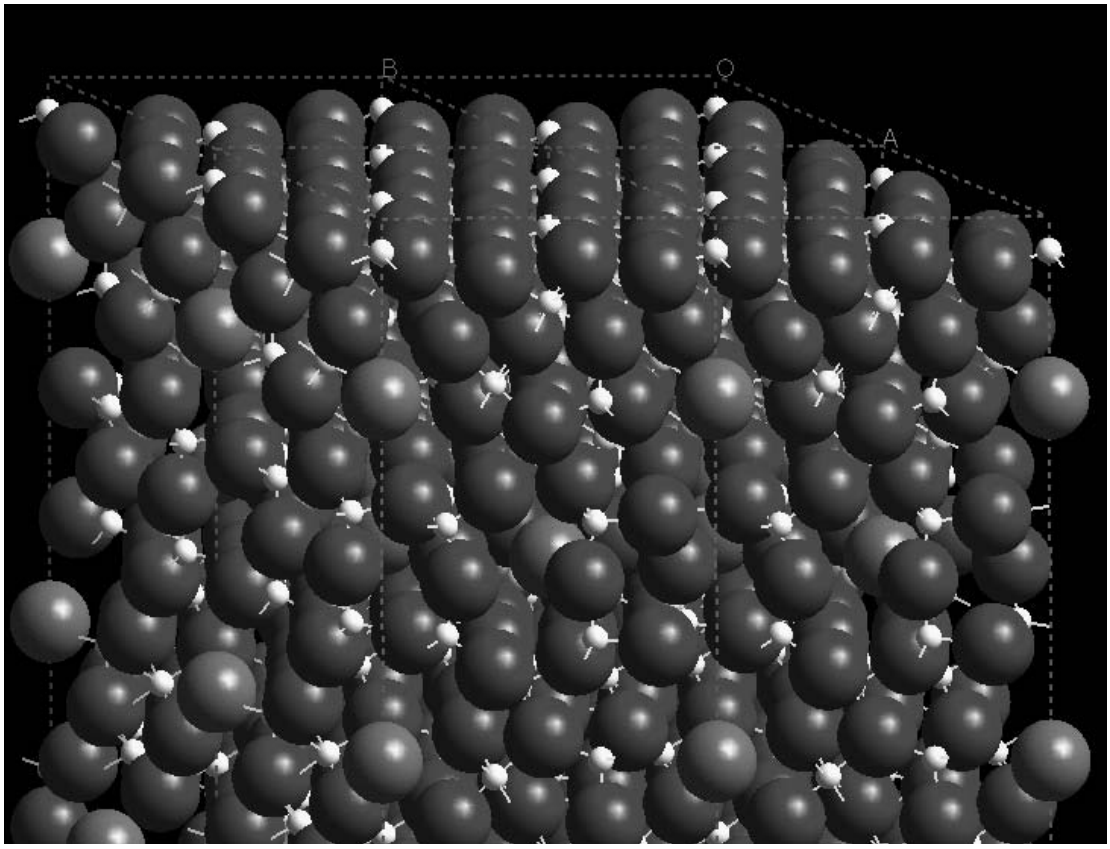

Figure 3.55. Unrelaxed {001} surface of barium β(II)-alumina.
Ions are color coded as follows: red - O^{2-}, white - Al^{3+}, and blue - Ba^{2+}. Surface image is of four blocks of unit cells of the modeled surface area. The unrelaxed surface shows rumpling in the O^{2-} layer.

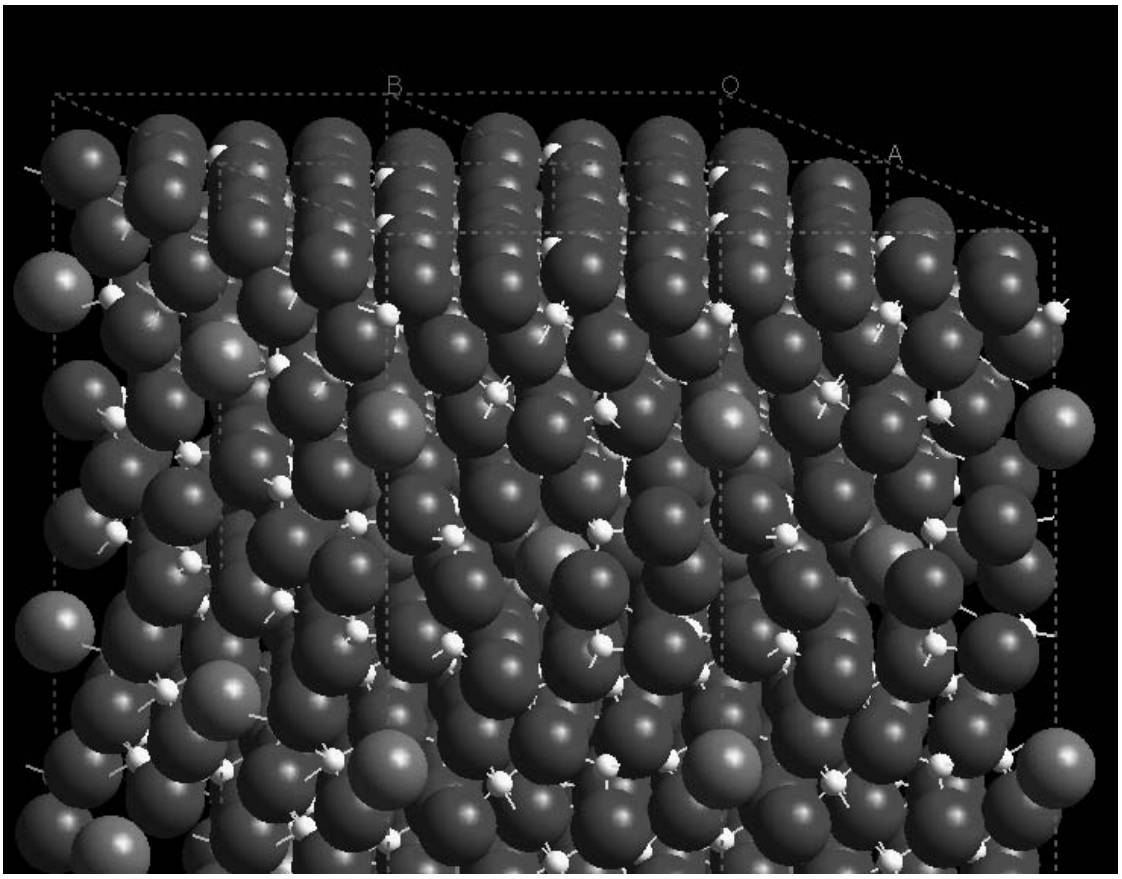

Figure 3.56. Relaxed {001} surface of barium β(II)-alumina.
Ions are color coded as follows: red - O^{2-}, white - Al^{3+}, and blue - Ba^{2+}. Surface image is of four blocks of unit cells of the modeled surface area. The O^{2-} layer has a slight increase in rumpling although it is not evident by visual examination.

Table XX. Surface Energies of the Barium Hexa-Aluminates

Surface	**Ba-MP (J/m^2)**	**Ba β(I) (J/m^2)**	**Ba β(II) (J/m^2)**
{100}	2.09	2.18	2.14
{110}	2.58	2.31	1.97
{120}	2.62	n/a	2.88
{101}	n/a	2.62	1.65
{201}	n/a	1.65	2.15
{102}	n/a	2.22	2.32
{111}	n/a	2.47	2.81
{121}	n/a	n/a	2.82
{112}	2.26	2.41	2.06
{122}	2.40	n/a	3.04
{001}	1.03	1.48	1.25

small enough to lower overall energy to remain stable.

A simple model was used to determine if the surface energy of the barium magnetoplumbite could be stabilized via surface energy effects. The model used the plate-like nature of the crystals, consisting of the {001} and {100} surfaces. The resulting crystal had six {100} and two {001} surfaces for each of the three barium hexa-aluminate phases. The relative values of the surface energy determined the area of each of the facets for each crystal structure. As the surface energy decreases, the area of the surface increases so that each facet has the same total surface energy for a given size crystal. The total surface energy for each crystal was calculated for a given size crystal. The total surface energy of a crystal plus the lattice energy equals the total energy of the crystal. If stabilization is possible, the total surface energy of the barium magnetoplumbite crystal must be more than 1.79 eV lower than that of the two β-alumina crystals with the same molar concentration of their constituent ions at equilibrium so that the total energy of the barium magnetoplumbite crystal is lower. The size of the barium magnetoplumbite crystal with the same total crystal energy was calculated.

The size of the barium magnetoplumbite crystal for which the reaction would be in equilibrium was 0.405 formula units. Below this size, the barium magnetoplumbite crystal is the stable phase. This result shows that the barium magnetoplumbite cannot be stabilized by its lower surface energy, since the size of 0.405 formula units is smaller than one formula unit of barium magnetoplumbite. This is not physically possible.

Each model used in the surface calculations has several formula units of atoms within the surface block and many times that in the bulk block needed to make these calculations. That is true for each surface calculated. In each direction normal to the surface there must be several blocks of atoms present to make the surface models accurate. Even at eight formula units of barium magnetoplumbite, where all three phases have at least one formula unit, the modeling conducted in this investigation would not create a valid picture of the crystal surfaces.

The overall structures of the {001} surfaces for the three barium hexa-aluminates modeled are very similar. In each of these systems, the Al^{3+} ions relax into the surface

structure while the O^{2-} layer rumples to accommodate the space needed for the Al^{3+} ions. The {001} surface for the barium β(II)-alumina had two termination planes that result in identical calculated surface energies. These corresponded to the O^{2-} and Al^{3+} layer immediately below the mirror plane. The barium β(I)-alumina had only one lowest energy termination. This occurred on the O^{2-} and Al^{3+} layer immediately below the mirror plane containing the barium vacancy and the Reidinger defect. Manual surface construction of the {001} plane was necessary to model the barium magnetoplumbite surface.

The more open structure of the barium β(II)-alumina phase resulted in a high number of low dipole moment termination surfaces that were acceptable starting configurations. Many of these surfaces relaxed to highly polarized structures. Such a degree of polarization results in high surface energies. Excessive polarization and divergent surface energy terminations, where relaxation resulted in an increase in the dipole moment normal to the surface, caused cessation of several calculations. There were some occurrences of this in the barium β(I)-alumina system, but the less open nature of the mirror plane in this phase substantially reduced the number of terminations affected in this way.

J. Defects in Alkaline Earth Hexa-Aluminates

Defects in materials can have a substantial effect on their properties.[96] There has been extensive work in the area of bulk defects.[54] Surface defects can play a large role in both the properties and phase stability of a system.[54,97] The first step in determining the properties of materials due to defects is determining what defects are present and where they occur.

1. Bulk Defects in Alkaline Earth Hexa-Aluminates

In this study, the main concern is with the substitution of cations. The point defect energies of calcium, strontium and barium hexa-aluminates are given in Table XXI. All point defects were the substitution of cations with the same valence to avoid the creation of charged defects on the surface, which are not easily handled by the METADISE code. The defect substitution of Ca^{2+}, Sr^{2+}, and Ba^{2+} were chosen because they were the divalent

Table XXI. Bulk Point Defect (eV) of Alkaline Earth Hexaaluminates Where M is the Divalent Cation

Defect	Ca-MP	Sr-MP	Ba-MP	Ba-β(I)	Ba-β(II)
Mg_M	-2.46	-4.55	-7.92	-6.18	-9.95
Ca_M	0.00	-2.28	-5.64	-3.44	-4.48
Sr_M	1.87	0.00	-3.61	-2.15	-2.50
Ba_M	5.48	3.32	0.00	0.00	0.00
Mn_M	-1.20	-3.31	-6.69	-4.51	-6.90
Mn_{Al}	3.46	3.62	3.31	3.83	3.58

cations used in this study and to illustrate the effect of the size of ions on surface defect energies and structure. Mg^{2+} ion substitutional defects were chosen also to illustrate cation defect size effect and because of its use to stabilize strontium and barium hexa-aluminates.[98] It should be noted that the Mg^{2+} ion will occupy an Al^{3+} site and not the divalent cation position.[7,22] Again, the difficulty in calculating charged surface defects is the reason why in this study the Mg^{2+} ion is substituted on the divalent cation site only. The addition of Mn to the barium hexa-aluminate system has many applications in the field of catalysis.[57,99] The Mn adopts the Mn^{2+} valence state and occupies the Al^{3+} tetrahedral sites at low concentrations. At higher concentrations, the Mn occupies octahedral Al^{3+} sites as Mn^{3+}.[99] In this study, Mn^{2+} ions were assumed to occupy the divalent cation site and Mn^{3+} ions occupy Al^{3+} sites to eliminate charged surface defects.

The purpose of the bulk defect calculations in this study is to compare their values to surface defects and the resultant modified surface energies. They are not reaction enthalpy values to be compared across different crystal structures nor are they meant to determine defect concentrations within a crystal.

2. Surface Defects in Alkaline Earth Hexa-Aluminate

The point defect energies for the {100} and {001} calcium, strontium, and barium hexa-aluminate surfaces are given in Table XXII. The surface defects occupy the top-most divalent cation position in the {100} surfaces. The Mn^{3+} defect ion was substituted in the exposed Al^{3+} sites in the {001} surfaces. Each was calculated as an isolated defect with one defect per unit cell.

The size of the defect ion has a large effect on the defect energy of the defective surface structure in the {100} surfaces. A defect cation substituted on a larger divalent cation relaxes to a position deeper in the bulk structure than the original host cation's surface position. This lowers the surface energy. A defect cation substituted on a smaller divalent cation relaxes to a position away from the bulk. This increases the surface energy.

There are two calculated defects in the strontium magnetoplumbite {100} surface that were noteworthy. The first is the Mg_{Sr} defect. The calculation was unsuccessful because

Table XXII. Segregation Energy, Defect Energy, Surface Energy, and Change in Surface Energy for the {100} Surface of Calcium Magnetoplumbite

Defect	**E_{SD} (eV)**	**E_{seg} (eV)**	**γ (J/m^2)**	**$\Delta\gamma$ (J/m^2)**
Mg_{Ca}	-4.44	-1.98	1.81	-0.58
Sr_{Ca}	0.89	-0.98	2.51	0.12
Ba_{Ca}	2.32	-3.14	2.70	0.31
Mn_{Ca}	-0.83	0.37	2.28	-0.11

of an increase in the dipole moment normal to the surface. This was the only occurrence of an increase in the dipole moment for all surface defect calculations. The second is the calculated Mn_{Sr} defect energy. Although the surface point defect energies cannot be directly compared across systems nor between different defects without a complete reaction enthalpy, the calculated energy of -7.40 eV does not fit in with the trends seen in the other systems. Since the Mn^{2+} cation is smaller than the host Sr^{2+} ion, a negative defect energy was expected, based on the results for the other systems, but its value was much lower than anticipated. Although smaller defect cations show a lower defect energy, as evident for example in the Mg_{Ba} substitution in barium magnetoplumbite, the possible explanation of the low value in the Mn_{Sr} defect is due to the fact that it is not an alkaline earth element. Since it is not an alkaline earth element, the defect energy decreases more rapidly, than with an alkaline earth ion, with its smaller size compared to the host ion. The value for the surface defect energy is lower than in calcium magnetoplumbite which follows the trend for its size. The surface defect energy would then be expected to be lowest in barium magnetoplumbite. The difference must be in the surface structure of barium magnetoplumbite. The rumpling and distortion of the polyhedral of the O^{2-} ions, interacts with the Mn_{Ba} defect more than with the alkaline earth substitutions so that its energy is not as low as the trend exhibited by the alkaline earth ions.

The Mn_{Al} defect energies for the {001} alkaline earth hexa-aluminate surfaces all result in positive defect energies. This is due to the fact that the Mn^{3+} ion is larger than the Al^{3+} ion. The Mn^{3+} ion relaxes out of the bulk because the size of the Al^{3+} surface site is not large enough to accommodate the defect.

There are two factors in determining if a defect will be present on the surface. The first is the difference in the defect energy between a bulk and surface position. The segregation energy of a defect from the bulk to the surface is given by:[100]

$$E_{seg} = E_{sur} - E_{bulk.}$$

(56)A negative segregation energy indicates that the defect will prefer to occupy a surface position. The second factor in determining if a defect will occupy a surface position is whether or not there is a reduction of the surface energy.

There are four possibilities based on these two factors. The first is when there is a negative segregation energy and a reduction in the surface energy. When this occurs, the defect will occupy a surface position regardless of the size of the crystal. The second possibility is when there is a positive segregation energy and an increase in the surface energy. This case results in the defect always occupying a bulk position.

The implications from the other two possibilities are not as straight forward. The third possibility is when there is a negative segregation energy and an increase in the surface energy. The fourth is when the segregation energy is positive and there is a decrease in the surface energy. In each of these cases, the size of the crystals may determine whether or not a defect occupies a surface position.

The larger the crystal, the smaller the effect the surface energy has on the overall energy of the crystal. In the third case, the negative segregation energy of the crystal must overcome the increase in the surface energy for a defect to occupy a surface position. This indicates that there might be some minimum size for the crystal, larger than for which the defect will occupy the surface position. The increase in the surface energy might be too large for the defect to segregate to the surface. It also possible that the minimum size of a crystal needed to cause segregation of the defect is too large for a single crystal to be grown.

In the fourth case, the lowering of the surface energy must overcome the positive segregation energy. This indicates that there might be some maximum size crystal, smaller than for which, the defect will occupy a surface position. Similar to the third case, occupying a surface position might not be thermodynamically possible for a defect at any size since the decrease in the surface energy cannot overcome the segregation energy of the defect.

Tables XXIII - XXVII show the surface defect energy, segregation energy, defect surface energy, and the change in surface energy due to the presence of surface defects for the {100} calcium, strontium, and barium hexa-aluminates. Table XXVIII contains the {001} surface defect energy, segregation energy, defect surface energy, and the change in surface energy.

All four above-mentioned cases occur in the results presented in this work. The calcium magnetoplumbite system illustrates three of the four cases. The substitution of Mg_{Ca}

Table XXIII. Segregation Energy, Defect Energy, Surface Energy, and Change in Surface Energy for the {100} Surface of Strontium Magnetoplumbite

Defect	**E_{SD} (eV)**	**E_{seg} (eV)**	**γ (J/m^2)**	**$\Delta\gamma$ (J/m^2)**
Ca_{Sr}	-1.19	1.09	2.44	-0.13
Ba_{Sr}	1.39	-1.93	2.77	0.20
Mn_{Sr}	-7.40	-4.09	1.62	-0.95

Table XXIV. Segregation Energy, Defect Energy, Surface Energy, and Change in Surface Energy for the {100} Surface of Barium Magnetoplumbite

Defect	**E_{SD} (eV)**	**E_{seg} (eV)**	**γ (J/m^2)**	**$\Delta\gamma$ (J/m^2)**
Mg_{Ba}	-8.12	-0.20	1.04	-1.05
Ca_{Ba}	-2.47	3.17	1.77	-0.32
Sr_{Ba}	-1.46	2.15	1.90	-0.19
Mn_{Ba}	-3.41	3.28	1.65	-0.44

Table XXV. Segregation Energy, Defect Energy, Surface Energy, and Change in Surface Energy for the {100} Surface of Barium Magnetoplumbite

Defect	E_{SD} (eV)	E_{seg} (eV)	γ (J/m^2)	$\Delta\gamma$ (J/m^2)
Mg_{Ba}	-8.12	-0.20	1.04	-1.05
Ca_{Ba}	-2.47	3.17	1.77	-0.32
Sr_{Ba}	-1.46	2.15	1.90	-0.19
Mn_{Ba}	-3.41	3.28	1.65	-0.44

Table XXVI. Segregation Energy, Defect Energy, Surface Energy, and Change in Surface Energy for the {100} Surface of Barium β(I)-Alumina

Defect	E_{SD} (eV)	E_{seg} (eV)	γ (J/m^2)	Δγ (J/m^2)
Mg_{Ba}	-6.27	-0.09	1.79	-0.39
Ca_{Ba}	-3.45	-0.01	1.92	-0.26
Sr_{Ba}	-2.16	-0.01	1.94	-0.24
Ca_{Ba}	-4.45	0.06	1.90	-0.28

Table XXVII. Segregation Energy, Defect Energy, Surface Energy, and Change in Surface Energy for the {100} Surface of Barium β(II)-Alumina

Defect	E_{SD} (eV)	E_{seg} (eV)	γ (J/m^2)	Δγ (J/m^2)
Mg_{Ba}	-5.92	4.03	1.67	-0.47
Ca_{Ba}	-2.45	2.06	1.92	-0.22
Sr_{Ba}	-1.00	1.50	2.02	-0.12
Mn_{Ba}	-3.88	3.02	1.82	-0.32

Table XXVIII. Mn_{Al} Segregation Energy, Defect Energy, Surface Energy, and Change in Surface Energy for the {001} Surface of the of Alkaline Earth Hexa-Aluminates

Defect	E_{SD} (eV)	E_{seg} (eV)	γ (J/m^2)	Δγ (J/m^2)
Ca-MP	4.16	0.70	2.60	0.64
Sr-MP	3.64	0.02	2.22	0.52
Ba-MP	3.61	0.30	1.55	0.52
Ba-β(I)	3.64	-0.19	2.00	0.52
Ba-β(II)	4.34	0.76	2.07	0.83

is an example of the first case. There is a negative segregation energy and a reduction in the surface energy. The Mg^{2+} ion will segregate always prefer a surface substitution on the Ca^{2+} site than a bulk Ca^{2+} position. The third case can be seen in the Sr_{Ca} and Ba_{Ca} {100} defects. In each of these defect surfaces, there is a negative segregation energy and an increase in the surface energy. The fourth case can be seen in the Mn_{Ca} {100} defect. There is a positive segregation energy and a reduction in the surface energy. The second case can be seen in the all the Mn_{Al} defects on {001} surfaces with the exception of the barium β(I)-alumina system. For each of these defects, there is a positive segregation energy and an increase in the surface energy. This indicates that the Mn^{3+} ion will always prefer a bulk position for these surfaces.

A simple model was developed to determine if a defect will segregate to the surface for the calcium, strontium, and barium hexa-aluminates crystal systems. This model assumes a spherical crystal where the entire surface is the same and thus has the same surface energy. This also means that each modeled unit cell area of surface contains one defect. As the size of the crystal is increased, the number of surface defects increases proportionally with the number of surface unit cells. Implications of these assumptions will be discussed later in this section. The possible number of bulk defect positions increases at a much faster rate than the number of surface positions as the size of the crystal is increased. The change in the surface energy due to defects is compared to the segregation energy of same number of bulk defects. If the sum of the segregation energy and the change in the surface energy results in a lowering of the total energy, segregation is assumed to occur. The results of these calculations for the {100} and {001} surfaces are given in Table XXIX.

Ba^{2+}, Mg^{2+} and Mn^{2+} ions always segregate to the {100} surface in all systems. The Mn^{3+} ion never segregates to the {001} surface. The Ca^{2+} and Sr^{2+} ions always segregate to the {100} surface except in the barium magnetoplumbite system where they never segregate. In the barium magnetoplumbite system, the Ca^{2+} and Sr^{2+} defect ions have a positive segregation energy and a reduction in the surface energy. The thermodynamics of the system does not allow segregation of the defects for any size crystal.

The fourth case for segregation of defects, where the segregation energy is positive

Table XXIX. Segregation of Defects from Bulk to Surface Sites for the {100} and {001} Surfaces of Alkaline Earth Hexa-Aluminates Where M is the Divalent Cation

Defect	Ca-MP	Sr-MP	Ba-MP	Ba-β(I)	Ba-β(II)
Mg_M {100}	Always	n/a	Always	Always	Always
Ca_M {100}	n/a	Always	Never	Always	Always
Sr_M {100}	Always	n/a	Never	Always	Always
Ba_M {100}	Always	Always	n/a	n/a	n/a
Mn_M {100}	Always	Always	Alway	Always	Always
Mn_{Al} {001}	Never	Never	Never	Never	Never

and there is a decrease in the surface energy, occurs for the Ca^{2+} defect ion in the strontium magnetoplumbite system. Unlike in the barium magnetoplumbite system, segregation always occurs. There is no maximum size crystal for which segregation does not occur. The segregation energy never overcomes the reduction in the surface energy for any size crystal.

The third case for segregation of defects where the segregation energy is negative and there is an increase in the surface energy occurs for the Ba^{2+} defect ion segregating in the strontium magnetoplumbite system. The results calculated here always indicate that the segregation of the defect from the bulk to the surface will occur. There is no minimum size crystal below which the defects will not segregate.

In addition to the results presented in this study, this model was used to calculate whether the third and fourth cases can yield results where the size of the crystal does affect segregation of defects. Each of the five surfaces was tested to see if there was a set of values of the segregation energy and change in surface energy that predicted a minimum size crystal for defect segregation. It was found for all five systems that there are sets of segregation energies and changes in the surface energy that show that crystal size can affect the stability of surface defects.

One instance where this model may be too simple to give a valid physically result is the number of surface defect sites. The assumption that the all the unit cells have defects can lead to difficulties. Not all sites would be expected to have a defect present. This means that only the area immediately surrounding the defect will have a lower surface energy. The Ca^{2+} defect ion segregating to the {100} surface in the strontium magnetoplumbite system might not occur because of this assumption.

This assumption could also cause the opposite effect to occur. In the {001} surface of the barium β(I)-alumina system, Mn^{3+} defect ion never occupies a surface position. It has a negative segregation energy and results in an increase in the surface energy. Using this simple model, there is no minimum size crystal below which the segregation will occur. The segregation of the Mn^{3+} ion might occur because the increase in the surface energy will be a local effect if not all sites are occupied.

Avoiding this simplification for this model is difficult, but the idea of localization of

defects has some experimental evidence. It has been found that the addition of MgO to Al_2O_3 can cause the surface to form hills and valleys at the atomic level on the {0001} surface.[101] This could be an indication that the defect has a negative segregation energy and increases the surface energy causing the surface to lower its surface energy by faceting.

The assumption that the crystal is spherical with only one surface can also an over simplification. In a cubic crystal such as NaCl, where each face is symmetrically equivalent and thus has the same surface energy, this simply model might work well. As the complexity of the crystal morphology increases, the limitation of this model become more evident. In the hexa-aluminates, the model used to calculate the stability of barium magnetoplumbite is an improvement since it has eight surfaces, two {001} and six {100} facets.

Experimental results show that high concentrations of Mn in barium β(I)-alumina, where Mn^{3+} occupies Al^{3+} sites, causes a reduction in the surface area.[98] Reduction of the surface area indicates larger crystals are being formed. This agrees with the calculated surface defect energies but not with the segregation of defects. This model predicts that the Mn will not segregate to the surface, but the change in surface area indicates that this does occur. Again, the model used to determine if a defect segregates to the surface might be too simple a representation. The solution to this seeming failure of this model is to have crystals with more than one surface, i.e., not make them spherical crystals but add other facets. Another possibility is that the Mn will be not be present in the form of Mn^{3+} but Mn^{2+} since it prefers this state in the bulk at low concentrations. This change in oxidation state makes it necessary to have a charge compensating defect. That might lead to defect clusters with the Mn^{2+} defect that further reduce the surface energy and thus a minimum sized crystal is possible to have segregation to occur.

3. Effect of Surface Defects on Phase Stability of Barium Magnetoplumbite

Five cases of surface defects were examined using the same model used to determine if the barium magnetoplumbite phase could be stabilized (i.e., the {100} and {001} surfaces are the only surfaces in the model). The same assumption in the segregation model, that all surface unit cells contain a defect, was used to determine stability. This means that the modified surface energy for the defective surface was used to model the whole surface.

The first case modeled was when Mg^{2+} occupied defect positions on the {100} surface with no defects present on the {001} surfaces for all three barium hexa-aluminate phases. The Mg^{2+} defect ion was used because of the indication that the defect will always occupy a surface position occurs in all three phases. The barium magnetoplumbite phase is stable below 1.35 formula units.

The second model was chosen for the same reason as in the first case. In this model, the Mn^{2+} ion occupy the Ba^{2+} ion {100} surface site and there are no defects on the {001} surface. It was found the barium magnetoplumbite phase was stable below 2.35 formula units in size. The third model assumed that no defects were present on the {100} surface, with Mn^{3+} ion occupying {001} Al^{3+} sites. This resulted in the barium magnetoplumbite phase being stable below 4.73 formula units. The fourth case had Mn^{2+} ions occupying {100} surface Ba^{2+} positions and Mn^{3+} ions occupying {001} surface Al^{3+} sites. The barium magnetoplumbite phase is stable below 3.42 formula units. The last was with Mg^{2+} defect ions on the {100} surface and Mn^{3+} defect ion on the {001} surface. The barium magnetoplumbite phase is stable below 1.64 formula units.

The initial indication that barium magnetoplumbite can be stabilized via surface stabilization in the presence of surface defects has one serious drawback. The model used to calculate the perfect and defective surface has five unit cells in Region I and fifteen unit cells in Region II. Each unit cell contains two formula units. This means that each surface modeled contains 40 formula units, substantially larger than the formula units needed for stability for the barium magnetoplumbite phase. In order for the surface energy calculation presented in this thesis to be valid, a crystal must be twice as large as used in the calculation of each surface. In other words, one side of the crystal would need 20 unit cells and the other side would need an additional 20 unit cells. That is the limit for a two-sided crystal. When additional faces are added to the crystal, they too must have 20 unit cells per side. This means that, even if the intersection of two surfaces is ignored, the crystal must be at least 600 A in diameter in order for these results to have any credibility. Given this, the barium magnetoplumbite phase cannot be predicted to be stable based on these calculations presented in this thesis.

IV SUMMARY AND CONCLUSIONS

Atomistic computer simulation techniques were used to model five crystal structures in the hexa-aluminate family. Calcium and strontium hexa-aluminates adopt the magnetoplumbite-type structure. Barium hexa-aluminate phase separates from the theoretical magnetoplumbite structure into the barium β(I)-alumina and barium β(II)-alumina phases, which is thermodynamically unstable because of the large size of the Ba^{2+} ion.

The structure of the crystal influences the morphology of the crystal. Each system modeled resulted in a plate-like crystals. It was also determined that chemistry, in addition to crystal structure, can lead to differences in the number of low dipole termination planes within a given surface orientation and thus differences in their morphology. Calculations performed during this study indicate that each has subtle differences in their final crystal shape. The complexity of these unit cells presents the possibility that planes with initial configurations that relax to the lowest surface energy for a given orientation are missed because they initially possess a dipole moment normal to the surface. One example where the chemistry of the system changes the morphology of the crystal is in the {012} surfaces in the calcium and strontium magnetoplumbite systems. The calcium magnetoplumbite has fewer low dipole moment terminations than the strontium magnetoplumbite system. The extra termination in the strontium magnetoplumbite, that has a low dipole moment, results in the lowest surface energy structure. This changes the order of relative values of surface energy structures. This change causes a change in the crystal morphology of these two crystals.

Calcium magnetoplumbite was used as the initial model system in this study. The {001} surface was found to have the lowest surface energy configuration as expected from experimental observations of the crystal shape. Manual construction of the termination plane was necessary to calculate the surface energy of its {001} surface. Manual construction of the {001} surface was also necessary for the strontium and barium magnetoplumbite structures. The lowest surface energy orientation was also found to be the {001} surface for these two crystals.

The depth of the divalent cation in the {100} calcium magnetoplumbite surfaces is the dominant factor in the calculated surface energy. Smaller depths of the Ca^{2+} ion positions result in lower surface energies. The system prefers the Ca^{2+} ion in an exposed position in the unrelaxed surface structure. When the Ca^{2+} ion is not exposed, subsurface relaxations are more difficult to achieve in the dense mirror plane. The constraint of the these subsurface relaxations increases the surface energy for the given termination plane.

Coordination of the exposed surface ions in orientations other than the {100} surface plays a more prominent role than the depth of the divalent cation in the surface structure and thus the surface energy. Since the mirror plane in no longer perpendicular to the surface, the subsurface relaxations in these orientations are not as hindered by the size of the divalent cations. Exposure of the Ca^{2+} ion is not as critical to lower surface energy structures as in the {100} orientation. Dangling O^{2-} ions that occupy low coordinated positions thus become the most important factor in determining which termination in a family of orientations has the lowest surface energy structure.

The metastable surface structures found while modeling the (1_0) orientation are due to limitations in the METADISE program. Minor differences in the surface vectors cause slight changes in the starting configurations of symmetrically equivalent surfaces. The smaller calculated size of the surface area during the reorientation of the unit cell causes an increase in the repulsive energy between neighboring ions and thus a small increase in the surface energy of the given orientation. This does not allow for complete relaxation of the termination which should result in the same surface structure for the symmetrically equivalent orientations. Examination of all the symmetrically equivalent orientations ensures that the global minimum surface energy structure is found.

The strontium magnetoplumbite system is very similar to the calcium magnetoplumbite system. The {001} surface is again the lowest surface energy orientation. The exposure of the Sr^{2+} ion plays a lesser role in the lowest calculated surface structure. Two factors have been identified as the cause of the difference between the strontium and calcium magnetoplumbite systems. The first is the more open nature of the spinel blocks due to the larger size of the Sr^{2+} ion. This allows for more subsurface relaxation to occur in

these blocks. The second is the higher polarizability of the Sr^{2+} ion. This allows for greater relaxation of the "electron cloud" of the Sr^{2+} ions to occur. Both the exposure of the divalent cation and the coordination of the surface atoms control the calculated surface structure and energy.

The theoretical barium magnetoplumbite structure has a different space group than the other two structures. The large size of the Ba^{2+} ion causes the O^{2-} ions to rumple in the layers near the mirror plane. This rumpling lowers the symmetry of the system. Again, the {001} surface has the lowest surface energy for this crystal structure. The larger size of the Ba^{2+} ion, and thus the unit cell, reduces the differences in the surface vectors for symmetrically equivalent termination planes. The hindering of subsurface relaxations due to the large Ba^{2+} ion is offset by the coordination of surface ions, namely dangling O^{2-} ions.

The calcium and strontium magnetoplumbite systems show an increase in surface energy with increasing divalent cation size for most surfaces. The above mentioned {012} surface is the only exception. Subsurface divalent cations in the closely packed mirror plane can hinder relaxation of the surface atoms and thus increase the surface energy for a given orientation. The lower calculated surface energies for the barium magnetoplumbite system are due to the rumpling of the oxygen layer above and below the mirror plane in the bulk. The difference between the bulk structure and the relaxed surface structure is smaller in the barium magnetoplumbite than in calcium and strontium magnetoplumbite. Since the surface structure, thus its energy, is closer to the bulk structure, this results in lower surface energies for the barium magnetoplumbite than those of the calcium and strontium magnetoplumbite structures that do not have the rumpling. Low coordination of the surface atoms may negate any decreases in energy created by exposing the divalent cation.

The location of the Ba^{2+} ion plays only a minor role in the lowering of surface energies in the β-aluminas. The openness of the mirror planes allows subsurface relaxations to occur that are sometimes lost with the larger cation in the magnetoplumbite system. The coordination of the surface atoms, mostly the number of dangling O^{2-} ions, and the reduction of polarization in the surface structure have the greatest impact on the surface energy of a given orientation.

The barium β(I)- and β(II)-alumina systems have the lowest surface energy for the {001} orientation, as in the magnetoplumbite systems. Unlike in the magnetoplumbite systems, the exposure of the Ba^{2+} ion is not critical for the structure to be the lowest surface energy termination for a given orientation. This is due to the more open nature of the mirror plane in these systems. There is more room for subsurface relaxations to occur, even with the large Ba^{2+} ion occupying positions deeper in the surface structure. The coordination of surface ions, especially the number of dangling O^{2-} ions, and the constraint of relaxation of surface O^{2-} ions control the calculated surface structure and energy.

One problem that occurs in modeling of these two systems is the high number of calculations that were prematurely ended. There are two causes for these calculations to end. The first is excessive polarization in the surface structure. The second occurs because some terminations relax to structures that increase the dipole moment normal to the surface. This results in a divergent surface energy. Real surfaces will not have a dipole moments normal to the surface. Surface structures that result in a highly polarized configuration will have very high surface energies. These terminations would not be stable and thus will not occur in nature.

The stabilization of the pure barium magnetoplumbite phase in very small crystals is very unlikely. The calculated size of a surface energy stabilized crystal is less than one formula unit of barium magnetoplumbite. Crystals of this size would not exist. One limitation of the modeling used in this study is the minimum size of crystals for which these models are accurate because of the number unit cells used to model each surface structure. The surface energies calculated in this study are valid for crystals larger than about 600 A in diameter.

The calculation of surface defects and the prediction of segregation to the surface of substitutional point defects were also included in this study. Defect cations that are smaller than the host surface cation result in a lowering of the surface energy of the defective surface. This is due to the relaxation of the defect cation toward the bulk of the crystal. In the case of the Mn^{2+} substitution on the divalent cation surface site, the rumpling of the O^{2-} layers of barium magnetoplumbite and the differences in chemistry of the Mn^{2+} ion and

alkaline earth elements results in a higher than expected surface defect energy.

The two factors in determining if a defect will occupy a surface position are the segregation energy and the change in surface energy. A positive segregation energy and an increase in the surface energy will always result in a defect occupying a bulk position. A negative segregation energy and a decrease in the surface energy will always have the defect occupy a surface position. The size of the crystal can determine if a defect occupies a surface position for the case when the segregation energy is positive and there is a decrease in the surface energy. Crystal size can also effect defect positions when the segregation energy is negative and there is an increase in the surface energy.

It was found that Mg^{2+}, Mn^{2+}, and Ba^{2+} substitution on the divalent cation site always result in a segregation of the defect to the surface for the {100}orientations for the alkaline earth hexa-aluminates. Ca^{2+} and Sr^{2+} defect ions occupy surface positions for the calcium and strontium magnetoplumbite and the two barium β-alumina systems in the {100} orientations, but not in the barium magnetoplumbite system. In all five crystal systems for the {001} orientation, the Mn^{3+} substitution on the Al^{3+} surface sites never occurs. The size of the crystal does not effect the segregation of defects in all of the calculated results. There are values for the segregation energy and change in surface energy where crystal size does effect the segregation of defects to the surface.

The simplicity of the segregation model does have limitations. The segregation of Mn^{3+} defect ions to positions on the {001} surface of the barium β(I)-alumina system is not predicted by this segregation model. It does have a positive segregation energy and decreases the surface energy based on the calculated defect energies. Experimental results suggest that the Mn^{3+} defect ions occupy surface positions.[98] It is accompanied by a reduction in surface area which indicates an increase in the size of the crystal. This indicates that the segregation model must be more complex to have complete confidence in its results. One solution is to increase the number of facets in the model for the more complex structures.

The possibility of stabilization of the barium magnetoplumbite phase in very small crystals was revisited when surface defects were included in the model. Five cases for

defect surface stabilization were examined. It was found that the barium magnetoplumbite phase cannot be predicted stabilized by inclusion of surface defects since the minimum size since the range of the model validity was exceeded. No experimental evidence has been found that indicate that the barium magnetoplumbite phase will be stable.

Two main features of the calculations on these models show the validity of their use in surface science. The calculations predict the experimentally observed crystal's plate-like geometries for the alkaline earth hexa-aluminates.[91] The second evidence for the validity of these models comes from the {001} surfaces. Relaxation of the surface Al^{3+} ions into the bulk and the rumpling of the basal plane were predicted by these calculations. This type of surface relaxations were found in the similar structured α-Al_2O_3 crystals.[59]

The results of this study do show that atomistic simulation techniques can be used to model surface structures of fairly complicated systems. The use of these techniques have potential applications in many areas of ceramic and materials science. Surfaces play an important role in the solid state reactions and the joining of materials. CVD, biomaterials, catalysis, and the advance of nanotechnology all have at there core the surfaces of the materials.[53,67,101,102,103] The use of atomistic surface modeling to examine a large number of possibilities quickly and inexpensively have great potential for all of these technologies.

V FUTURE WORK

Four advancements in the area of atomistic simulations would further their use in development of new materials and technology. The first is in the area of modeling non-vacuum conditions of physical systems. This can be achieved by using molecular dynamics in conjunction with modeling that was used in this study. Catalytic reactions and CVD could potentially be modeled using these two techniques in conjunction.

The second relies on the ability to model larger number of atoms. Modeling the joining of materials need modification of existing programs to handle the large number of atoms necessary for these more complicated systems. Modeling the joining of materials requires that the surface area of both materials match. Systems that do not have similar size surface unit cells or when the lattices are of different crystal systems, several surface unit cells might be necessary for both materials. This greatly increases the number of necessaria atoms used for accurate models. Lack of computer resources prevented calculations of calcium magnetoplumbite and YAG interfaces.

The ability to model charged surface defects also needs to addressed. Using the existing METADISE code, it is not possible to calculate the Mg^{2+} and Mn^{2+} ions occupying a Al^{3+} surface site. Bulk calculations[22] and experimental results[100] indicate that these ions prefer the Al^{3+} sites. Performing these charged surface defects would lead to a better understanding of the overall surface and bulk defect occupancy.

The fourth improvement to this technique is in the rotation of the unit cell to model symmetrically equivalent surfaces. Rotation of the unit cell sometimes results in slight changes in the surface vectors. On smaller sized cells, this can lead to non-equivalent results on surfaces that have identical starting configurations. Although these differences can be overcome by modeling all surfaces that are expected to be symmetrically equivalent, this is a problem that should be addressed. These errors are the result of the storage of values in the systems memory and the rounding of values of trigometric functions during the rotation process.

The last modification that is necessary for modeling of complicated systems is the way in which low dipole moment surfaces are found. Although not encountered this study,

work on the YAG system revealed a major problem in determining low dipole moment surfaces. A more complicated approach is needed in the way in which atoms are removed from the surface. Using the current system, atoms are removed one at a time. At each step, the dipole moment normal to the surface is calculated and the surface is accepted or rejected based on this value. The atom that is removed is determined by the order of input into the model. The atoms are ordered in the input by depth of their positions with the core and shell placed together. In simple systems, it does matter which atom is removed because the atoms occupy symmetrical equivalent sites. As the system become more complicated, the number of surface atoms that occupy different symmetrical positions increases. The order in which atoms are removed then plays a role in the calculated dipole moment. It is then possible to remove an atom and reject this surface due to a high dipole moment when the removal of a different atom would result in a very low dipole moment. It is then possible to miss a termination plane that would relax to the lowest energy configuration.

REFERENCES

1. P.E.D. Morgan and E.H. Cirlin, "The Magnetoplumbite Crystal Structure as a Radwaste Host," *J. Am. Ceram. Soc.,* **66** [11] C-114-115 (1982).

2. C.M. Jantzen and R.R. Neurgaonkar, "Solid State Reaction in the System Al_2O_3-Nd_2O_3-CaO: A System Pertinent to Radioactive Waste Disposal," *Mater. Res. Bull.,* **16** [5] 519-524 (1981).

3. W.J. Buykx, K. Hawkins, D.M. Levins, H. Mitamura, R. Smart, G.T. Stevens, K.G. Watson, D. Weedon, and T.J. White, "Titanate Ceramics for the Immobilization of Sodium-Bearing High Level Nuclear Waste," *J. Am. Ceram. Soc.,* **71** [8] 678-688 (1988).

4. A. Kahn, A.M. Lejus, M. Macdsac, J. Thery, and D. Vivien, "Preparation, Structure, Optical and Magnetic Properties of Lanthanide Aluminate Single Crystal ($LnMAl_{11}O_{19}$)," *J. Appl. Phys.,* **52** [11] 6864-6869 (1981).

5. J.M.P.J. Vertegen, J.L. Sommerdijk, and J.G. Verriet, "Cerium and Terbium Luminescence in $LaMgAl_{11}O_{19}$," *J. Lumin.,* **6** [5] 425-431 (1973).

6. A.L.N. Stevels and J.M.P.J. Vertegen, "Eu^{3+} - Mn^{2+} Energy Transfer in Hexagonal Aluminates," *J. Lumin.,* **14** [3] 207-218 (1976).

7. A.L.N. Stevels and A.D.M. Schrama-de Pauw, "Ce^{3+} Luminescence in Hexagonal Aluminates Containing Large Divalent or Trivalent Cations," *J. Electrochem. Soc.,* **125** [4] 588-594 (1978).

8. A.L.N. Stevels, "Red Mn^{2+}-Luminescence in Hexagonal Aluminates," *J. Lumin.,* **20** [2] 99-109 (1979).

9. H. Inoue, K. Sekizawa, K. Eguchi, and H. Arai, "Thermal Stability of Hexaaluminate Film Coated on SiC Substrate for High-Temperature Catalytic Application," *J. Am. Ceram. Soc.,* **80** [3] 584-588 (1997).

10. H. Inoue, K. Sekizawa, K. Eguchi, and H. Arai, "Preparation of Hexaaluminate Catalyst Thick Films on α-SiC Substrate for High Temperature Application," *J. Mater. Sci.,* **32** [17] 4627-4632 (1997).

11. M.K. Cinibulk, "Reactions Between Hot-Pressed Calcium Hexaaluminate and Silicon Carbide in the Presence of Oxygen," *J. Am. Ceram. Soc.,* **81** [11] 2789-2798 (1998).

12. P.E.D. Morgan, D.B. Marshall, and R.M. Housley, "High-Temperature Stability of Monazite-Alumina Composites," *Mater. Sci. Eng.,* **A195** [1] 215-222 (1995).

13. T.A. Parthasarathy, E. Boakye, M.K. Cinibulk, and M.D. Petry, "Fabrication and Testing of Oxide/Oxide Microcomposites with Monazite and Hibonite as Interlayers," *J. Am. Ceram. Soc.,* **82** [12] 3575-3585 (1999).

14. M.K. Cinibulk and R.S. Hay, "Textured Magnetoplumbite Fiber-Matrix Interphase Derived from Sol-Gel Fiber Coatings," *J. Am. Ceram. Soc.,* **79** [5] 1233-1246 (1996).

15. N. Iyi, Z. Inoue, S. Takekawa, and S. Kimura, "The Crystal Structure of Barium Hexaaluminate (Phase I) Single Crystals," *J. Solid State Chem.*, **74** [2] 295-303 (1988).

16. H.W. Zandbergen, F.C. Mijlhoff, D.J.W. Ijdo, and G. van Tendeloo, "A Model for the Structure of $1.31BaO{\cdot}6M_2O_3$; M=Al, Ga; An Electron Microscopic Study, " *Mater. Res. Bull.,* **19** [11] 1443-1450 (1984).

17. J. Park and A.N. Cormack, "Crystal/Defect Structures and Phase Stability in Ba-Hexaaluminates," *J. Solid State Chem.*, **121** [2] 278-260 (1996).

18. M. Gobbels, S. Kimura, and E. Woermann, " The Aluminum-Rich Part of the System BaO-Al_2O_3-MgO: I: Phase Relationships," *J. Solid State Chem.*, **136** [2] 253-257 (1998).

19. V. Adelskold, "X-ray Studies on Magnetoplumbite $PbO{\cdot}Fe_2O_3$ and Other Substance Resembling 'β-Alumina' $Na_2O{\cdot}11Al_2O_3$," *Ark. Kemi, Mineral. Geol.,* **12A** [1] 29-37 (1938).

20. R. Amin, Y. Abbas, M. Fayak, A. Murasik, and I. Hamouda, "A Neutron Diffraction Study on Magnetoplumbite $PbFe_{12}O_{19}$," pp. 437-444 in *Interaction of Radiation with Solids*. Edified by A. Bishay. Plenum, New York, 1967.

21. A.J. Lindop, C. Matthews, and D. W. Goodwin, "Refined Structure of $SrO{\cdot}6Al_2O_3$," *Acta Crystallogr., Sect. B: Struct. Crystallogr. Cryst. Chem.,* **B31** [12] 2940-2941 (1975).

22. J. Park, "Structure, Stoichiometry, and Stability in Magnetoplumbite and β-Alumina Type Ceramics"; Ph.D. Thesis, Alfred University, Alfred, NY, 1995.

23. N. Iyi, Z. Inoue, S. Takekawa, and S. Kimura, "The Crystal Structure of Barium Lead Hexaaluminate Phase II," *J. Solid State Chem.,* **60** [1] 41-50 (1985).

24. N. Iyi, Y. Bando, S. Takekawa, Y. Kitami, and S. Kimura, "Superstructure of Barium Lead Hexaaluminate Phase II (BaPb β(II)-Alumina) Reveled by High-Resolution Electron Microscopy," *J. Solid State Chem.,* **64** [2] 220-224 (1986).

25. W. Wimmer and A.J. Freeman, "Fundamentals of the Electronic Structure of Surfaces," Ch. 1 in *Electronic Structures: Handbook of Surface Science,* Vol. 2. Edited by K. Horn and M. Scheffler. Elsevier Science, Amsterdam, Holland, 2002.

26. M.S.D. Read, M.S. Islam, G.W. Watson, F. King, and F.E. Hancick, "Defect Chemistry and Surface Properties of $LaCoO_3$," *J. Mater. Chem.,* **10** [10] 2298-2305 (2000).

27. F.P. Santos, E. Compos, M. Costa, F.C.L. Melo, R.Y. Honda, and R.P.Mota, "Superficial Modifications in TiO_2 and Al_2O_3," *Mater. Res. (Sao Carlos, Braz.),* **6** [3] 1-5 (2003).

28. *Concise Encyclopedia of Materials Characterization*; pp. 502-503. Edited by R.W. Cahn and E. Lifshin. Pergamon Press, Oxford, 1993.

29. R.J. Cventanovic and Y. Amenomiya, "A Temperature Programmed Desorption Technique for Investigation of Practical Catalysts," *Catal. Rev.,* **6** [1] 21-48 (1972).

30. M. Prutton, *Surface Physics*; Ch. 6. Oxford University Press, Oxford, 1983.

31. I.M. Campbell, *Catalysis at Surfaces*, Chapman and Hall, London, 1988.

32. *Concise Encyclopedia of Materials Characterization*; pp. 53-58. Edited by R.W. Cahn and E. Lifshin. Pergamon Press, Oxford, 1993.

33. J.C. Riviere, *Surface Analytical Techniques*; Ch. 10. Claredon Press, Oxford, 1990.

34. *Encyclopedia of Materials Characterization: Surfaces, Interfaces, and Thin Films*; pp. 416-427. Edited by C.R. Brundle, C.A. Evans, Jr., and S. Wilson. Butterworth-Heinemann, Boston, 1992.

35. *Encyclopedia of Materials Characterization: Surfaces, Interfaces, and Thin Films*; pp. 40-41. Edited by C.R. Brundle, C.A. Evans, Jr., and S. Wilson. Butterworth-Heinemann, Boston, 1992.

36. *Encyclopedia of Materials Characterization: Surfaces, Interfaces, and Thin Films*; pp. 198-213. Edited by C.R. Brundle, C.A. Evans, Jr., and S. Wilson. Butterworth-Heinemann, Boston, 1992.

37. *Encyclopedia of Materials Characterization: Surfaces, Interfaces, and Thin Films*; pp. 240-251. Edited by C.R. Brundle, C.A. Evans, Jr., and S. Wilson.

Butterworth-Heinemann, Boston, 1992.

38. *Encyclopedia of Materials Characterization: Surfaces, Interfaces, and Thin Films*; pp. 252-263. Edited by C.R. Brundle, C.A. Evans, Jr., and S. Wilson. Butterworth-Heinemann, Boston, 1992.

39. J.C. Riviere, *Surface Analytical Techniques*; Ch. 22. Claredon Press, Oxford, 1990.

40. *Concise Encyclopedia of Materials Characterization*; pp. 23-28. Edited by R.W. Cahn and E. Lifshin. Pergamon Press, Oxford, 1993.

41. C.R.A. Catlow, "Need and Scope of Modeling Techniques," pp. 1-20 in *Computer Modeling in Inorganic Crystallography.* Edited by C.R.A. Catlow. Academic Press, San Diego, California, 1997.

42. M. Born and K. Huang, *Dynamical Theory of Crystal Lattices*; Ch. 1. Oxford University Press, Oxford, 1954.

43. J.M. Thijssen, *Computational Physics;* Ch. 3. Cambridge University Press, Cambridge, United Kingdom, 1999.

44. J.M. Thijssen, *Computational Physics;* Ch. 4. Cambridge University Press, Cambridge, United Kingdom, 1999.

45. J.M. Thijssen, *Computational Physics;* Ch. 5. Cambridge University Press, Cambridge, United Kingdom, 1999.

46. C.R.A. Catlow, "An Introduction to Computer Modeling of Condensed Matter," pp. 1-28 in *Computer Modeling of Fluids Polymers and Solids*. Edited by C.R.A. Catlow, S.C. Parker, and M.P. Allen. Kluwer Academic Publishers, Dordrecht, Netherlands, 1990.

47. H.L. Tuller and T.S. Stratton, "Defect Structure and Transport in Oxygen Excess Cerium Oxide-Uranium Oxide Solid Solutions," pp. 87-99 in *Transport in Nonstoichiometric Compounds.* Edited by G. Simkovich and V.S. Stubican. Plenum Press, New York, 1985.

48. P.J. Lawrence and S.C. Parker, "Computer Modelling of Oxide Surfaces and Interfaces," pp. 219-248 in *Computer Modelling of Fluids Polymers and Solids*. Edited by C.R.A. Catlow, S.C. Parker, and M.P. Allen. Kluwer Academic Publishers, Dordrecht, Netherlands, 1990.

49. S.C. Parker and G.D. Price, "Computer Modelling of the Structure and

Thermodynamic Properties of Silicate Minerals," pp. 405-429 in *Computer Modelling of Fluids Polymers and Solids*. Edited by C.R.A. Catlow, S.C. Parker, and M.P. Allen. Kluwer Academic Publishers, Dordrecht, Netherlands, 1990.

50. P.W.M. Jacobs and Z.A. Rycerz, "Molecular Dynamics Methods," pp. 83-115 in *Computer Modelling in Inorganic Crystallography.* Edited by C.R.A. Catlow. Academic Press, San Diego, California, 1997.

51. B. Vessal, "Amorphous Solids," pp. 295-332 in *Computer Modelling in Inorganic Crystallography.* Edited by C.R.A. Catlow. Academic Press, San Diego, California, 1997.

52. M. Haneda, Y. Kintaichi, I. Nakamura, T. Fujitani, and H. Hamda, "Effect of Surface Structure of Supported Palladium Catalysts on the Activity for Direct Decomposition of Nitrogen Monoxide," *J. Catal.,* **218** [2] 405-410 (2003).

53. H.M. Kim, "Bioactive Ceramics: Challenges and Perspectives," *J. Ceram. Soc. Jpn.*, **109** [4] 549-557 (2001).

54. R.F. Stewart and W.C. Mackrodt, "Defect Properties of Ionic Solids: I. Point Defects at the Surfaces of Face-Centered Cubic Crystals," *J. Phys. C: Solid State Phys.,* **10** [9] 1431-1446 (1977).

55. P.W. Tasker, "The Surface Energies, Surface Tensions, and Surface Structure of the Alkali Halide Crystals," *Philos. Mag. A,* **39** [2] 119-136 (1979).

56. P.W. Tasker, "The Stability of Ionic Crystal Surfaces," *J. Phys. C: Solid State Phys.,* **12** [22] 4977-4984 (1979).

57. J.H. Harding, "Defects, Surfaces, and Interfaces," pp. 185-199 in *Computer Modeling in Inorganic Crystallography*. Edited by C.R.A. Catlow. Academic Press, San Diego, California, 1997.

58. S. Pugh and M.J. Gillan, " The Energetics of NH_3 Adsorption at the MgO (001) Surface," *Surf. Sci.*, **320** [3] 331-343 (1994).

59. I. Manassidis and M.J. Gillan, "Structure and Energetics of Alumina Surfaces Calculated from First Principles," *J. Am. Ceram. Soc.,* **77** [2] 335-343 (1994).

60. P.W. Tasker, E.A. Colbourn, and W.C. Mackrodt, "Segregation of Isovalent Impurity Cations at the Surfaces of MgO and CaO," *J. Am. Ceram. Soc.,* **68** [2] 74-80 (1985).

61. P.W. Tasker and D.M. Duffy, "The Structure and Properties of the Stepped

Surfaces of MgO and NiO," *Surf. Sci.,* **137** [1] 91-102 (1984).

62. S.C. Parker, E.T. Kelsey, P.M. Oliver, and J.O. Titiloye, "Computer Modelling of Inorganic Solids and Surfaces," *Faraday Discuss.,* **95**, 75-84 (1993).

63. N.L. Allan, P. Kenway, W.C. Mackrodt, and S.C. Parker, "Calculated Surface Properties of La_2CuO_4: Implications for High-T_c Behavior," *J. Phys.: Condens. Matter,* **1** [B] SB119-123 (1989).

64. B. Slater, J.O. Titloye, F.M. Huggins, and S.C. Parker, "Atomistic Simulation of Zeolite Surfaces," *Solid State Mater. Sci.,* **5** [2] 417-424 (2001).

65. A. Pavese, M. Catti, S.C. Parker, and A. Wall, "Modeling of the Thermal Dependence of Structural and Elastic Properties of Calcite, $CaCO_3$," *Phys. Chem. Miner.,* **23** [2] 89-93 (1996).

66. P.J. Lawrence, "The Role of Defects and Impurities at Surfaces, Interfaces and in the Bulk of Chromium (III) Oxide"; Ph.D. Thesis, University of Bath, Bath, UK 1988.

67. M. Gautier, G. Renaud, L.P. Van, B. Villette, M. Pollack, N. Thromat, F. Jollet, and J. Duraud, "α-Al_2O_3 (0001) Surfaces: Atomic and Electronic Structure," *J. Am. Ceram. Soc.,* **77** [2] 323-334 (1994).

68. P.P. Ewald, "Die Berechnung Opticsher und Elektrostatischer Gitterpotentiale," *Ann. Phys.,* **84** 253-287 (1921).

69. M.J. Gillan, "The Volume of Formation of Defects in Ionic Crystals," *Philos. Mag. A.*, **43** [2] 301-312 (1981).

70. J.H. Harding, "Computer Simulation of Defects in Ionic Solids," *Rep. Prog. Phys.,* **53** [11] 1403-1466 (1990).

71. C.R.A. Catlow, M. Dixon, and W.C. Mackrodt, "Interatomic Potentials in Ionic Solids," pp. 130-161 in *Computer Simulation of Solids*. Edited by C.R.A. Catlow and W.C. Mackrodt. Springer-Verlag, Berlin, 1982.

72. M.J. Gillan and M.J. Dixon, "Molecular Dynamics Simulation of Fast-Ion Conduction in $SrCl_2$: I. Self-Diffusion," *J. Phys. C: Solid State Phys.*, **13** [10] 1901-1917 (1980).

73. M.J. Norgett, "A Born Model Calculation of the Energies of Vacancies, Ion Interstitials, and Inert Gas Atoms in Calcium Fluoride," *J. Phys. C: Solid State Phys.,* **4** [3] 298-306 (1971).

74. I.D. Faux, "The Catastrophe in Defect Calculations in Ionic Crystals," *J. Phys. C: Solid State Phys.,* **4** [10] L211-L215 (1971).

75. B.G. Dick and A.W. Overhauser, "Theory of the Dielectric Constants of Alkali Halide Crystal," *Phys. Rev.,* **112** [1] 90-103 (1958).

76. M.J. Norgett and R.J. Fletcher, "Fast Matrix Methods for Calculating the Relaxation about Defects in Crystals," *J. Phys. C: Solid State Phys.,* **3** [1] L190-L192 (1970).

77. A.B. Lidiard and M.J. Norgett, "Point Defects in Ionic Crystals," pp. 385-412 in *Computational Solid State Physics.* Edited by F. Herman, N.W. Dalton, and T.R. Koelher. Plenum, New York, 1972.

78. M.J. Norgett, "A General Formulation of the Problem of Calculating the Energies of Lattice Defects in Ionic Crystals," *UKAEA AERE Harwell Report,* **AERE-R 7650,** 1974.

79. N.F. Mott and M.J. Littleton, "Conduction in Polar Crystals. I. Electrolytic Conduction in Solid Salts," *Trans. Faraday Soc.,* **34** [1] 485-499 (1938).

80. S.C. Parker, "Prediction of Mineral Crystal Structures," *Solid State Ionics*, **8** [3] 179-186 (1983).

81. A.M. Stoneham, *Defects and Their Structure in Non-Metallic Solids*. Edited by B. Henderson and A.E. Hughes. Plenum, New York, 1976.

82. F. Bertart, "Physique du Cristal - Le Terme Electrostatic de L'Energie de Surface, Par M.," *Compt. Rendu,* **246** [25] 3447-3450 (1958).

83. P.M. Oliver, S.C. Parker, W.C. Mackrodt, " Computer Simulation of the Morphology of NiO," *Modell. Simul. Mater. Sci. Eng.,* **1** [5] 755-760 (1993).

84. G.W. Watson, E.T. Kelsey, N.H. de Leeuw, D.J. Harris, and S.C. Parker, "Atomistic Simulation of Dislocations, Surfaces and Interfaces in MgO," *J. Chem. Soc., Faraday Trans.,* **92** [3] 433-438 (1996).

85. K. Jensen, "Uber die Existenz Negativer Ionen im Rahmen des Statistischen Modells," *Z. Phys,* **101** [10] 141-163 (1936).

86. N.L. Allen and W.C. Mackrodt, "Density Functional Theory and Interatomic Potentials," *Philos. Mag. B*, **69** [5] 871-878 (1994).

87. S.C. Parker, "Computer Modelling of Minerals"; Ph.D. Thesis, University

College, London, England, 1983.

88. C.R.A. Catlow, C.M. Freeman, M.S. Islam, R.A. Jacson, M. Leslie, and S.M. Tomlinson, "Interatomic Potentials for Oxides," *Philos. Mag. A.*, **58** [1] 123-142 (1988).

89. G.V. Lewis and C.R.A. Catlow, "Potential Models for Ionic Oxides," *J. Phys. C: Solid State Phys.,* **18** [6] 1149-1161 (1985).

90. M.K. Cinibulk, "Effect of Precursors and Dopants on the Synthesis and Grain Growth of Calcium Hexaluminate," *J. Am. Ceram. Soc.,* **81** [12] 3127-3168 (1998).

91. L. Di Filippo, E. Lucchini, V. Sergo, and S. Maschio, "Synthesis of Pure Monolithic Calcium, Strontium, and Barium Hexaluminates for Catalytic Applications," *J. Am. Ceram. Soc.,* **83** [6] 1524-1526 (2000).

92. M.A. Gulgun, O.O. Popoola, and W.M. Kriven, "Chemical Synthesis and Characterization of Calcium Aluminate Powders," *J. Am. Ceram. Soc.,* **77** [2] 531-539 (1994).

93. M. Machida, K. Eguchi, and H. Arai, "Analytical Electron Microscope Analysis of the Formation of $BaO{\cdot}6Al_2O_3$," *J. Am. Ceram. Soc.,* **71** [12] 1142-1147 (1988).

94. C. Debsikdar and O.S. Sowemimo, "Some Characteristics of Barium Hexaaluminate/Celsian Composites," *J. Mater. Sci. Lett.*, **11** [10] 637-638 (1992).

95. D.A. Porter and K.E. Easterling, *Phase Transformation in Metals and Alloys*; Ch. 3. T.J. International, Padstow, Germany, 1992.

96. R.J.D. Tilley, *Defect Crystal Chemistry and Its Applications*; Ch. 1. Chapman and Hall, New York, 1987.

97. J.H. Harding, "Defects, Surfaces, and Interfaces," pp. 185-200 in *Computer Modelling in Inorganic Crystallography*. Edited by C.R.A. Catlow. Academic Press, San Diego, California, 1997.

98. T. Mathews, R. Subasri, and O.M. Sreedharan, "A Rapid Combustion Synthesis of MgO Stabilized Sr- and Ba-β-Alumina and Their Microwave Sintering," *Solid State Ionics*, **148** [1-2] 135-143 (2002).

99. P. Artizzu-Duart, J.M. Miller, N. Guilhaume, E. Garbowski, and M. Primet, "Catalytic Combustion of Methane on Substituted Barium Hexaaluminates," *Catal. Today,* **59** [1-2] 163-177 (2000).

100. G.V. Lewis, C.R.A. Catlow, and R.E.W. Casselton, "PTCR Effect in $BaTiO_3$," *J. Am. Ceram. Soc.,* **68** [10] 555-558 (1985).

101. C.W. Park and D.Y. Yoon, "Effect of Magnesium Oxide on Faceted Vicinal (0001) Surface of Aluminum Oxide," *J. Am. Ceram. Soc.*, **84** [2] 456-458 (2001).

102. N-A.M. Deraz, "Effect of Ag_2O Doping on Surface and Catalytic Properties of Cobalt-Magnesia Catalysts," *Mater. Lett.,* **51** [6] 470-477 (2001).

103. D. Coster, V. Gruver, and A. Blumenfeld, "Relationship between the Structure and the Surface Activity of Nanosized Alumina in Acid Catalysis," *Mater. Res. Soc. Symp. Proc.,* **346** 961-966 (1984).